The Dissertation Committee for Corey Michael Bryant
certifies that this is the approved version of the following dissertation:

On goal-oriented error estimation and adaptivity for nonlinear systems with uncertain data and application to flow problems

Committee:

Serge Prudhomme , Co-Supervisor

Clint Dawson , Co-Supervisor

Omar Ghattas

Robert D Moser

J. Tinsley Oden

Todd A Oliver

On goal-oriented error estimation and adaptivity for nonlinear systems with uncertain data and application to flow problems

by

Corey Michael Bryant, B.S.; M.S.C.A.M

DISSERTATION

Presented to the Faculty of the Graduate School of

The University of Texas at Austin

in Partial Fulfillment

of the Requirements

for the Degree of

DOCTOR OF PHILOSOPHY

THE UNIVERSITY OF TEXAS AT AUSTIN

December 2014

Dedicated to my family.

Acknowledgments

I wish to thank the many friends and colleagues who helped me to get to this point. First of all, Albert Romkes who originally encouraged me to attend graduate school and was instrumental in my decision to go to The University of Texas; he has continued to provide me with advice, and I owe him a great deal of gratitude. I wish to acknowledge the support of The Institute for Computational Engineering and Sciences and the Center for Predictive Engineering and Computational Sciences. I have learned a great deal from the faculty, research scientists, and graduate students that comprise these two centers, and for that, I am grateful. I would not be in the position I am today without the guidance of my committee: J. Tinsley Oden, Robert Moser, Omar Ghattas, Todd Oliver, and my supervisors Clint Dawson and Serge Prudhomme; through lectures, office meetings, and less formal discussions your teaching and direction has been invaluable. In particular, I must thank Clint Dawson for agreeing to act as my primary supervisor upon Serge Prudhomme's departure from the university. I am thankful that Serge Prudhomme remained actively involved in my research, despite being remote; the countless questions and resulting discussions have, without doubt, improved the quality of my work and will have permanent impact on my research philosophy. I have to thank Gabriel Terejanu for his influence in my understanding of numerous subjects, specifically Bayesian techniques; his insights were crucial in the beginning of my graduate

career. John Red-Horse and Roger Ghanem participated in several discussions on the subject of error analysis in the context of uncertainty quantification, which provided an alternative perspective and ultimately contributed to the idea for statistical quantities of interest. While interning at Sandia National Laboratory, Tim Wildey served as an excellent mentor, fostering discussions that lead to continuing collaborations including elements of this dissertation. I was also given the opportunity to visit King Abdullah University of Science and Technology, under the support of Raul Tempone; I value my time there for more than just the research collaborations that grew from my visit. To my fellow graduate students who have been helpful in too many ways to count, thank you. While I certainly can't list everyone, I am obliged to list a few who have had a significant impact during my time in graduate school: Steve Mattis, Andrea Hawkins-Daarud, Vikram Garg, Rebecca Morrison, Kathryn Farrell, Lindley Graham, and Jonathan Young. Finally, I should thank my family, to whom this work is dedicated, for their encouragement throughout my studies and for teaching me the value of dedication and hard work.

On goal-oriented error estimation and adaptivity for nonlinear systems with uncertain data and application to flow problems

Corey Michael Bryant, Ph.D.
The University of Texas at Austin, 2014

SUPERVISORS: Serge Prudhomme
Clint Dawson

The objective of this work is to develop a posteriori error estimates and adaptive strategies for the numerical solution to nonlinear systems of partial differential equations with uncertain data. Areas of application cover problems in fluid mechanics including a Bayesian model selection study of turbulence comparing different uncertainty models. Accounting for uncertainties in model parameters may significantly increase the computational time when simulating complex problems. The premise is that using error estimates and adaptively refining the solution process can reduce the cost of such simulations while preserving their accuracy within some tolerance.

New insights for goal-oriented error estimation for deterministic nonlinear problems are first presented. Linearization of the adjoint problems and quantities of interest introduces higher-order terms in the error representation

that are generally neglected. Their effects on goal-oriented adaptive strategies are investigated in detail here. Contributions on that subject include extensions of well-known theoretical results for linear problems to the nonlinear setting, computational studies in support of these results, and an extensive comparative study of goal-oriented adaptive schemes that do, and do not, include the higher-order terms.

Approaches for goal-oriented error estimation for PDEs with uncertain coefficients have already been presented, but lack the capability of distinguishing between the different sources of error. A novel approach is proposed here, that decomposes the error estimate into contributions from the physical discretization and the uncertainty approximation. Theoretical bounds are proven and numerical examples are presented to verify that the approach identifies the predominant source of the error in a surrogate model. Adaptive strategies, that use this error decomposition and refine the approximation space accordingly, are designed and tested.

All methodologies are demonstrated on benchmark flow problems: Stokes lid-driven cavity, 1D Burgers equation, 2D incompressible flows at low Reynolds numbers. The procedure is also applied to an uncertainty quantification study of RANS turbulence models in channel flows. Adaptive surrogate models are constructed to make parameter uncertainty propagation more efficient. Using surrogate models and adaptivity in a Bayesian model selection procedure, it is shown that significant computational savings can be gained over the full RANS model while maintaining similar accuracy in the predictions.

Table of Contents

List of Tables

List of Figures

Chapter 1

Introduction

In nearly all computational models of physical phenomena, there are inaccuracies due to an imperfect representation of the true system. Imperfections can result from uncertainties due to the miss-specification, or intentional simplification, of the governing equations and/or from discretization errors due to the approximate nature of solving an infinite dimensional problem in a discrete, computational environment.

A characteristic example is the simulation of turbulent flow. Direct simulation of the chaotic velocity field is impractical for many systems of engineering interest. Instead one often adopts a statistical approach, seeking a description of the flow in terms of the mean velocity. This leads to the well-known Reynolds-averaged Navier-Stokes (RANS) equations, governing the mean flow velocity which must be closed in order to be solved. Unfortunately, closure models introduce additional model parameters that are, *a priori*, unknown.

Not only are the parameters uncertain, and possibly dependent on specifics of the flow scenario under study, but the equations are solved numerically, which may introduce additional error. Quantifying these errors, and eventually reducing them, is vital in assessing the validity of the models

and increasing confidence in the resulting predictions.

Computational simulation of turbulent flows by the RANS equations with uncertain parameters presents a number of challenges. Firstly, the RANS equations represent a nonlinear system. The addition of uncertain parameters means one must solve an even more complex set of equations, often requiring the solution of the nonlinear equations many times to thoroughly quantify the uncertainty in model outputs.

Motivated by the RANS equations, the aim of the present work is to make the uncertainty quantification process for nonlinear problems more efficient through the application of goal-oriented error estimation techniques and surrogate modeling.

1.1 Background

Increasingly, computational models are being used to inform design and policy decisions, which raises the concern: how accurate are the predictions obtained from these models? Computational scientists have long sought to establish trust in numerical solutions to complicated engineering problems through the use of error estimation techniques. In the past few decades noteworthy advances have been made for numerous solution algorithms, in particular the finite element method.

Error estimators naturally lend themselves to the design of adaptive strategies for reducing the error in a systematic manner. In particular, in the

finite element community, methodologies based on *a posteriori* error estimation of the solution have been shown to be effective at reducing approximation errors in computed solutions [16, 56]. Some approaches focus on estimating errors in a global sense such as energy norms. However, it is often more effective to quantify the error with respect to specific features of the solution, the so-called quantities of interest. Methods for error estimation in quantities of interest, referred to as dual-weighted residual methods or goal-oriented error estimation methods, are based on the solution of an adjoint problem related to the particular quantity of interest (see, e.g. [16, 108, 57, 69, 101, 102] and the references therein). Theoretical results for goal-oriented error estimation of linear problems are well established, and have contributed to the popularity of the technique.

In contrast, the theory on goal-oriented error estimation for nonlinear systems is somewhat less advanced. The current state-of-the-art relies on the definition of a linearized adjoint problem to derive the relationship between the error in the quantity of interest and the residual but neglects the higher-order terms due to linearization in order to provide computable error estimates and refinement indicators [16, 118]. Some recent work has investigated the effect of these terms on the quality of the error estimators and on the performance of the adaptive strategy [54, 71], but more in-depth studies are still needed to better understand the consequences of neglecting these terms. One main concern is the whether ignoring these terms could have dramatic consequences in the refinement process.

Similarly to the nonlinear case, there is also a growing interest in extending goal-oriented error estimation to initial and boundary-value problems with uncertain model parameters or random boundary conditions and external forcing data [84, 91, 3, 33, 32]. Mathelin and Le Maître [91] (also presented in [84]) for example, successfully extended the goal-oriented error estimation approach to the stochastic Galerkin method. Similarly, Butler et al. [33] developed error estimates in a stochastic Galerkin framework using polynomial chaos expansions for the forward and adjoint solutions and they demonstrated the efficiency of their methodology on a non-linear transport problem. Interestingly, the authors constructed a polynomial chaos representation for the discretization error as well. In contrast to these previous works, Almeida and Oden [3] used truncated Karhunen-Loève expansions to model the random variables. Similar to an eigen decomposition, this allows for a reduction in dimensionality as fewer terms are needed to express the dominant behavior of the response. To discretize the random variables in the resulting Karhunen-Loève expansion the authors used a stochastic collocation method and computed *a posteriori* error estimates for the quantity of interest evaluated at each collocation point. Butler and collaborators later extended their work to the use of a non-intrusive approach based on an approximate projection, or pseudospectral projection; they showed that it provides similar computational benefits to the approach proposed by Almeida and Oden [3].

One major shortcoming of the previously mentioned approaches is, while they could successfully estimate the overall approximation error, they did

not provide separate estimates of the error contributions due to the physical discretization and the uncertainty representation. That is, one can not easily decide which approximation space to refine first in an adaptive refinement algorithm.

The need for surrogate models and adaptive methods can be best appreciated when one is interested in parameter estimation based on a Bayesian calibration procedure. In the case of RANS models, the literature on Bayesian inference is rather scarce. One should nevertheless mention the work of Cheung et al. [40], which describes a Bayesian approach for the calibration of parameters in the Spalart-Allmaras turbulence model. The previous work was further extended by Oliver and Moser in [104] to showcase a Bayesian model selection procedure, in which four different models to characterize uncertainties and four different turbulence models were considered. They were able to identify the most probable turbulence model and uncertainty representation that best captured the flowfield obtained from direct numerical simulation data. However, these numerical experiments were performed on relatively simple scenarios due to the computational cost and complexity of the simulations. If one is interested in engineering applications, the proposed calibration procedure will need to be greatly accelerated in order to be viable. A motivation for this work is the development of a methodology combining surrogate modeling and goal-oriented error estimation for fast and reliable parameter identification that can be applied to turbulence modeling.

1.2 Objectives and contributions of this work

As mentioned above, the main objective of this work is to develop a technique based on surrogate modeling and goal-oriented error estimation for efficient and reliable parameter estimation in turbulence modeling. To achieve this objective, we proceeded by considering the following goals:

1. Extension of goal-oriented error estimation for nonlinear models in a deterministic setting: As noted previously, nonlinear contributions to *a posteriori* error estimators are typically neglected. We seek here to perform a more thorough analysis of the application of goal-oriented error estimation to nonlinear problems. Previous theoretical results by [1, 118, 119] are extended to present a nonlinear form of Céa's lemma. We also present numerical justification for scenarios where the nonlinear error contributions cannot be neglected. Adaptive strategies based on the previously neglected terms are investigated for Navier Stokes flow past an obstacle at moderate Reynolds number ($Re = 40$).

2. Goal-oriented error estimation for partial differential equations with uncertain data: On that topic, further improvement of the current state-of-the-art is also needed. Le Maître and Knio [84, Ch. 9], stated in a section on refinement strategies for uncertainty quantification that:

   > "Specifically, it is not possible to decide (a) between h or p refinement and (b) whether one should enrich the approximation space $\mathcal{V}^h$ [physical] or $\mathcal{S}^h$ [stochastic]."

They go on to emphasize further that,

> "[...] better approaches, yet to be conceived, are consequently needed."

Development of novel methods that address this issue is one of the aims of the proposed work. Adaptive procedures for surrogate construction that have been developed to date typically lack this feature. With the exception of Butler et al. [33], all of the previously referenced works on the subject did not have the ability to distinguish between the two sources of the error. We propose here a computable error estimator that is capable of separating the two contributions and an adaptive strategy that refines the approximations either in physical space and/or in parameter space. The new approach is tested first on synthetic examples before being applied to the case of incompressible flows past a cylinder at low Reynolds numbers. We also demonstrate the efficiency of the error estimator and adaptive strategy for anisotropic refinement on a diffusion example that depends on ten random parameters.

3. Application of adaptive surrogate modeling to Bayesian model comparison: Contributions of the present work culminate with the application to a Bayesian model comparison for the Spalart-Allmaras turbulence model with four proposals for the uncertainty characterization. A comparative study is performed against the work of Oliver and Moser [104], and our preliminary results look extremely promising. Only minor discrepancies

are observed between the full model and the use of the adaptive surrogate in the Bayesian posterior distribution.

1.3 Overview

The dissertation is organized as follows. We begin by reviewing the well established theory of goal-oriented error estimation for linear problems in Chapter 2. After presenting the general theory in Section 2.2, results are presented in 2.3 for benchmark flow scenarios including the Stokes lid-driven cavity problem. Extensions to the nonlinear setting are presented in Chapter 3. Section 3.2 includes a review and extension of theoretical results, followed by numerical justifications. In Section 3.3 we investigate the need to include previously neglected terms associated with the linearization. Adaptive strategies are then examined in Section 3.4. Focus shifts in Chapter 4 to goal-oriented error estimation for partial differential equations with uncertain data. Foundations of probability, and the representation of uncertainty into the differential equation are detailed in Section 4.1. Error estimation and decomposition into physical approximation error and uncertainty representation error are discussed in Sections 4.2 and 4.4, respectively. Finally, adaptive strategies are examined in Section 4.5. To conclude the work the previously discussed components are used to perform an efficient Bayesian model comparison for RANS in Chapter 5. Section 5.1 reviews the RANS equations and the Spalart-Allmaras turbulence model. General results of the application of the newly proposed adaptive surrogate construction for the RANS model are given

in Section 5.2. Efficient Bayesian calibration with surrogate models is examined in Section 5.3 and the comparison with the Bayesian study performed by Oliver and Moser [104] is presented in Section 5.4. Concluding remarks, and a brief discussion on possible extensions and future work are provided in the final chapter, Chapter 6.

Chapter 2

Goal-oriented error estimation: Linear theory

In the computational mechanics community *a posteriori* error estimation techniques are effective tools in estimating and eventually reducing approximation errors in numerical solutions of initial and boundary-value problems. Goal-oriented error estimation methods are of particular interest when specific features of the solution are the primary concern of the simulation. The practical objective of such techniques is a computable estimate of the discretization error with proven accuracy and reliability. Babuška and Rheinboldt [11] first considered the use of *a posteriori* error estimation for adaptive finite element methods. Their pioneering work paved the way for goal-oriented error estimation and adaptive methods beginning in the 1990s with seminal works by Eriksson et al. [51, 52], Becker and Rannacher [16], and Prudhomme and Oden [108], among others. Since, publications concerning *a posteriori* error estimation and adaptivity for finite element methods have gained tremendous popularity. The books of Ainsworth and Oden [1], Babuška and Strouboulis [6], and Verfürth [119] provide more extensive reviews of the field as a whole.

Of continued interest is the application of *a posteriori* error estima-

tion to non-linear problems [106, 16, 119] and, more recently, to the field of uncertainty quantification [33, 32, 84]. Theoretical results for these more complicated problems are far less mature than for deterministic linear problems and will be explored in the subsequent chapters. In this chapter we review the foundations of the linear theory for goal-oriented error estimation. We will restrict our analysis to standard, conforming, continuous finite element spaces, but the theoretical results extend to more sophisticated discretizations with minor modification, for example see [19] for the case of nonconforming finite elements. Starting in Section 2.1, we consider an abstract differential equation for which we derive the weak formulation and recall classic results for existence and uniqueness of solutions and for the numerical error in Galerkin approximation of the problem. In Section 2.2 we proceed with a discussion on quantities of interest and the corresponding adjoint problem. Again well-posedness of the adjoint problem and classic error results are included before focusing on error estimation for quantities of interest and adaptive refinement of the approximation spaces in Section 2.2.4. Finally, in Section 2.3, the entire process including error estimation and mesh adaptivity, is illustrated for Stokes flow in a lid-driven cavity.

2.1 Abstract linear model

For linear operators, general results on the existence of a unique solution and convergence of Galerkin approximations are readily available and can be found in [20, 53], among others. We briefly review these results while

introducing the notation which will be used throughout this monograph. To begin, we describe an abstract differential equation as motivation for the weak formulation of the problem detailed thereafter.

2.1.1 Weak formulation

Let Ω be an open bounded domain in $\mathbb{R}^d, d = 1, 2$, or 3, with Lipschitz boundary $\partial\Omega$. We use the notation $\mathcal{A}$ to represent an abstract linear (second-order) differential operator and f to represent external forcing. We consider the abstract differential equation governing the behavior of solution $u = u(\boldsymbol{x})$, written as

$$0 = f(\boldsymbol{x}) - \mathcal{A}u(\boldsymbol{x}), \ \boldsymbol{x} \in \Omega. \tag{2.1}$$

Subjected to homogeneous Dirichlet boundary conditions on the boundary $\partial\Omega$,

$$u(\boldsymbol{x}) = 0, \quad \boldsymbol{x} \in \partial\Omega. \tag{2.2}$$

Inhomogeneous Dirichlet boundary conditions can be accommodated through the use of a lift function; we employ this technique for the cavity problem in Section 2.3.

Let U be a Banach space and V a reflexive Banach space on Ω[1] with norms $\|\cdot\|_U$ and $\|\cdot\|_V$. Multiplying (2.1) by an arbitrary $v \in V$ integrating over Ω, performing integration by parts, and applying the boundary conditions (2.2)

[1] Appropriate spaces U and V will depend on the specific structure of the operator, as well as boundary conditions. These statements are kept general on purpose and will be made more concrete in the context of specific problems.

leads to the weak formulation,

$$\begin{aligned} &\text{Find } u \in U \text{ such that} \\ &\mathcal{R}(u;v) := \ \mathcal{F}(v) - \mathcal{B}(u,v) = 0 \quad \forall v \in V, \end{aligned} \tag{2.3}$$

where $\mathcal{B} : U \times V \to \mathbb{R}$ and $\mathcal{F} : V \to \mathbb{R}$ are bilinear and linear forms, respectively. Equation (2.3) also introduces the residual form $\mathcal{R} : U \times V \to \mathbb{R}$.

2.1.2 Well-posedness: existence and uniqueness

Existence of a unique solution to (2.3) is established by the Generalized Lax-Milgram Theorem, a proof of which can be found in [53] (note that Theorem 2.1.1 is also referred to as the Babuška Lax-Milgram Theorem or Banach-Nečas-Babuška Theorem).

Theorem 2.1.1 (Generalized Lax-Milgram Theorem)**.** *Let U and V be Banach spaces, V reflexive. Assume $\mathcal{B}$ also satisfies the following conditions:*

a.) $\mathcal{B}$ is continuous, i.e. there is some constant $c_{\mathcal{B}} > 0$ such that

$$|\mathcal{B}(u,v)| \leq c_{\mathcal{B}} \|u\|_U \|v\|_V \quad \forall u \in U, \forall v \in V \ ; \tag{2.4}$$

b.) $\mathcal{B}$ satisfies the inf-sup condition, i.e. $\exists \gamma_{\mathcal{B}} > 0$ such that

$$\inf_{u \in U \setminus \{0\}} \sup_{v \in V \setminus \{0\}} \frac{\mathcal{B}(u,v)}{\|u\|_U \|v\|_V} \geq \gamma_{\mathcal{B}} \ ; \tag{2.5}$$

c.) $\mathcal{B}$ satisfies a non-degeneracy condition on U

$$\forall v \in V, \quad (\forall u \in U, \mathcal{B}(u,v) = 0) \Rightarrow (v = 0) \tag{2.6}$$

If $\mathcal{F}$ is continuous, i.e. $\mathcal{F}$ is in the dual space V^* of V, then (2.3) *has a unique solution and*

$$\|u\|_U \leq \frac{1}{\gamma_{\mathcal{B}}} \|F\|_{V^*} \tag{2.7}$$

2.1.3 Functional representation

Equivalently, the abstract model problem (2.3) can be written in operator form. Let $\langle \cdot, \cdot \rangle_{V^*,V}$ be the duality pairing on $V^* \times V$ and let $B : U \to V^*$ be the unique continuous linear operator such that,

$$\langle Bu, v \rangle_{V^*,V} = \mathcal{B}(u, v), \quad \forall u \in U, \ \forall v \in V, \tag{2.8}$$

and let $F \in V^*$ be given by $\langle F, v \rangle_{V^*,V} = \mathcal{F}(v)$, $\forall v \in V$. Additionally, we define the residual operator, $R : U \to V^*$ by $R(u) = F - Bu$; uniqueness of B and F implies that R is also unique. Then (2.3) is equivalent to,

$$\begin{aligned} &\text{Find } u \in U \text{ such that} \\ &\langle R(u), v \rangle_{V^*,V} = 0, \quad \forall v \in V. \end{aligned} \tag{2.9}$$

We will make use of this formulation in the discussion on nonlinear problems in Chapter 3. As a result of the equivalence between the formulations, if $\mathcal{B}$ satisfies the conditions of Theorem 2.1.1, then B is bijective [53, Corollary A.46].

2.1.4 Galerkin approximation

We will focus on standard conforming Galerkin approximations of (2.3). Let $U^h \subset U$ and $V^h \subset V$ represent appropriate trial and test finite element

spaces, respectively. The Galerkin approximation of (2.3) is then given by,

$$\begin{aligned} &\text{Find } u^h \in U^h \text{ such that} \\ &\mathcal{F}(v^h) - \mathcal{B}(u^h, v^h) = 0 \quad \forall v^h \in V^h. \end{aligned} \tag{2.10}$$

Provided that $\mathcal{B}$ satisfies the conditions of Theorem 2.1.1 on $U^h \times V^h$ the discrete problem (2.10) is also well posed. Furthermore, the error $u - u^h \in U^h$ satisfies the Galerkin orthogonality property, i.e.

$$\mathcal{R}(u^h; v^h) = \mathcal{B}(u - u^h, v^h) = 0 \quad \forall v^h \in V^h. \tag{2.11}$$

Convergence of Galerkin approximations is provided by the well-known Céa's Lemma and is the foundation of *a priori* error estimates. We first state Céa's Lemma and then review the results from approximation theory to establish *a priori* convergence rates for a family of approximation spaces parameterized by h.

Theorem 2.1.2. *(Céa's Lemma) Assume that* (2.3) *and* (2.10) *are well-posed in the sense of Theorem 2.1.1, with solutions* u *and* u^h*, respectively. Then the error,* $u - u^h$*, satisfies the upper bound*

$$\left\| u - u^h \right\|_U \leq \left(1 + \frac{c_{\mathcal{B}}}{\gamma_{\mathcal{B}}^h} \right) \inf_{\varphi \in U^h} \left\| u - \varphi \right\|_U , \tag{2.12}$$

where $c_{\mathcal{B}}$ *is the continuity constant given in* (2.4) *and* $\gamma_{\mathcal{B}}^h$ *is the discrete inf-sup constant established by* (2.5) *for* (2.10)*.*

In order to establish convergence rates, we recall a result from approximation theory on the interpolation of functions in Sobolev spaces. The following results are provided without proof, see [53, Corollary 1.110] [20, Theorem

14.3.3] for more details. First recall the definition of a finite element $\{K, P, \Sigma\}$: a triplet consisting of K a compact connected subset of $\mathbb{R}^d$, P a vector space of functions on K, and Σ a set of n linear forms $\sigma_i, i = 1, \ldots, n$ such that the linear mapping $P \ni p \mapsto (\sigma_1(p), \ldots, \sigma_n(p)) \in \mathbb{R}^n$ is bijective. The linear forms σ_i are called the degrees of freedom and form a basis for the space of linear maps from P into $\mathbb{R}$ [53]. Let $\mathcal{T}_h$ represent a partition of Ω where the subscript h denotes the maximum element size of the mesh, namely $h = \max_{K \in \mathcal{T}_h} h_K$, where $h_K = \text{diam}(K)$. We also define the polynomial space $\mathbb{P}_k$, the space of polynomials in $\boldsymbol{x} \in \mathbb{R}^d$ with total degree at most k. We denote the integer ordered Sobolev spaces by $W^{m,p}(\Omega) = \{u \in L^p(\Omega) : D^\alpha u \in L^p(\Omega),\ |\alpha| \leq m\}$. Furthermore, when $p = 2$ we adopt the common notation $H^m = W^{m,2}$.

Theorem 2.1.3. *Let $\{K, P, \Sigma\}$ and $V(K)$ an associated normed vector space. Assume there exists an integer k such that*

$$\mathbb{P}_k \subset P \subset W^{k+1,p}(K) \subset V(K) \tag{2.13}$$

where $1 \leq p \leq \infty$. Let $\{\mathcal{T}_h\}$ be a shape-regular[2] family of affine meshes on the polyhedron domain Ω. Let V_k^h be the approximation space associated with $\mathcal{T}_h$ and $\{K, P, \Sigma\}$, and assume that V_k^h is $W^{1,p}$-conformal (i.e. $V_k^h \subset W^{1,p}$). Let $\mathcal{I}_k^h$ be the global interpolation operator on V_k^h, then there exists a constant $c_\mathcal{I}$, independent of h, such that, for all h and $v \in W^{s+1,p}$, $0 \leq s \leq k$,

$$\left|v - \mathcal{I}_k^h v\right|_{W^{1,p}} \leq c_\mathcal{I} h^s \left|v\right|_{W^{s+1,p}}. \tag{2.14}$$

[2] The term *shape-regular* means that for the family of meshes $\{\mathcal{T}_h\}$ there exists an r such that $\forall h, \forall K \in \mathcal{T}_h,\ h_K/\rho_K \leq r$, where ρ_K is the diameter of the largest ball that can be inscribed inside of element K.

Equation (2.14) combined with Theorem 2.1.2 can be used to prove the following result

Theorem 2.1.4. *In addition to the assumptions of Theorem 2.1.3, if* $u \in H^{s+1}$*, then*

$$\left\|u - u^h\right\|_{H^1} \leq \bar{C} h^s \left|u\right|_{H^{s+1}}, \tag{2.15}$$

where $\bar{C} = 2\left(1 + \frac{c_{\mathcal{B}}}{\gamma_B^h}\right) c_{\mathcal{I}}$.

Error estimates in weaker norms can also be established if $U = V$ and the linear operator $\mathcal{B}(\cdot, \cdot)$ satisfies two additional assumptions required by the Lemma of Aubin and Nitsche:

(AN1) The space V can be continuously embedded into a Hilbert space L, equipped with a continuous, symmetric, and positive definite bilinear form $l(\cdot, \cdot)$ and corresponding seminorm $\left|\cdot\right|_L = \sqrt{l(\cdot, \cdot)}$. Furthermore, there exists a Banach space $Z \subset V$ and a stability constant $c_S > 0$ such that, for all $g \in L$, the solution $\zeta(g)$ to the adjoint problem:

$$\begin{aligned} &\text{Find } \zeta(g) \in V \text{ such that} \\ &\mathcal{B}(v, \zeta(g)) = l(g, v), \quad \forall v \in V, \end{aligned} \tag{2.16}$$

satisfies the *a priori* estimate $\left\|\zeta(g)\right\|_Z \leq c_S \left|g\right|_L$.

(AN2) There exists an interpolation constant $c_i > 0$ such that

$$\forall h, \forall v \in Z, \quad \inf_{v^h \in V^h} \left\|v - v^h\right\|_V \leq c_i h \left\|v\right\|_Z. \tag{2.17}$$

Lemma 2.1.5. *(Aubin-Nitsche) Provided the operator $\mathcal{B}(\cdot,\cdot)$ satisfies (AN1) and (AN2), then,*

$$\left|u-u^h\right|_L \leq c_A h \left\|u-u^h\right\|_V \quad \forall h, \tag{2.18}$$

where $c_A = c_{\mathcal{B}} c_i c_S$.

Proof. See [19] [53, p.98]. □

Letting $V = H^1, L = L^2$ and combining (2.18) and (2.15) allows one to establish the following theorem.

Theorem 2.1.6.

$$\left\|u-u^h\right\|_{L^2} \leq c_A \bar{C} h^{s+1} \left|u\right|_{H^{s+1}} \sim h^{s+1} \tag{2.19}$$

The results of this section provide a strong theoretical foundation on which the remainder of the chapter will rely. Furthermore, the linear theory will be crucial in the examination of nonlinear problems in the next chapter.

2.2 *A posteriori* error estimation

2.2.1 Quantities of Interest (QoI) and the adjoint problems

One is often interested in a particular feature of the response, referred here to as a quantity of interest. A quantity of interest can usually be represented as a functional of the solution, $\mathcal{Q}(u)$. We restrict ourselves, for the moment, to bounded linear functionals of the form:

$$\mathcal{Q}(u) = \langle q, u \rangle_{U^*,U}\,, \tag{2.20}$$

where $q \in L^2(\Omega)$ is the kernel associated with quantity of interest $\mathcal{Q}$. We list below some common choices for quantities of interest.

Averaged values. The average of the solution u over a subregion ω of the domain is represented as the linear functional

$$\mathcal{Q}(u) = \frac{1}{|\omega|} \int_\Omega \kappa_\omega u dx, \tag{2.21}$$

where κ_ω is the characteristic function:

$$\kappa_\omega = \begin{cases} 1, & x \in \omega, \\ 0, & x \in \Omega \setminus \omega, \end{cases} \tag{2.22}$$

and $|\omega| = \int_\Omega \kappa_\omega dx$.

Pointwise value. The value of the solution at a specific point x_0 in the domain is given by $\mathcal{Q}(u) = u(x_0)$. If $u \in H^1(\Omega)$ then this quantity may not be well defined for $d \geq 2$. Thus, we define a local average of the solution,

$$\mathcal{Q}(u) = \int_\Omega \kappa_\varepsilon(x - x_0) u(x)\ dx, \tag{2.23}$$

using a mollifying kernel κ_ε given by:

$$\kappa_\varepsilon(x) = \begin{cases} C \exp\left(\frac{1}{|x|^2/\varepsilon^2 - 1}\right), & |x| < \varepsilon \\ 0, & |x| \geq \varepsilon, \end{cases} \tag{2.24}$$

where C is such that $\int_\Omega \kappa_\varepsilon(x - x_0) dx = 1$.

The aim of goal-oriented *a posteriori* error estimation is to estimate the error in the quantity of interest for the discrete solution $u^h \in V^h$, i.e.

$$\mathcal{E} = \mathcal{Q}(u) - \mathcal{Q}\left(u^h\right). \tag{2.25}$$

It requires the definition of the so-called adjoint problem, which seeks a generalized Green's function associated with the particular quantity of interest $\mathcal{Q}$ [16, 108, 14, 57]. The definition of the adjoint problem is based on the form $\mathcal{B}$ and the quantity of interest $\mathcal{Q}$,

$$\begin{aligned} &\text{Find } z \in V \text{ such that} \\ &\mathcal{B}(v, z) = \mathcal{Q}(v), \quad \forall v \in U. \end{aligned} \tag{2.26}$$

Provided the primal problem (2.3) is well-posed and the Banach space U is also reflexive, the well-posedness of (2.26) follows from (2.1.1) and the fact that $\mathcal{Q}$ is continuous [118].

2.2.2 Error representation formula

The key feature of the adjoint solution is that it provides an error representation formula on which error estimates can be established. Let u and z be the solutions to (2.3) and (2.26), respectively, and let $e = u - u^h$, where u^h is the solution of (2.10), then

$$\mathcal{E} = \mathcal{Q}(u) - \mathcal{Q}(u^h) = \mathcal{B}(e, z), \tag{2.27}$$

$$= \mathcal{B}(e, z - \varphi), \quad \forall \varphi \in V^h, \tag{2.28}$$

$$= \mathcal{F}(z - \varphi) - \mathcal{B}(u, z - \varphi), \quad \forall \varphi \in V^h, \tag{2.29}$$

$$= \mathcal{R}(u^h; z - \varphi), \quad \forall \varphi \in V^h. \tag{2.30}$$

Here, we made use of the residual form $\mathcal{R} : U \times V \to \mathbb{R}$.

Remark 2.2.1. In Equation (2.30) we also employed Galerkin orthogonality (2.11) to introduce the test function φ. In the literature the motivation for

introducing such a function is not always made clear. In fact, due to orthogonality, it has no effect on the value of the error itself. From a theoretical standpoint this step is key in deriving convergence estimates and establishing error estimators for the error in the quantity of interest, which we demonstrate below. A practical motivation, in terms of adaptivity, is seldom discussed however. Using the difference of the adjoint solution and a function in the primal approximation space (usually the projection of the adjoint solution itself) does impact the quality of the error indicators used to guide adaptive refinement; we provide further insight on the topic and demonstrate the effect in the example at the end of this chapter.

A priori estimates for the error in the quantity of interest are readily obtained from (2.28). Applying the continuity of $\mathcal{B}$ and then taking the infimum of all $\varphi \in V^h$ proves the following Theorem, originally due to Babuška and Miller [8, 9, 10]; see also [6, 118].

Theorem 2.2.1. *Let u and u^h be the solutions to* (2.3) *and* (2.10)*, respectively, and let z be the solution to the adjoint problem* (2.26)*. Then, under the assumptions of Céa's Lemma 2.1.2, the following estimate holds for the error in the quantity of interest,*

$$\left|\mathcal{Q}(u) - \mathcal{Q}(u^h)\right| \leq c_{\mathcal{B}} \left\|u - u^h\right\|_U \inf_{\varphi \in V^h} \|z - \varphi\|_V . \tag{2.31}$$

Since (2.31) involves the product of two errors, it is expected that the error in the quantity of interest, $\mathcal{E}$, will converge at a higher rate than the

error in the primal solution $\left\|u - u^h\right\|_U$; higher rates are generally observed in practice.

In fact, provided the primal and adjoint solutions are smooth enough, *a priori* convergence rates can be established for the error in the quantity of interest in a similar fashion to what was done in the previous section. Using (2.15) and (2.14) the following corollary is easily proved [118].

Corollary 2.2.2. *Using the notation of Theorem 2.1.3, let* $u^h \in V^h$ *be the solution of* (2.10) *with* $V^h = \{v \in H_0^1(\Omega) : \ \forall K \in \mathcal{T}_h, \ v|_K \in \mathcal{P}_k(K)\}$*, and assume* $u \in H^{s+1} \cap H_0^1$*, where* $0 \leq s \leq k$*. Additionally, assume* $z \in H^{t+1} \cap H_0^1$*,* $0 \leq t \leq k$*, to be the solution to* (2.26)*. Then,*

$$\left|\mathcal{Q}(u) - \mathcal{Q}(u^h)\right| \leq ch^{s+t} \left|u\right|_{H^{s+1}} \left|z\right|_{H^{t+1}}, \tag{2.32}$$

where c *is independent of* h*, but involves the constants* $c_{\mathcal{B}}, \bar{C}$*, and* $c_{\mathcal{I}}$*.*

Thus, the optimal rate of convergence for the error in the quantity of interest of h^{2k} can be achieved if $t = s = k$ [118].

2.2.3 Error estimation

The error representation (2.30) is the point of departure from the derivation of *a posteriori* error estimates and adaptive strategies with respect to quantities of interest. However, it involves the adjoint solution z, that cannot be solved exactly, apart from simple cases. Hence, one must resort to an appropriate approximation of the adjoint solution z. Several approaches

have been proposed for establishing error estimates based on (2.30), see [16] for example. Here we will focus on the straightforward method of solving for z in a larger approximation space V^+, such that $V^h \subset V^+ \subset V$. A common choice for the enriched space is to increase the polynomial order of the finite element basis, yielding the discrete function space V^+ [16]. The discrete adjoint problem is thus,

$$\text{find } z^+ \in V^+ \text{ s.t.} \quad \mathcal{B}(v, z^+) = \mathcal{Q}(v) \quad \forall v \in V^+.$$

A computable error estimate can then be obtained using the discrete primal and adjoint solutions. Let π^h denote the projection operator on V^h and let us choose $\varphi^h = \pi^h z^+$. Then

$$\mathcal{Q}(u) - \mathcal{Q}(u^h) = \mathcal{R}(u^h; z - \pi^h z^+), \tag{2.33}$$

$$= \mathcal{R}(u^h; z^+ - \pi^h z^+) + \mathcal{R}(u^h; z - z^+), \tag{2.34}$$

We introduce the computable error estimator $\eta(u^h, z^+)$,

$$\mathcal{Q}(u) - \mathcal{Q}(u^h) \approx \mathcal{R}(u^h; z^+ - \pi^h z^+) =: \eta(u^h, z^+). \tag{2.35}$$

Since, z^+ is higher order, the adjoint error $z - z^+$ is expected to be relatively small so that the second term of (2.34) can be neglected to obtain the computable estimate (2.35) [16].

Remark 2.2.2. Alternatively, some authors [108, 8, 10] have proposed estimators based on the product of primal and dual error estimates,

$$\left|\mathcal{B}(u - u^h, z - z^+)\right| \leq c_{\mathcal{B}} \left\|u - u^h\right\|_U \left\|z - z^+\right\|_V \approx \eta_u \eta_z. \tag{2.36}$$

If $U = V$ and $\mathcal{B}$ defines an inner product on U, then equality is obtained in the equation above with $c_{\mathcal{B}} = 1$. The parallelogram identity can then be used to establish the estimate [8, 10],

$$|B(e_u, e_z)| = \frac{1}{4} \|e_u + e_z\|_U^2 - \frac{1}{4} \|e_u - e_z\|_U , \tag{2.37}$$

where $e_u = u - u^h$ and $e_z = z - z^h$. In either case, the error in the energy norms can be approximated using one of the many techniques discussed in the literature, see [108, 1, 119] for an overview of some such methods. Since estimates of the primal and adjoint error are obtained independently, this approach even allows for the solution of the adjoint problem in the same approximation space. Energy based estimates such as (2.36) are often argued to be overly pessimistic compared to the dual-weighted residual methods, but it is possible to obtain upper *and* lower bounds on the estimators which provides a theoretical foundation for the accuracy and reliability of such estimates [108, 109]. In any case, we choose to focus on the dual-weighted residual techniques.

2.2.4 Refinement indicators for mesh adaptivity

For the purpose of mesh refinement one has to decompose the global error quantity (2.35) into local contributions, defined on subdomains of Ω. The most straightforward approach is to consider contributions on each element of the mesh. In order to so, (2.35) can be recast as:

$$\eta(u^h, z^+) = \mathcal{R}(u^h; z^+ - \pi^h z^+) = \sum_{K \in \mathcal{T}_h} \mathcal{R}(u^h; z^+ - \pi^h z^+)\big|_K , \tag{2.38}$$

where the element restriction of the residual is obtained by doing element-wise integration by parts,

$$\begin{aligned}\mathcal{R}(u^h; z^+ - \pi^h z^+)\big|_K = &\int_K r_K(z^+ - \pi^h z^+)dx \\ &+ \int_{\partial K} j_K(z^+ - \pi^h z^+)ds,\end{aligned} \tag{2.39}$$

where r_K is the interior residual $f - \mathcal{A}u^h$ and the boundary term j_K restricted to element edge e, or $j_K|_e$, represents the boundary flux terms for $e \in \partial K \setminus \Omega$ and the Neumann boundary conditions if $e \in \partial\Omega$ [16, 118].

For example, consider Laplace's equation, $\mathcal{A} = \Delta$ and $f = 0$, with homogeneous Dirichlet boundary conditions, then

$$\mathcal{R}(u^h; z^+ - \pi^h z^+) = -\int_\Omega \nabla u^h \cdot \nabla(z^+ - \pi^h z^+)dx, \tag{2.40}$$

$$= \sum_{K\in\mathcal{T}_h} -\int_K \nabla u^h \cdot \nabla(z^+ - \pi^h z^+)dx, \tag{2.41}$$

$$= \sum_{K\in\mathcal{T}_h} \int_K \Delta u^h \ (z^+ - \pi^h z^+)dx \tag{2.42}$$

$$- \sum_{K\in\mathcal{T}_h} \int_{\partial K\setminus\Omega} (\boldsymbol{n}_K \cdot \nabla u^h)(z^+ - \pi^h z^+)ds, \tag{2.43}$$

where $\boldsymbol{n}_K$ is the outward normal vector on element K. In practice however, the boundary integrals are typically decomposed into integrals over the edges of elements e that belong to the interior of the domain Γ_{int},

$$\begin{aligned}&\sum_{K\in\mathcal{T}_h} -\int_{\partial K} (\boldsymbol{n}_K \cdot \nabla u^h)(z^+ - \pi^h z^+)ds \\ &\qquad = \sum_{K\in\mathcal{T}_h} \sum_{e\in\partial K\cap\Gamma_{\text{int}}} -\frac{1}{2}\int_e \boldsymbol{n}_K \cdot [\![\nabla u^h]\!](z^+ - \pi^h z^+)ds,\end{aligned} \tag{2.44}$$

where $[\![\nabla u^h]\!]$ denotes the jump across element boundaries, $[\![\nabla u^h]\!] = \nabla u^h|_{K^+} - \nabla u^h_{K-}$, for elements K^+ and K^- adjacent to edge e in the positive and negative directions, respectively. This form of the estimator suggests an obvious choice of error indicators, namely

$$\eta_K = \left| \int_K (\Delta u^h)(z^+ - \pi^h z^+) dx - \sum_{e \in \partial K \cap \Gamma_{\text{int}}} \frac{1}{2} \int_e \boldsymbol{n} \cdot [\![\nabla u^h]\!](z^+ - \pi^h z^+) ds \right| \tag{2.45}$$

The general form of the error indicators is, thus the absolute value of the expression given by (2.39), where the boundary terms have been decomposed in the manner of (2.45). That is, the element indicators are defined by,

$$\eta_K := \left| \int_K r_k(z^+ - \pi^h z^+) dx + \sum_{e \partial K \cap \Gamma_{\text{int}}} \int_e j_K|_e (z^+ - \pi^h z^+) ds \right|, \tag{2.46}$$

where $j_K|_e$ will typically involve the jump in fluxes across element interfaces. Alternatively, the triangle inequality can be applied to (2.46) to limit the cancellation of errors [119].

Once a set of element error indicators η_K is obtained there are a number of different ways to use the indicators to drive mesh refinement. In regards to controlling global error, optimal refinement techniques have been investigated by numerous researchers, see for example Binev, Dahmen, and DeVore [18], Carstensen and collarborators [38, 37], and Stevenson [114], to name a few. Optimal convergence for goal-oriented adaptive refinement has also been investigated, to a lesser extent, notably by Mommer and Stevenson [94]; although, they focused on the product of global error estimates (Remark 2.2.2) instead

of dual-weighted approaches. The present work is primarily concerned with extending goal-oriented error estimation to new problems, rather than investigating optimal methods for refinement for established areas of research. We will therefore consider two classical marking strategies for adaptive mesh refinement:

- An element fraction marking strategy which consists of choosing a fixed fraction α of elements to be refined. The elements corresponding to the largest indicators are refined.
- Error fraction marking strategy, which consists of refining all elements within the fraction α of the maximum contribution, i.e.

$$|\eta_{K'}| \geq \alpha \max_{K \in \mathcal{T}} |\eta_K| \,. \tag{2.47}$$

In addition to the references on optimal adaptive schemes, see [118, 16] for other standard marking strategies.

Once an element is marked for refinement, one must also make the choice between raising the polynomial order of approximation in that element, often termed enrichment or p-refinement, or splitting the element into new 'child' elements, called h-refinement or simply refinement. For refinement of the finite element mesh, we will restrict our approach to h refinement, although we do explore a type of p refinement for parameter space later in Chapter 4.

When performing the refinement we also take into account the relative level of neighboring elements. No element is allowed to be more than one refinement level above its nodal neighbors. We enforce this limit prior to actually

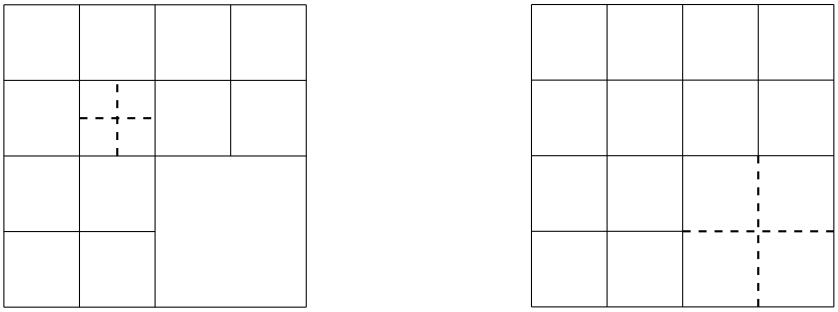

Figure 2.1: Diagram of the mesh smoothing procedure. Although the smaller element is marked for refinement (left), the procedure just refines the lower right element to homogenize the levels of refinement (right).

performing refinement. Each element marked for refinement is compared to its neighbors, if any neighbor is a refinement level above the marked element we mark the neighbor element instead. This can be thought of as a smoothing procedure that reduces the number of spurious refinements. Figure 2.1 depicts an example of the smoothing process, where the dashed lines indicate an element marked for refinement.

2.3 Stokes problem

In order to illustrate the goal-oriented error estimation and adaptivity procedures, we consider the Stokes equations in a 2D lid-driven cavity. This problem represents a common benchmark application for testing fluid flow simulations and we follow closely here the work of Prudhomme and Oden [109]. We follow the same structure as above; we start by deriving the variational setting, show that the problem satisfies the conditions of Theorem 2.1.1 and thus possesses a unique solution; we describe one possible quantity of interest,

the resulting adjoint equation, and the error representation; finally numerical results are shown demonstrating the use of the error estimate to drive adaptive h-refinement and the superior convergence compared to uniform refinement.

2.3.1 Variational formulation

To develop the weak formulation for the Stokes equations in a lid-driven cavity, we begin by considering the Stokes equations with homogeneous Dirichlet boundary conditions,

$$\left.\begin{aligned} -\Delta \boldsymbol{u} + \nabla p &= \boldsymbol{f}, \quad \text{in } \Omega, \\ \nabla \cdot \boldsymbol{u} &= 0, \quad \text{in } \Omega, \\ \boldsymbol{u} &= 0, \quad \text{on } \partial\Omega. \end{aligned}\right\} \tag{2.48}$$

In this work, we will use a mixed formulation, although a constrained formulation, such as that suggested in [53], could also be used. Let $\boldsymbol{v} \in V = [H_0^1(\Omega)]^2$ and $q \in Q = L_0^2(\Omega) = \{q \in L^2(\Omega) : \int_\Omega q = 0\}$ be test functions for the velocity and pressure variables, respectively. The zero-mean restriction on Q is used to remove constant functions from the test space, which are not needed since $\int_\Omega \nabla \cdot u \; dx = 0$. Note also that, if p is a solution to (2.48), then so is $p + c$ for some constant c, thus it makes sense to seek $p \in Q$.

Multiplying the momentum and continuity equations in (2.48) by the appropriate test functions, and integrating by parts we obtain the weak formulation: find $\boldsymbol{u} \in V, p \in Q$ such that

$$\begin{aligned} a(\boldsymbol{u}, \boldsymbol{v}) + b(\boldsymbol{v}, p) &= \mathcal{F}(\boldsymbol{v}), \quad \forall \boldsymbol{v} \in V \\ b(\boldsymbol{u}, q) &= 0, \qquad \forall q \in Q, \end{aligned} \tag{2.49}$$

where $a(\cdot,\cdot) : V \times V \to \mathbb{R}$, $b(\cdot,\cdot) : V \times Q \to \mathbb{R}$, and $\mathcal{F}(\cdot) : V \to \mathbb{R}$ are defined by

$$a(\boldsymbol{u}, \boldsymbol{v}) = \int_\Omega \nabla u : \nabla v \; dx, \tag{2.50}$$

$$b(\boldsymbol{v}, q) = -\int_\Omega q \nabla \cdot v \; dx, \tag{2.51}$$

$$\mathcal{F}(\boldsymbol{v}) = \int_\Omega \boldsymbol{v} \cdot \boldsymbol{f} \; dx. \tag{2.52}$$

Alternatively, we will write (2.49) as:

$$\begin{aligned} &\text{find } (\boldsymbol{u}, p) \in V \times Q \text{ such that} \\ &\mathcal{B}((\boldsymbol{u}, p), (\boldsymbol{v}, q)) = \mathcal{F}(\boldsymbol{v}) \quad \forall (\boldsymbol{v}, q) \in V \times Q, \end{aligned} \tag{2.53}$$

where $\mathcal{B}((\boldsymbol{u}, p), (\boldsymbol{v}, q)) = a(\boldsymbol{u}, \boldsymbol{v}) + b(\boldsymbol{v}, p) + b(\boldsymbol{u}, q)$.

For the lid-driven cavity problem some care must be taken to account for the inhomogeneous top boundary (lid) of the domain. Let $\Omega = (0,1) \times (0,1)$ and for the top boundary (or lid) of the domain define $\Gamma = \{\boldsymbol{x} = (x, y) : \; 0 \leq x \leq 1, \; y = 1\}$ and suppose $\boldsymbol{u} = (4x(1-x), 0)^T$ on Γ. We introduce a *lift function* $\boldsymbol{u}_D \in [H^1(\Omega)]^2$, with $\nabla \cdot \boldsymbol{u}_D = 0$, that satisfies the Dirichlet boundary condition on Γ so that there exists $V \ni \boldsymbol{w} = \boldsymbol{u} - \boldsymbol{u}_D$. The weak formulation for the lid-driven cavity is thus,

$$\begin{aligned} &\text{find } (\boldsymbol{w}, p) \in V \times Q \text{ such that} \\ &\mathcal{B}((\boldsymbol{w}, p), (\boldsymbol{v}, q)) = \tilde{\mathcal{F}}(\boldsymbol{v}, q) \quad \forall (\boldsymbol{v}, q) \in V \times Q, \end{aligned} \tag{2.54}$$

where

$$\tilde{\mathcal{F}}(\boldsymbol{v}, q) = \mathcal{F}(\boldsymbol{v}) - a(\boldsymbol{u}_D, \boldsymbol{v}). \tag{2.55}$$

2.3.2 Well-posedness and Galerkin approximation

We will focus on (2.53) for the moment and deal with the lift function after well-posedness is established for the case of homogeneous boundary conditions.

Continuity of $\mathcal{B}$ is rather straightforward by equipping the space $V \times Q$ with the norm $\|(\boldsymbol{v}, q)\|_{V\times Q} = \|\boldsymbol{v}\|_V + \|q\|_Q$, where $\|\boldsymbol{v}\|_V^2 = \|\boldsymbol{v}\|_{[H_0^1(\Omega)]^2}^2 = \|v_1\|_{H_0^1}^2 + \|v_2\|_{H_0^1}^2$, and applying Cauchy-Schwarz to (2.50) and (2.51). Furthermore, conditions b) and c) of Theorem 2.1.1 applied to (2.53) are equivalent to the following conditions for $a(\cdot,\cdot)$ and $b(\cdot,\cdot)$ [53, Theorem 2.34 and Prop. 2.36],

$$\begin{cases} \exists \gamma_a > 0, & \inf\limits_{\boldsymbol{u}\in \mathrm{Ker}(b)} \sup\limits_{\boldsymbol{v}\in \mathrm{Ker}(b)} \dfrac{a(\boldsymbol{u},\boldsymbol{v})}{\|\boldsymbol{u}\|_V \|\boldsymbol{v}\|_V} \geq \gamma_a \\ \forall \boldsymbol{v} \in \mathrm{Ker}(b), & (\forall \boldsymbol{u} \in \mathrm{Ker}(b), a(\boldsymbol{u},\boldsymbol{v}) = 0) \Rightarrow (\boldsymbol{v} = 0), \end{cases} \tag{2.56}$$

where $\mathrm{Ker}(b) = \{\boldsymbol{v} \in V : \ \forall q \in Q, \ b(\boldsymbol{v}, q) = 0\}$ and

$$\exists \gamma_b > 0, \qquad \inf_{q\in Q} \sup_{\boldsymbol{v}\in V} \frac{b(\boldsymbol{v},q)}{\|\boldsymbol{v}\|_V \|q\|_Q} \geq \gamma_b. \tag{2.57}$$

That $a(\cdot,\cdot)$ satisfies (2.56) is due to the fact that

$$a(\boldsymbol{u},\boldsymbol{u}) = \|\nabla u_1\|_{L^2(\Omega)}^2 + \|\nabla u_2\|_{L^2(\Omega)}^2 \tag{2.58}$$

and thus Poincaré's inequality can be applied for each component, proving a is coercive. Proving that equation (2.57) is satisfied for the Stokes problem relies on the divergence operator being surjective from V into Q, i.e. $\nabla\cdot : [H_0^1(\Omega)]^2 \to L_0^2(\Omega)$ is surjective [53, Lemma B.69] [20, Lemma 12.2.3]. Furthermore, if

$\nabla \cdot \hat{\boldsymbol{v}} = q$ then, there exists a positive constant C_{div} such that

$$\|\hat{\boldsymbol{v}}\|_{[H^1(\Omega)]^2} \leq C_{\text{div}} \|q\|_{L^2(\Omega)} . \tag{2.59}$$

This allows for the supremum to be bounded from below by choosing the particular function $\hat{\boldsymbol{v}} \in V$ such that $\nabla \cdot \hat{\boldsymbol{v}} = q$,

$$\begin{aligned} \inf_{q \in Q} \sup_{\boldsymbol{v} \in V} \frac{b(\boldsymbol{v}, q)}{\|\boldsymbol{v}\|_V \|q\|_Q} &\geq \inf_{q \in Q} \frac{b(\hat{\boldsymbol{v}}, q)}{\|\hat{\boldsymbol{v}}\|_V \|q\|_Q} \\ &= \inf_{q \in Q} \frac{\|q\|_Q^2}{\|\hat{\boldsymbol{v}}\|_V \|q\|_Q} \geq \frac{1}{C_{\text{div}}} > 0. \end{aligned} \tag{2.60}$$

These results are easily extended to the case of inhomogeneous boundary conditions through the lift function. Since the additional terms only appear on the right-hand side of (2.53), the analysis for $\mathcal{B}$ holds the same as in the homogeneous case. We simply must verify that $\tilde{\mathcal{F}}$ still represents a continuous form on $V \times Q$, i.e. $\tilde{\mathcal{F}} \in (V \times Q)^*$, which follows immediately since $\mathcal{F}(\boldsymbol{v}) = 0$ and $a(\boldsymbol{u}_d, \cdot)$ is clearly continuous on $V \times Q$.

Well-posedness of the infinite dimensional problem does not immediately imply that all choices of finite-dimensional approximation spaces result in a well posed discrete problem; more care must be taken for establishing a well-posed discrete formulation of (2.53). Let $V^h \subset V$ and $Q^h \subset Q$, the finite dimensional formulation is given by,

$$\begin{aligned} &\text{Find } (\boldsymbol{u}^h, p^h) \in V^h \times Q^h \text{ such that} \\ &\mathcal{B}\left((\boldsymbol{u}^h, p^h), (\boldsymbol{v}^h, q^h)\right) = \tilde{\mathcal{F}}\left((\boldsymbol{v}^h, q^h)\right) \quad \forall (\boldsymbol{v}^h, q^h) \in V^h \times Q^h. \end{aligned} \tag{2.61}$$

In order to guarantee existence of a unique solution to (2.61), certain compatibility conditions must be satisfied. Specifically (2.57) must hold on the

discrete spaces V^h and Q^h [53],

$$\exists \gamma_{b^h} > 0, \qquad \inf_{q^h \in Q^h} \sup_{\boldsymbol{v}^h \in V^h} \frac{b(\boldsymbol{v}^h, q^h)}{\|\boldsymbol{v}^h\|_{V^h} \|q^h\|_Q^h} \geq \gamma_{b^h}. \tag{2.62}$$

Equation (2.62) was first examined by Babuška [7] and Brezzi [21], and is thus often referred to as the Babuška-Brezzi condition. It is well known that Taylor-Hood elements, where the pressure is approximated with continuous linear funcitons $\mathbb{P}_1$ and the velocity approximated by continuous quadratic polynomials $\mathbb{P}_2$, satisfy the discrete inf-sup condition (2.62) in two dimensions. See for example [53, Lemma 4.24]. This statement can be generalized to include higher-order Taylor-Hood type elements ($\mathbb{P}_k/\mathbb{P}_{k-1}$) as well [22, 53]. Thus, elements of this type are well suited for the present application since we also require a higher-order enriched space in which to approximate the adjoint solution.

Let $\{\mathcal{T}_h\}$ be a collection of shape-regular affine meshes on Ω. For solution of the primal problem (2.61) we seek a continuous solution u^h, whose transformation to the reference element belongs to $[\mathbb{P}_2]^2$, and likewise for p^h with $\mathbb{P}_1$. That is,

$$V^h = \left\{ u^h \in [C^0(\Omega)]^2 : \ \forall K \in \mathcal{T}_h, \ u^h(T_K(\cdot)) \in [\mathbb{P}_2]^2 \right\}, \tag{2.63}$$

$$Q^h = \left\{ q^h \in C^0(\Omega) : \ \int_\Omega q^h = 0 : \ \forall K \in \mathcal{T}_h, \ q^h(T_K(\cdot)) \in \mathbb{P}_1 \right\}, \tag{2.64}$$

where $T_K : \hat{K} \to K$ represents the transformation operator from the reference element $\hat{K}$ to the physical element K.

2.3.3 Error estimate and error indicators

In the present section we provide a more concrete explanation of the components of the goal-oriented error estimation framework described in Section 2.2 in the case of the Stokes cavity problem. However, since each numerical example examined in the subsequent sections considers a different quantity of interest, the definition of $\mathcal{Q}$ remains abstract.

Assuming that $\mathcal{Q}$ is a bounded linear functional on $V \times Q$, the adjoint equation for Stokes reads,

$$\begin{aligned} &\text{Find } (\boldsymbol{z}_u, z_p) \in V \times Q \text{ such that} \\ &\mathcal{B}\left((\boldsymbol{v}, q), (\boldsymbol{z}_u, z_p)\right) = \mathcal{Q}\left((\boldsymbol{v}, q)\right), \quad \forall (\boldsymbol{v}, q) \in V \times Q. \end{aligned} \tag{2.65}$$

Equation (2.65) is well-posed since $\mathcal{B}$ has already been shown to satisfy the conditions of Theorem 2.1.1 and $\mathcal{Q} \in (V \times Q)^*$.

As previously suggested, we seek approximate solutions of (2.65) in an enriched space. For the present case we use higher-order elements (p-refinement) to construct an enriched approximation space for the adjoint solution. Let

$$V^+ = \left\{ u^+ \in [C^0(\Omega)]^2 : \ \forall K \in \mathcal{T}_h, \ u^+(T_K(\cdot)) \in [\mathbb{P}_3]^2 \right\}, \tag{2.66}$$

$$Q^+ = \left\{ q^+ \in C^0(\Omega) : \ \int_\Omega q^+ = 0 : \ \forall K \in \mathcal{T}_h, \ q^+(T_K(\cdot)) \in \mathbb{P}_2 \right\}, \tag{2.67}$$

where $\mathcal{T}_h$ and T_K are as defined earlier. The discrete adjoint equation is as follows,

$$\begin{aligned} &\text{Find } (\boldsymbol{z}_u^+, z_p^+) \in V^+ \times Q^+ \text{ such that} \\ &\mathcal{B}\left((\boldsymbol{v}^+, q^+), (\boldsymbol{z}_u^+, z_p^+)\right) = Q\left(\boldsymbol{v}^+, q^+\right)), \quad \forall (\boldsymbol{v}^+, q^+) \in V^+ \times Q^+. \end{aligned} \tag{2.68}$$

As an error indicator we use the form motivated by (2.46); for the lid-driven cavity,

$$\eta_K = \left| \int_\Omega \left(\Delta \boldsymbol{u}^h - \nabla p^h\right)\left(\boldsymbol{z}_u^+ - \pi^h \boldsymbol{z}_u^+\right) + \left(\nabla \cdot \boldsymbol{u}^h\right)\left(z_p^+ - \pi^h z_p^+\right) dx \right. \\ \left. - \sum_{e \in \partial K \cap \Gamma_{\text{int}}} \frac{1}{2} \int_e \boldsymbol{n} \cdot [\![\nabla u^h - pI]\!] (\boldsymbol{z}_u^+ - \pi^h \boldsymbol{z}_u^+) ds \right|, \tag{2.69}$$

where I represents the (2×2) identity matrix.

2.3.4 Numerical results

We explore here three different scenarios for adaptive refinement. First, we use the global error in the solution to guide adaptivity. A common feature of interest in the lid-driven cavity is the formation of small eddies in the lower corners. In order to accurately capture the small eddies, we also examine two local quantities of interest; the vorticity in the lower right region of the domain, and the pointwise value of the x-velocity at $\boldsymbol{x}_0 = (0.955, 0.015)^T$.

2.3.4.1 Global refinement

If the global accuracy of the solution is the main concern of the analysis, *a posteriori* error estimates and indicators can be used to perform adaptivity. Numerous techniques have been developed for computing error estimates that focus on the primal solution only; explicit estimators originating from the work of Babuška and Rheinboldt [11, 12], implicit estimators which require the solution of additional 'auxiliary' local problems [81, 79], and recovery methods of Zienkiewicz and Zhu [130, 131, 132], to name a few, see [1, 119] and the

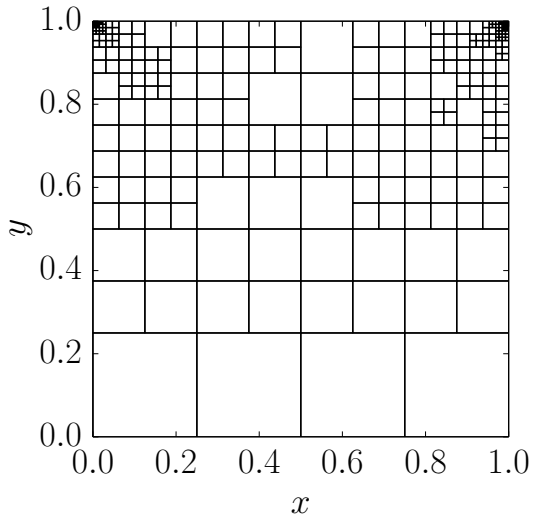

Figure 2.2: Globally adapted mesh for the Stokes lid-driven cavity.

references therein for more extensive examinations of the methods.

The final adapted mesh is shown in Figure 2.2. Notice that the global refinement focuses on refining the upper corners where the singularities in the pressure cause significant errors. The fact that $\nabla \cdot u^h \neq 0$ may also contribute to the refinement pattern in the interior of the domain. In Figure 2.3 we show the streamlines obtained after global adaptivity. It is clear that the globally adapted mesh does a poor job of capturing the flow in the lower corners of the domain; the global adaptivity focuses on the upper corners where the singularities in the pressure are the dominant source of the error. If the main feature of interest is the flow in the lower corner of the domain, we can use a local quantity of interest to adaptively refine the region.

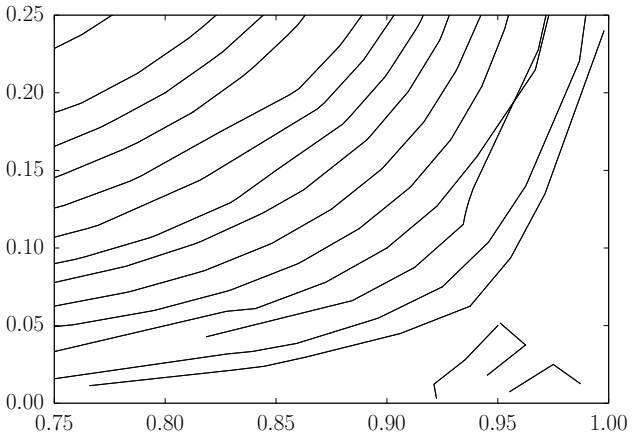

Figure 2.3: Streamlines in the lower corner of the globally adapted mesh for Stokes cavity problem.

2.3.4.2 Local vorticity

Using a local quantity of interest we can obtain a better representation of the flow in the corner. We take the quantity of interest to be the vorticity in the triangular region ω bounded by the two edges of the domain and the line connecting the points $\boldsymbol{x}_1 = (0.9, 0)$ and $\boldsymbol{x}_2 = (0, 0.9)$. As a linear functional we consider,

$$\mathcal{Q}\left((\boldsymbol{u}, p)\right) = \frac{1}{|\omega|} \int_{\omega} \nabla \times \boldsymbol{u} \; dx. \tag{2.70}$$

With the local vorticity as the quantity of interest we performed goal-oriented adaptive refinement using the error fraction marking strategy (2.47) with $\alpha = 0.7$. After 36 iterations we obtain the mesh and streamlines shown in Figures 2.4 and 2.5, respectively. Compared to the results for the globally

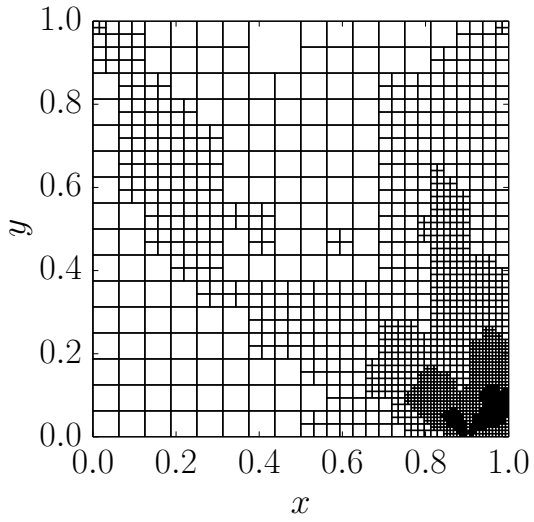

Figure 2.4: Adapted mesh for the local vorticity in the Stokes lid-driven cavity.

adapted mesh in Figure 2.3 the streamlines computed using the adapted mesh are more representative of the true flow in the region.

2.3.4.3 Pointwise x velocity

Following Prudhomme and Oden [109] we select the velocity in the x direction at a point $\boldsymbol{x}_0 = (0.955, 0.015)^T$ as the quantity of interest. We estimate this QoI by the weighted average

$$\mathcal{Q}\left((\boldsymbol{u}, p)\right) = \int_{\Omega} \kappa_{\varepsilon}(\boldsymbol{x} - \boldsymbol{x}_0)\ u_1(\boldsymbol{x})\ dx, \tag{2.71}$$

where κ_{ε} is the kernel defined in (2.24). We set $\varepsilon = 0.025$; Figure 2.6 shows the kernel for this choice of ε and x_0 parameters.

Using the error indicators discussed in Section 2.3.3 adaptive refinement

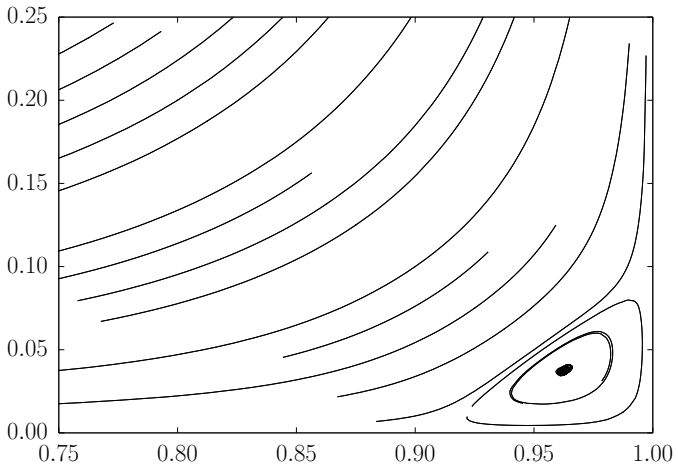

Figure 2.5: Streamlines for the Stokes lid-driven cavity using the adapted mesh.

was performed with the error fraction marking strategy with $\alpha = 0.7$. Since no exact solution is available, a reference solution was computed on the mesh in Figure 2.7. The quantity of interest evaluated for the reference solution is used as a replacement for the true quantity of interest in the results below, and we will denote its value by $\mathcal{Q}(u)$.

By targeting the lower-right region of the domain we obtain a much more accurate representation of the velocity field in that region. As a result we compute a more accurate estimation of the quantity of interest which we observe in the convergence results. Convergence of the relative error in the quantity of interest for uniform mesh refinement and adaptive mesh refinement is shown in Figure 2.8. Initially, we observe a significant advantage for the

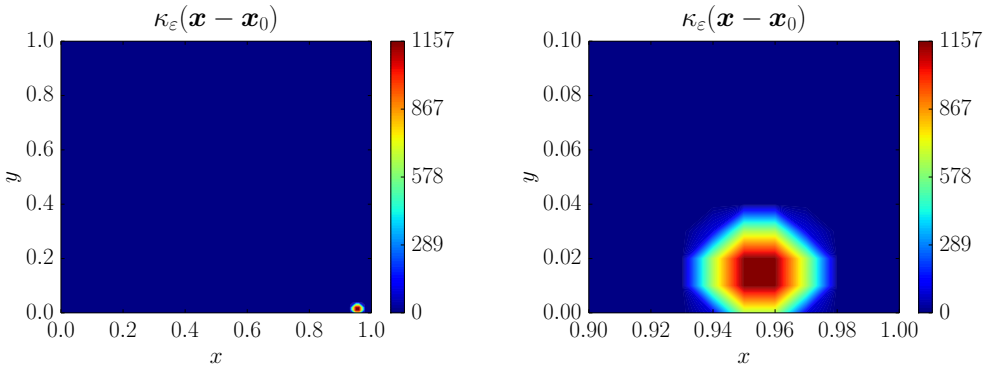

Figure 2.6: Integration kernel for local QoI defined in (2.71).

adaptive refinement; at this stage refinement is mostly occurring in the lower right-hand corner near the quantity of interest. After this initial stage both uniform and adaptive mesh refinement strategies converge at similar rate.

The effectivity of the estimator $\frac{\eta}{\left|\mathcal{Q}(u)-\mathcal{Q}(u^h)\right|}$, shown in Figure 2.9, degrades as the mesh is refined. This suggests that the estimator is no longer accurately capturing the error in the quantity of interest; in fact it is over estimating the error, hence $\frac{\eta}{\left|\mathcal{Q}(u)-\mathcal{Q}(u^h)\right|} > 1$. One contributing factor is the use of a reference solution. We expect that the estimate $\mathcal{Q}(u^h)$ will approach the reference value $\mathcal{Q}(u)$ sooner than than the true value of the quantity of interest. Thus, the ratio of the estimator to the reference error is larger than unity even though η may be a more accurate measure of the true error.

The final adapted mesh obtained after 36 refinement steps is shown in Figure 2.10. The region around the quantity of interest is clearly targeted for refinement, which was expected considering the adjoint solution in Figure 2.12. Additionally, some refinement in the upper corners is seen as a result of the

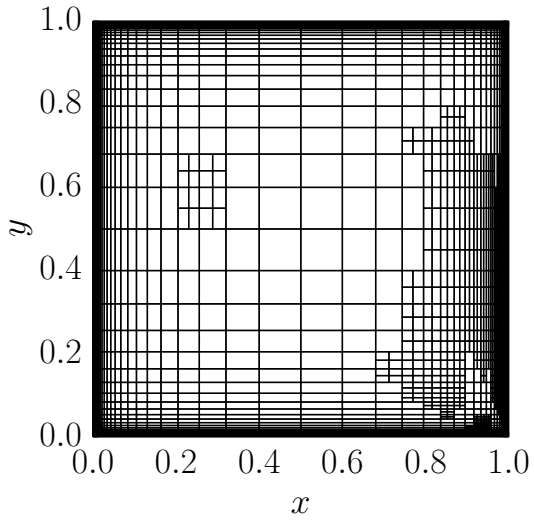

Figure 2.7: Reference mesh used to compute a substitute for the exact value of the quantity of interest ($N = 6697$).

singularities that exist in the pressure at these points; these singularities can be seen in Figure 2.11. Lastly, some refinement is observed in the interior of the domain, which can be attributed to the divergence constraint not being satisfied exactly.

As we mentioned in Remark 2.2.1 the introduction of the projection into the error representation formula, while unnecessary for the error estimate, is crucial for the decomposition of the error estimate into element contributions for refinement. Figure 2.13 shows the difference between the adjoint solution and its projection onto the coarse solution space, $z_{u_1}^+ - \pi^h z_{u_1}^+$. Comparing this figure to the adjoint solution z_u^+ in Figure 2.12 it is evident that the choice of weighting in the element residuals, and thus indicators, leads to different refine-

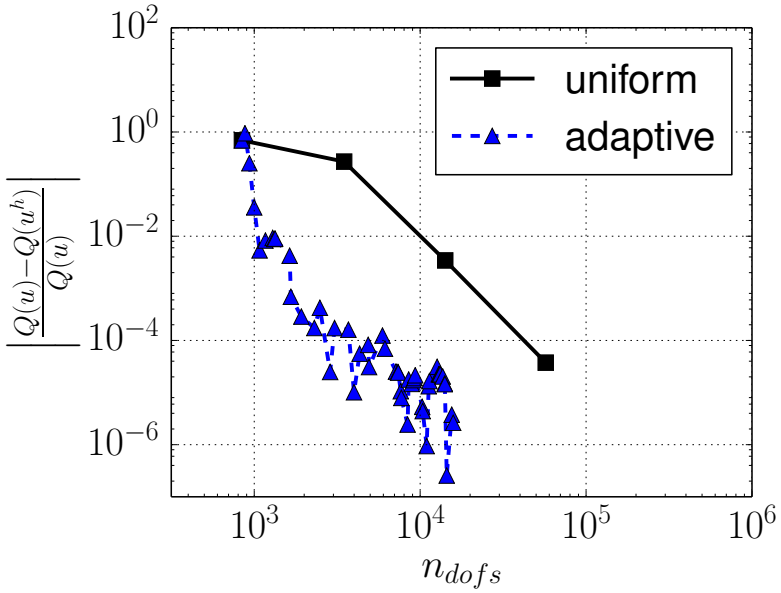

Figure 2.8: Convergence rates for uniform refinement and goal-oriented adaptive refinement.

ment patterns. Subtracting off the projection provides a more representative measure of what can be gained from improving the approximation *relative* to the current solution mesh. That is, the difference $z^+_{u_1} - \pi^h z^+_{u_1}$ only exhibits features of the adjoint solution that can not be discerned from approximations in V^h, whereas $z^+_{u_1}$ has features that may be adequately approximated on the current approximation space.

2.4 Concluding remarks

In this chapter, we have reviewed the established theory and fundamental framework for goal-oriented error estimation and adaptive mesh refinement. The methodology was applied to a benchmark linear problem, namely a Stokes

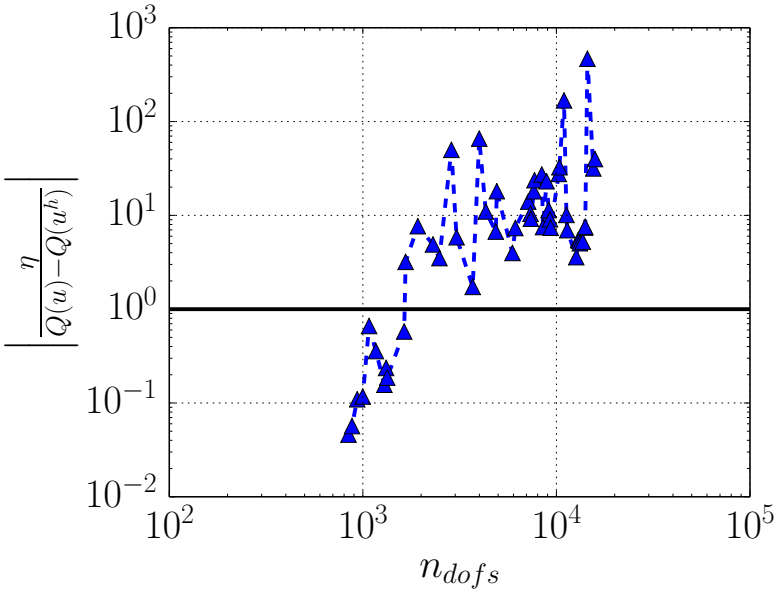

Figure 2.9: Effectivity of the estimator, $\left|\frac{\eta}{\mathcal{Q}(u)-\mathcal{Q}(u^h)}\right|$ for the Stokes cavity problem.

flow in a lid-driven cavity. The results are convincing for this straightforward application, however, the effectiveness of the goal-oriented error estimation technique for more complex situations is still not fully established. In particular, the application to nonlinear problems is still a topic of research. We examine this subject in the subsequent chapter.

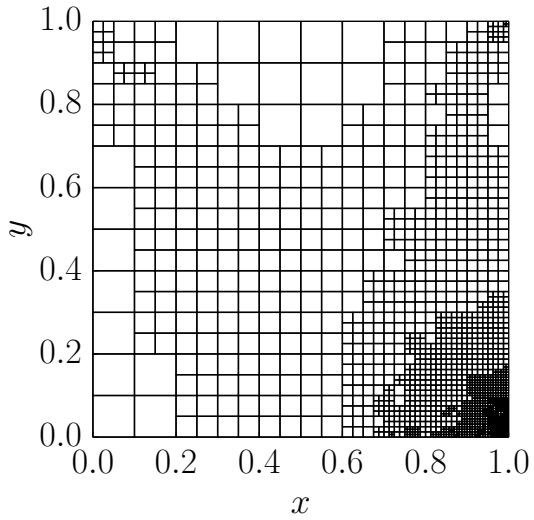

Figure 2.10: Adapted mesh for velocity u_1 in the lower-right region of the domain.

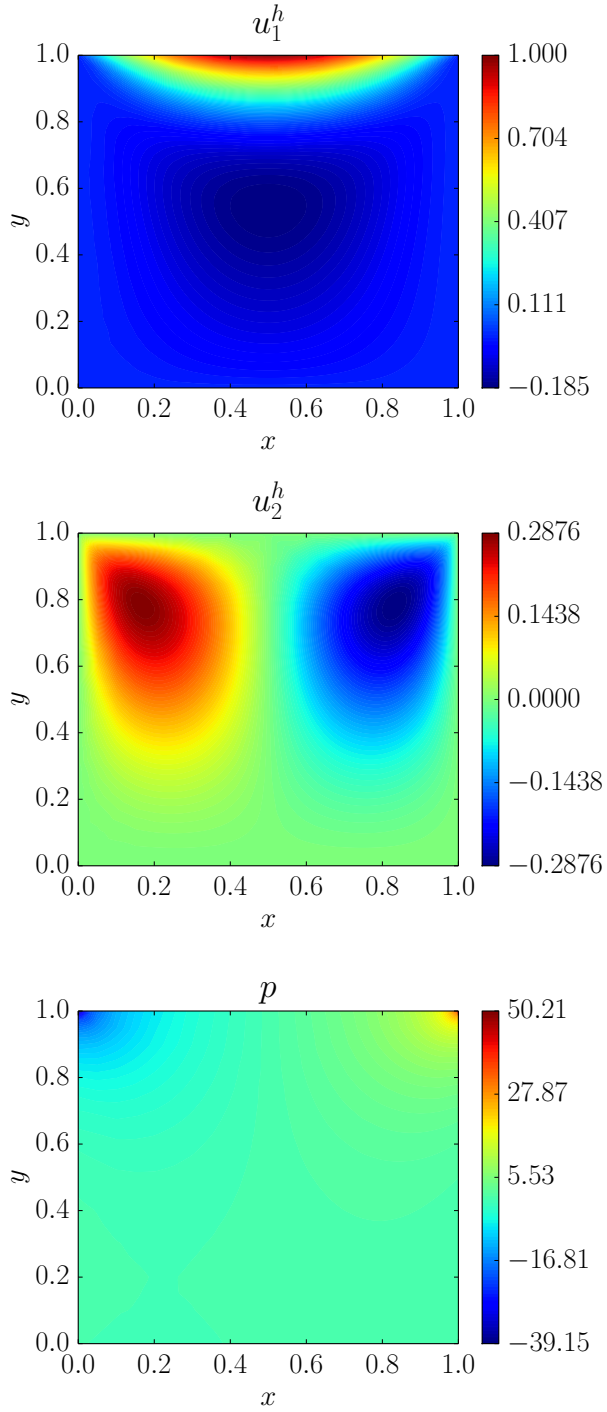

Figure 2.11: Primal solution fields for Stokes flow in lid-driven cavity.

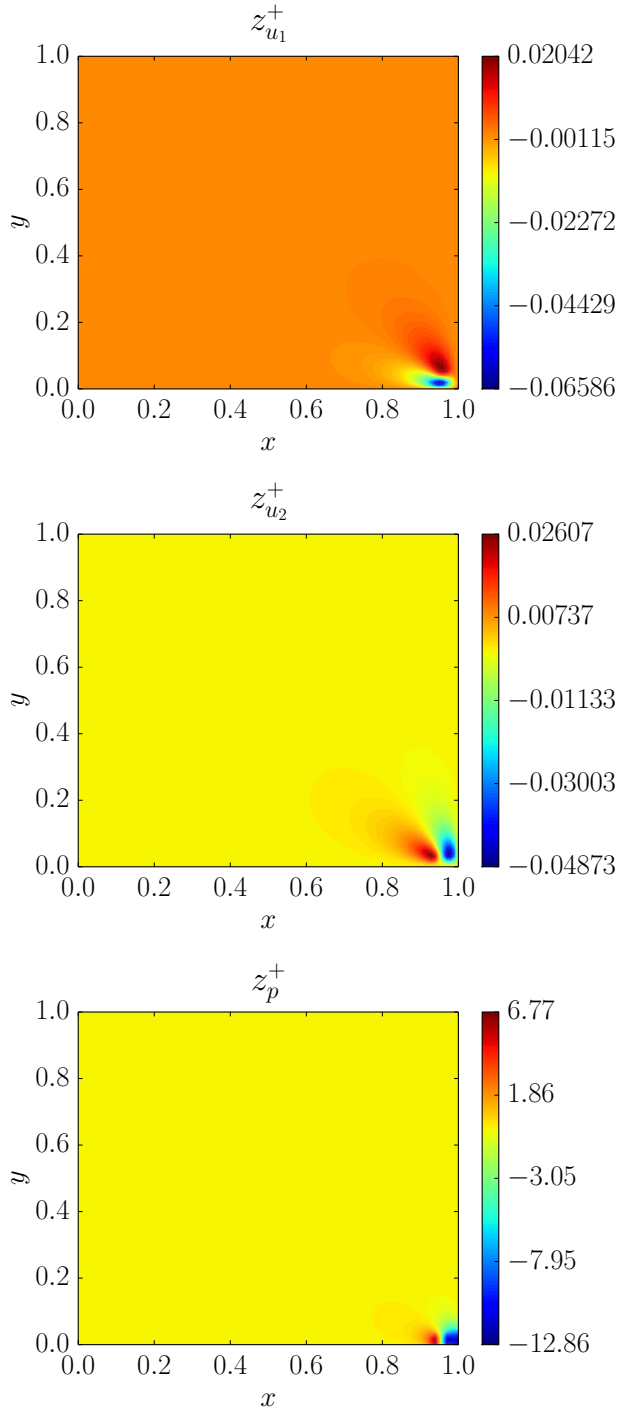

Figure 2.12: Adjoint solution fields for Stokes flow in lid-driven cavity.

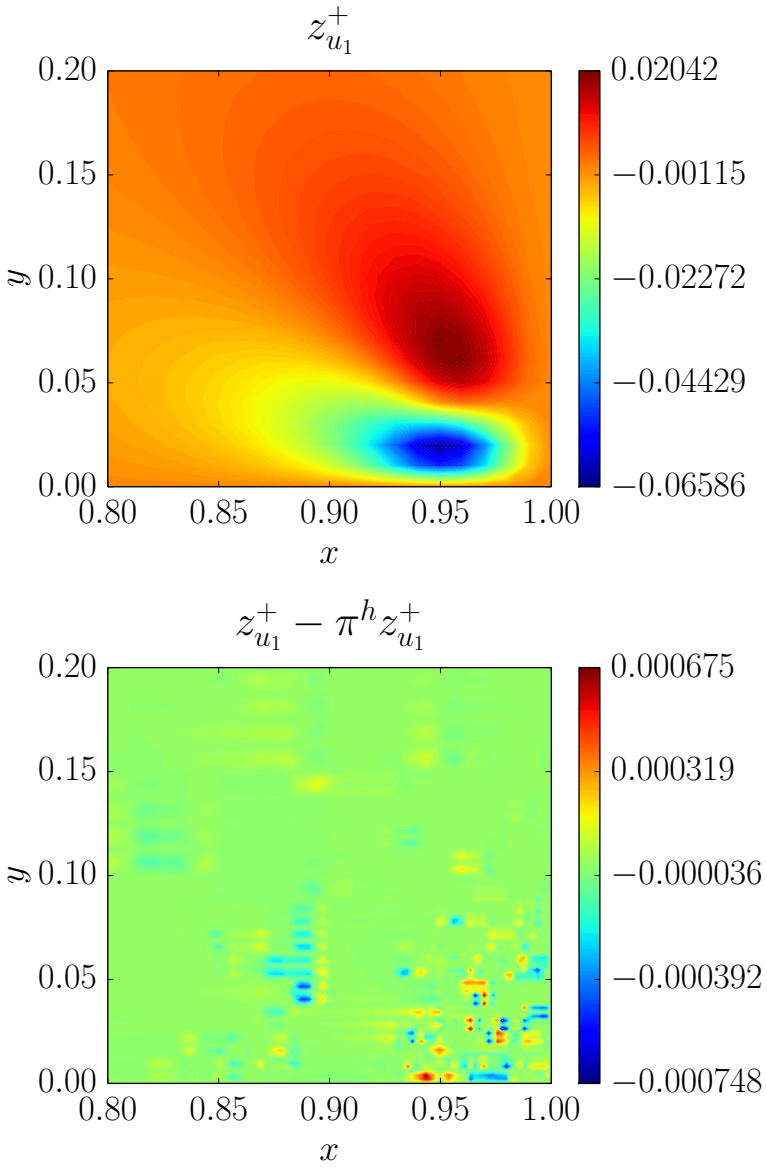

Figure 2.13: Comparison of adjoint solution $z^+_{u_1}$ (top) and $z^+_{z_1} - \pi^h z^+_{u_1}$ (bottom) in the lower right corner of the cavity.

Chapter 3

Goal-oriented error estimation: Nonlinear theory

In contrast to the linear case, general results on the existence and uniqueness of solutions to non-linear problems are limited and usually depend on the specifics of the given data: domain, boundary conditions, forcing, etc. We will focus on a particular form of nonlinear problems, described in Section 3.1, and make appropriate assumptions in order to prove results applicable to the class of problems we will consider.

Similarly to Chapter 2, we will begin by describing an abstract model problem in Section 3.1, first reviewing some necessary elements of differential calculus, and then discussing some results on the existence and uniqueness of solutions where available. In Section 3.2, we describe the extension of the goal-oriented error estimation framework to nonlinear problems, developing an exact error representation in the process. A practical representation of the exact error in the quantity of interest introduces a residual term, as in the linear case, and higher-order terms with respect to the error due to the linearization of the adjoint problem. The nonlinear terms are, in general, simply neglected without strong evidence for the terms to be negligible. We examine some of

the shortcomings of such an approach in Section 3.3. Finally, in Section 3.4 we propose error indicators based on estimating the contribution of the nonlinear terms, and demonstrate their use on a Navier-Stokes problem.

3.1 Abstract nonlinear model

3.1.1 Differential calculus in Banach spaces

We begin with a review of relevant concepts on differentiation in Banach spaces. Most of the content can be found in texts on nonlinear functional analysis, for example [129, 46, 4], and as a result are provided without proof or further discussion.

In more than one dimension, there are two basic notions for the concept of differentiability. The stronger of the two is Fréchet differentiability and stems from the idea of approximating a nonlinear map by an affine function.

Definition 3.1.1. (Fréchet differentiable map) Let $B : U \to Y$ be a nonlinear map where $U \subset X$ is open and X and Y are normed linear spaces. For an element $u \in U$, B is said to be *Fréchet differentiable* at u if there exists a bounded linear map, denoted $B^{'}(u) : U \to Y$ such that

$$\left\| B(u+w) - B(u) - B^{'}(u)(w) \right\|_Y = o(\|w\|_X), \quad \forall w \in U \tag{3.1}$$

meaning that as $w \to 0$ in X,

$$\frac{\left\| B(u+w) - B(u) - B^{'}(u)(w) \right\|_Y}{\|w\|_X} \to 0. \tag{3.2}$$

We call $B^{'}(u)$ the *Fréchet derivative* of B at u.

If B is Fréchet differentiable, then $B^{'}(u)$ is unique and B is continuous at u. A weaker notion of differentiability is given by Gâteaux differentiability.

Definition 3.1.2. (Gâteaux differentiable map) Let $B : U \to Y$. Then, the *Gâteaux derivative* of B at u in the direction w is given by,

$$B^{'}(u)(w) = \lim_{\theta \to 0} \frac{1}{\theta} \left[B(u + \theta w) - B(u) \right], \tag{3.3}$$

provided the limit exists. If the *Gâteaux derivative* exists for all $w \in U$ then B is said to be *Gâteaux differentiable* at u.

If B is Fréchet differentiable, then B is also Gâteaux differentiable; the converse however is not necessarily true.

With the notion of differentiability established, higher-order derivatives can be readily defined. We use the notation $B^{''}(u)(w_1, w_2)$ for second order derivatives and $B^{(n)}(u)(w_1, \ldots, w_n)$ for $n > 2$. Other concepts from finite-dimensional differentiation are readily established as well; of particular interest here is Taylor's theorem.

Theorem 3.1.1. *(Generalized Taylor's Theorem) Let $u \in U$ and assume that the derivatives $B^{(k)}(u)$ exist for $k = 1, \ldots, n$. Then, for w such that $u+w \in U$,*

$$\begin{aligned} B(u + w) = B(u) + B^{'}(u)(w) + \frac{1}{2} B^{''}(u)(w, w) \\ + \ \cdots \ + \frac{1}{n!} B^{(n)}(u)(w, \ldots, w) + r_n(u, w), \end{aligned} \tag{3.4}$$

where $r_n(u, w) = o(\|w\|_X^n)$ as $w \to 0$ in X. If $B^{(n+1)}$ is continuous, then

$$r_n(u, w) = \frac{1}{n!} \int_0^1 B^{(n+1)}(u + sw)(w, \ldots, w) \ (1 - s)^n \ ds, \tag{3.5}$$

and $r_n(u, w) = \mathcal{O}(\|w\|_X^{n+1})$.

3.1.2 A class of nonlinear problems

We are now equipped to discuss a particular class of nonlinear problems of interest: second-order nonlinear differential operators of the form

$$\begin{aligned} -\nabla \cdot a(x, u, \nabla u) &= b(x, u, \nabla u), \quad \text{in } \Omega, \\ u &= 0, \qquad\qquad\quad \text{on } \partial\Omega, \end{aligned} \tag{3.6}$$

where $b \in C(\Omega \times \mathbb{R} \times \mathbb{R}^d, \mathbb{R})$ and $a \in C^1(\Omega \times \mathbb{R} \times \mathbb{R}^d, \mathbb{R}^d)$ satisfies the condition that the matrix of partial derivatives,

$$A(x, y, z) = \frac{1}{2}\left(\frac{\partial a_i(x, y, z)}{\partial z_j} + \frac{\partial a_j(x, y, z)}{\partial z_i}\right), \quad 1 \leq i, j \leq d, \tag{3.7}$$

is positive definite for all $x \in \Omega$, $y \in \mathbb{R}$, $z \in \mathbb{R}^d$ [119, 1]. For appropriately chosen Banach spaces U and V, U reflexive, the weak formulation of (3.6) can be written as,

$$\begin{aligned} &\text{Find } u \in U \text{ such that} \\ &\mathcal{B}(u; v) = \mathcal{F}(v), \quad \forall v \in V, \end{aligned} \tag{3.8}$$

where the forms $\mathcal{B} : U \times V \to \mathbb{R}$ and $\mathcal{F} : V \to \mathbb{R}$ are linear in v and their specific definition depends on v. The spaces U and V are typically Sobolev spaces $W_0^{1,p}$ for appropriate choices of $1 < p < \infty$ that depend of the particular form of a and b. As we did for the linear case we also write (3.8) in operator form,

$$\begin{aligned} &\text{Find } u \in U \text{ such that} \\ &\langle B(u), v\rangle_{V^*,V} = \langle F, v\rangle_{V^*,V}, \quad \forall v \in V. \end{aligned} \tag{3.9}$$

where $\langle B(u), v\rangle_{V^*,V} = \mathcal{B}(u; v)$ for all $u \in U$ and $v \in V$. We will also use the residual operator $R : U \to V^*$ defined by,

$$\langle R(u), v\rangle_{V^*,V} = \mathcal{F}(v) - \mathcal{B}(u; v), \tag{3.10}$$

and the associated residual form $\mathcal{R}(u;v) = \langle R(u), v\rangle_{V^*,V}$

3.1.3 Regular solutions of nonlinear problems

In order to establish error estimates for approximations of (3.8) we introduce the concept of *regular* or *nonsingular* solutions.

Definition 3.1.3. If B is differentiable at u and, in addition, $B'(u) : U \to V^*$ is a bijection, then u is said to be a *regular* or *nonsingular* solution to (3.9).

Thus, we enforce more restrictive conditions on $B'(u)$, which will also allow us to establish a well-posed linearization of (3.8). We can relate these conditions on $B'(u)$ to the derivative of the form $\mathcal{B}$ by noting that

$$\langle B'(u)(w), v\rangle_{V^*,V} = \lim_{\theta\to 0} \frac{1}{\theta} \langle B(u+\theta w) - B(u), v\rangle_{V^*,V} \tag{3.11}$$

$$= \lim_{\theta\to 0} \frac{1}{\theta} \left[\mathcal{B}(u+\theta w; v) - \mathcal{B}(u; v)\right] := \mathcal{B}'(u; w, v). \tag{3.12}$$

Bijectivity of $B'(u)$ is equivalent to the linearized form $\mathcal{B}'(u;\cdot,\cdot) : U \times V \to \mathbb{R}$ satisfying the conditions of Theorem 2.1.1, meaning the linearized problem,

$$\begin{aligned} &\text{Find } w \in U \text{ such that} \\ &\mathcal{B}'(u; w, v) = \langle F, v\rangle_{V^*,V}, \quad \forall v \in V, \end{aligned} \tag{3.13}$$

is well-posed, with a unique solution w for any $F \in V^*$. Furthermore,

$$\|w\|_U \leq \frac{1}{\gamma_{\mathcal{B}'}(u)} \|F\|_{V^*}, \tag{3.14}$$

where $\gamma_{\mathcal{B}'}(u)$ is the inf-sup constant for $\mathcal{B}'(u;\cdot,\cdot)$ from condition (2.5) [118, 53].

Regular solutions exclude bifurcation points and limit points. Verfürth has extended in [119] these results to branches of solutions that include simple

limit and bifurcation points. The details are beyond the scope of the present work, but the extension essentially amounts to expanding the spaces U and V and modifying B [23, 119].

3.1.4 Galerkin approximation

Let $U^h \subset U$ and $V^h \subset V$ be finite-dimensional approximation spaces, then, the discrete version of (3.8) is given by,

$$\begin{aligned} &\text{Find } u^h \in U^h \text{ such that} \\ &\mathcal{B}(u^h; v^h) = \mathcal{F}(v^h), \quad \forall v^h \in V^h. \end{aligned} \tag{3.15}$$

Or, equivalently, in operator notation,

$$\begin{aligned} &\text{Find } u^h \in U^h \text{ such that} \\ &\left\langle B(u^h), v^h \right\rangle_{V^*,V} = \left\langle F, v^h \right\rangle_{V^*,V}, \quad \forall v^h \in V^h. \end{aligned} \tag{3.16}$$

Furthermore, we assume that $\mathcal{B}^{'}$ satisfies the discrete inf-sup condition,

$$\inf_{w^h \in U^h} \sup_{v^h \in V^h} \frac{\mathcal{B}'(u; w^h, v^h)}{\|w^h\|_{U^h} \|v^h\|_V} \geq \gamma_{\mathcal{B}'_h}(u) > 0, \tag{3.17}$$

where the inf-sup constant $\gamma_{\mathcal{B}'_h}(u)$ depends on the singular solution u, but is clearly independent of u^h and v^h.

Let $\mathcal{L}(U, V^*)$ represent the space of continuous linear maps from U into V^* and define the ball $B_\varepsilon(u) = \{w \in U : \|u - w\|_U \leq \varepsilon\}$. If $R^{'}(u)$ is Lipschitz continuous in a neighborhood of the singular solution u, i.e. there exists $\varepsilon > 0$ and $c_L > 0$ such that

$$\left\| R^{'}(u) - R^{'}(w) \right\|_{\mathcal{L}(U,V^*)} \leq c_L \|u - w\|_U, \quad \forall w \in B_\varepsilon(u) \tag{3.18}$$

then, provided that the approximate solution u^h is *close enough* to the singular solution, one can prove general error estimates for the discrete solution u^h [118, 119, 1]. Ainsworth and Oden [1] and Verfürth [119] both present similar bounds on the energy norm of the error in terms of the norm of the residual. Under similar assumptions, Van der Zee [118] proves an error estimate near nonsingular solutions similar to Céa's lemma, but with additional higher-order terms. We extend the results of Van der Zee and incorporate the results of Ainsworth and Oden [1] and Verfürth [119] to prove the following theorem and its corollary.

Theorem 3.1.2. *(Extension of Céa's Lemma to Nonlinear Problems) Assume that u is a nonsingular solution to* (3.8)*, that B is differentiable at u, and that $B^{'}(u) \in \mathcal{L}(U, V^*)$, which also implies $B^{'}(u)$ is a bijection. Furthermore, assume $R'(u)$ is Lipschitz continuous with constant c_L and the linearized problem* (3.13) *is well-posed with discrete inf-sup constant $\gamma_{\mathcal{B}_h'}(u)$. Then, the discrete solution u^h to* (3.15) *satisfies the bound,*

$$\left\|u - u^h\right\|_U \leq \left(1 + \frac{c_{\mathcal{B}'}(u)}{\gamma_{\mathcal{B}_h'}(u)}\right) \inf_{\varphi \in U^h} \|u - \varphi\|_U + \frac{c_L}{2\gamma_{\mathcal{B}_h'}(u)} \left\|u - u^h\right\|_U^2, \quad (3.19)$$

where $c_{\mathcal{B}'}(u)$ is the continuity constant for $\mathcal{B}'(u; \cdot, \cdot)$.

Proof. For any $\varphi \in U^h$, applying the triangle inequality, we have

$$\left\|u - u^h\right\|_U \leq \|u - \varphi\|_U + \left\|u^h - \varphi\right\|_U, \quad (3.20)$$

which we can bound using the discrete inf-sup condition

$$\leq \|u-\varphi\|_U + \frac{1}{\gamma_{\mathcal{B}_h'}(u)} \sup_{v^h \in V^h} \frac{\mathcal{B}'(u; u^h - \varphi, v^h)}{\|v^h\|_V} \tag{3.21}$$

and using the linearity of $\mathcal{B}'$

$$= \|u-\varphi\|_U + \frac{1}{\gamma_{\mathcal{B}_h'}(u)} \sup_{v^h \in V^h} \frac{\mathcal{B}'(u; u-\varphi, v^h) - \mathcal{B}'(u; u-u^h, v^h)}{\|v^h\|_V}. \tag{3.22}$$

The linearized form $\mathcal{B}'(u;\cdot,\cdot)$ is continuous, with continuity constant $c_{\mathcal{B}'}(u)$, thus

$$\left|\mathcal{B}'(u; u-\varphi, v^h)\right| \leq c_{\mathcal{B}'}(u) \|u-\varphi\|_U \left\|v^h\right\|_V. \tag{3.23}$$

Substitution into the previous result yields,

$$\begin{aligned} \left\|u-u^h\right\|_U \leq & \left(1 + \frac{c_{\mathcal{B}'}(u)}{\gamma_{\mathcal{B}_h'}(u)}\right) \|u-\varphi\|_U \\ & - \frac{1}{\gamma_{\mathcal{B}_h'}(u)} \sup_{v^h \in V^h} \frac{\mathcal{B}'(u; u-u^h, v^h)}{\|v^h\|_V}. \end{aligned} \tag{3.24}$$

Turning out attention to the second term of (3.24) we make use of the residual operator. Since u and u^h are solutions to (3.9) and (3.16), respectively,

$$\left\langle R(u^h), v^h \right\rangle = 0 = \left\langle R(u), v^h \right\rangle \quad \forall v^h \in V^h, \tag{3.25}$$

so that Taylor's Theorem (Theorem 3.1.1) implies,

$$\begin{aligned} \int_0^1 & \left\langle R'(u - s(u-u^h))(u-u^h), v^h \right\rangle_{V^*,V} \, ds \\ & = \left\langle R(u), v^h \right\rangle_{V^*,V} - \left\langle R(u^h), v^h \right\rangle_{V^*,V} = 0. \end{aligned} \tag{3.26}$$

Note that the definition of R suggests,

$$\left\langle R^{'}(u)(w), v \right\rangle_{V^*,V} = \lim_{\theta \to 0} \frac{1}{\theta} \left\langle R(u+\theta w) - R(u), v \right\rangle_{V^*,V} \tag{3.27}$$

$$= \lim_{\theta \to 0} \frac{1}{\theta} \left[-\mathcal{B}(u+\theta w; v) + \mathcal{B}(u; v) \right] \tag{3.28}$$

$$= -\mathcal{B}'(u; w, v). \tag{3.29}$$

Then, letting $e = u - u^h$,

$$-\mathcal{B}'(u; e, v^h) = \left\langle R^{'}(u)(e), v^h \right\rangle_{V^*,V} \tag{3.30}$$

$$= \left\langle R^{'}(u)(e), v^h \right\rangle_{V^*,V} - \int_0^1 \left\langle R^{'}(u - se)(e), v^h \right\rangle_{V^*,V} \, ds, \tag{3.31}$$

$$= \int_0^1 \left\langle R^{'}(u)(e), v^h \right\rangle_{V^*,V} - \left\langle R^{'}(u - se)(e), v^h \right\rangle_{V^*,V} \, ds, \tag{3.32}$$

and

$$-\mathcal{B}'(u; e, v^h) \leq \left| \int_0^1 \left\langle R^{'}(u)(e), v^h \right\rangle_{V^*,V} - \left\langle R^{'}(u - se)(e), v^h \right\rangle_{V^*,V} \, ds \right|, \tag{3.33}$$

$$\leq \int_0^1 \left\| R^{'}(u)(e) - R^{'}(u - se)(e) \right\|_{V^*} \left\| v^h \right\|_V \, ds, \tag{3.34}$$

$$\leq \left(\int_0^1 \left\| R^{'}(u) - R^{'}(u - se) \right\|_{\mathcal{L}(U,V^*)} \|e\|_U \, ds \right) \left\| v^h \right\|_V. \tag{3.35}$$

Lipschitz continuity of $R^{'}$ leads to,

$$-\mathcal{B}'(u; e, v^h) \leq \left(\int_0^1 c_L s \|e\|_U \, ds \right) \|e\|_U \left\| v^h \right\|_V = \frac{1}{2} c_L \|e\|_U^2 \left\| v^h \right\|_V. \tag{3.36}$$

Finally, returning to (3.24), we find

$$\left\| u - u^h \right\|_U \leq \left(1 + \frac{c_{\mathcal{B}'}(u)}{\gamma_{\mathcal{B}'_h}(u)} \right) \|u - \varphi\|_U + \frac{c_L}{2\gamma_{\mathcal{B}'_h}(u)} \|e\|_U^2, \tag{3.37}$$

and taking the infimum over all $\varphi \in V^h$ completes the proof. □

A stronger result easily follows given more restrictive conditions on u^h.

Corollary 3.1.3. *In addition to the assumptions of Theorem 3.1.2, if u^h satisfies,*

$$\left\|u - u^h\right\|_U \leq \frac{\gamma_{\mathcal{B}'_h}(u)}{c_L}, \tag{3.38}$$

the convergence of Galerkin approximations is bounded by the inequality

$$\left\|u - u^h\right\|_U \leq 2\left(1 + \frac{c_{\mathcal{B}'}(u)}{\gamma_{\mathcal{B}'_h}(u)}\right) \inf_{\varphi \in V^h} \|u - \varphi\|_U \tag{3.39}$$

Similar to the linear case, we can use the result of Céa's Lemma (specifically Corollary 3.1.3) and Theorem 2.1.3 to establish *a priori* convergence estimates for Galerkin approximations on a family of meshes.

Theorem 3.1.4. *Under the more restrictive assumptions of Corollary 3.1.3, and provided $u \in H^{s+1}(\Omega)$,*

$$\left\|u - u^h\right\|_{H^1} \leq \bar{C} h^s \left|u\right|_{H^{s+1}}, \tag{3.40}$$

where $\bar{C} = 2\left(1 + \frac{c_{\mathcal{B}'}(u)}{\gamma_{\mathcal{B}'_h}(u)}\right) c_{\mathcal{I}}$.

With the nonlinear version of Céa's Lemma 3.1.2, convergence in weaker norms can also be established in a similar manner to using the Aubin-Nitsche Lemma. To do so, we require an extension of the linear Aubin-Nitsche lemma that relates to the linearized operator; a similar result has been shown by Wheeler [124].

Theorem 3.1.5. *(Extension of Aubin-Nitsche Lemma to Nonlinear Problems) Let $u \in U$ and assume that the linearized operator $\mathcal{B}'(u;\cdot,\cdot)$ satisfies (AN1) and*

(AN2). Then, the Galerkin approximation u^h, which solves (3.15)*, satisfies the following inequality,*

$$\left|u - u^h\right|_L \leq c_A h \left\|u - u^h\right\|_V, \tag{3.41}$$

where $c_A = c_{\mathcal{B}'}(u) c_i c_S$ and L is as defined in (AN1).

Proof. Recall that L is a Hilbert space equipped with a continuous, symmetric, and positive definite bilinear form $l(\cdot,\cdot)$ and corresponding seminorm $|\cdot|_L = \sqrt{l(\cdot,\cdot)}$. The adjoint problem for (AN1) is now given by,

$$\begin{aligned} &\text{Find } \zeta(g) \in V \text{ such that} \\ &\mathcal{B}'(u; v, \zeta(g)) = l(g, v), \quad \forall v \in V, \end{aligned} \tag{3.42}$$

for any $g \in L$. By the definition

$$|e|_L = \sup_{g \in L} \frac{|l(g,e)|}{|g|_L} = \sup_{g \in L} \frac{\left|\mathcal{B}'(u; e, \zeta(g))\right|}{|g|_L}. \tag{3.43}$$

Galerkin orthogonality implies

$$\mathcal{B}'(u; e, \zeta(g)) = \mathcal{B}'(u; e, \zeta(g) - v^h), \quad \forall v^h \in V^h. \tag{3.44}$$

First using the continuity of $\mathcal{B}'$, and then taking the infimum on V^h we find,

$$\mathcal{B}'(u; e, \zeta(g)) \leq c_{\mathcal{B}'}(u) \|e\|_V \inf_{v^h \in V^h} \left\|\zeta(g) - v^h\right\|_V. \tag{3.45}$$

Making use of (AN2) followed by (AN1) we arrive at,

$$\mathcal{B}'(u; e, \zeta(g)) \leq c_{\mathcal{B}'}(u) c_i h \|e\|_V \|\zeta(g)\|_Z, \tag{3.46}$$

$$\leq c_{\mathcal{B}'}(u) c_i c_S h \|e\|_V |g|_L. \tag{3.47}$$

Substitution of this result into (3.43) completes the proof. □

Provided the linearized operator $\mathcal{B}'(u;\cdot,\cdot)$ satisfies the conditions of the Aubin-Nitsche Lemma (Lemma 3.1.5), we can establish a convergence result for the L^2-norm of the error in the discrete approximation.

Theorem 3.1.6. *Let $\mathcal{B}'$ satisfy the conditions of Theorem 3.1.5 and Theorem 3.1.4. The L^2 error in the discrete approximation u^h is bounded by:*

$$\left\|u - u^h\right\|_{L^2} \leq c_A \bar{C} h^{s+1} \left|u\right|_{H^{s+1}}. \tag{3.48}$$

We have demonstrated that, *a priori* error estimates can be proven with some fairly restrictive conditions on the nonlinear operator B and its Fréchet derivative B'. In addition, convergence rates in terms of mesh size h with respect to weaker norms can be established using a straightforward extension of the Aubin-Nitsche Lemma. These results will play an integral role in establishing *a posteriori* error estimates in the following section.

3.2 Nonlinear *a posteriori* error estimation

We now focus on the extension of the results of Section 2.2 to the nonlinear problem (3.8). In addition to the operator to being nonlinear, the quantity of interest functional can also be a nonlinear functional on V. For example, we will consider a functional that is representative of the kinetic energy in a flow,

$$\mathcal{Q}(u) = \int_\Omega u^2 dx. \tag{3.49}$$

Of course, the results in this section are general enough to apply to the case that either the differential operator or the quantity of interest functional only

is nonlinear.

3.2.1 Linearized adjoint equations and nonlinear QoI

In the case of nonlinear problems, the notion of the adjoint problem can be extended by considering a linearization of the operator associated with the primal problem. However, one question that immediately arises concerns the linearization point at which one should define the derivative.

One approach for constructing a linearized operator is to use the secant form, or a mean-value linearization. Assuming $\mathcal{B}$ is differentiable in a subset of V containing u *and* u^h, mean-value linearization yields,

$$\mathcal{B}^s(u, u^h; w, v) = \int_0^1 \mathcal{B}'(u^h + s(u - u^h); w, v)ds, \tag{3.50}$$

where $\mathcal{B}'(u; w, v)$ is given by (3.12). With this choice of linearization one can define an "exact adjoint problem" [16, 118],

$$\begin{aligned} &\text{find } z \in V \text{ such that} \\ &\mathcal{B}^s(u, u^h; w, z) = \mathcal{Q}^s(u, u^h; w), \quad \forall w \in V. \end{aligned} \tag{3.51}$$

As a result, one can derive an exact error representation for the error in the quantity of interest, similar to that in the linear case. However, this approach is impractical since the definition of the secant form depends on the unknown exact solution u.

Instead, we will proceed by linearizing around u^h and developing an exact representation, where the dependence on u only appears in the higher-order terms. Let $e = u - u^h$ and assume $\mathcal{B}$ is twice differentiable. We employ

Taylor's Theorem to linearize the residual about the approximate solution,

$$\mathcal{B}(u;v) - \mathcal{B}(u^h;v) = \mathcal{B}'(u^h;e,v) + \Delta_{\mathcal{B}}(u^h,e,v), \quad \forall v \in V, \tag{3.52}$$

where the higher-order remainder, $\Delta_{\mathcal{B}}$, can be written using (3.5) as

$$\Delta_{\mathcal{B}}(u^h,e,v) = \int_0^1 \mathcal{B}''(u^h + se;e,e,v)(1-s)\, ds. \tag{3.53}$$

Similarly, we can linearize the quantity of interest functional,

$$\mathcal{Q}(u) - \mathcal{Q}(u^h) = \mathcal{Q}'(u^h;e) + \Delta_{\mathcal{Q}}(u^h,e), \tag{3.54}$$

where, assuming $\mathcal{Q}$ is also twice differentiable,

$$\Delta_{\mathcal{Q}}(u^h,e) = \int_0^1 \mathcal{Q}''(u^h + se;e,e)(1-s)\, ds. \tag{3.55}$$

If $\mathcal{Q}$ is, in fact, a linear quantity of interest, then $\mathcal{Q}'(u^h;e) = \mathcal{Q}(e)$ and $\Delta_{\mathcal{Q}}(u^h,e) = 0$. The adjoint problem can then be defined as,

$$\begin{aligned} &\text{find } z \in V \text{ such that} \\ &\mathcal{B}'(u^h;v,z) = \mathcal{Q}'(u^h;v), \quad \forall v \in V. \end{aligned} \tag{3.56}$$

In an analogous way to the linear case, the primal problem being well-posed implies the well-posedness of the adjoint problem. However, in the nonlinear case it is the well-posedness of the linearized primal problem that is important. That is, provided (3.13) is well-posed for any $F \in V^*$, we must have that (3.56) is well-posed if $\mathcal{Q}'(u^h;\cdot) \in V^*$.

Remark 3.2.1. Notice that the operator $\mathcal{B}'$ is the same linearized operator one might use to compute updates in Newton's method for solving the nonlinear primal problem (3.8).

3.2.2 Error representation

With the definition of the linearized adjoint equation, we are now ready to establish an error representation formula for the error in a, possibly nonlinear, quantity of interest for a nonlinear differential equation of the form (3.6).

The procedure follows the same process as in the linear case. We are interested in the error in the quantity of interest for the discrete solution $u^h \in V^h$,

$$\mathcal{E} = \mathcal{Q}(u) - \mathcal{Q}(u^h), \tag{3.57}$$

where $\mathcal{Q}$ may be a nonlinear functional on V. Using the linearizations (3.54) and (3.52), and the definition of the linearized adjoint equation (3.56),

$$\begin{aligned}
\mathcal{E} = \mathcal{Q}(u) - \mathcal{Q}(u^h) &= \mathcal{Q}'(u^h; e) + \Delta_{\mathcal{Q}}(u^h, e), && (3.58)\\
&= \mathcal{B}'(u^h; e, z) + \Delta_{\mathcal{Q}}(u^h, e), && (3.59)\\
&= \mathcal{R}(u^h; z) - \Delta_{\mathcal{B}}(u^h, e, z) + \Delta_{\mathcal{Q}}(u^h, e), && (3.60)\\
&= \mathcal{R}(u^h; z - \varphi) - \Delta_{\mathcal{B}}(u^h, e, z) + \Delta_{\mathcal{Q}}(u^h, e), && (3.61)
\end{aligned}$$

for all $\varphi \in V$. Due to the complexity of estimating $\Delta_{\mathcal{B}}$ and $\Delta_{\mathcal{Q}}$, and the fact that they are deemed to be higher-order, the term is often neglected [16, 14, 57]. In many situations the remainder terms are in fact higher order. However, all that can be proven about them in general is that $\Delta_{\mathcal{B},\mathcal{Q}} = \mathcal{O}(\|e\|_U^2)$. When the approximation u^h is far from the exact solution u, $\|e\|_U$ may remain large for the remainders to be non negligible, and in fact the rate of convergence may be slow enough to make them rather important. The problem could, for example,

appear in an adaptive procedure with respect to a quantity of interest in which the resulting adapted meshes would fail to the global errors $\mathcal{O}(\|e\|_U^2)$. Incorporating the higher-order nonlinear terms into an error estimation procedure is the focus of the next section. For the remainder of this section, we proceed assuming the nonlinear contributions are negligible and demonstrate that this assumption is valid for some problems and provides reasonable results.

3.2.3 Classical error estimation

While we do not advise using this approach for all problems, we demonstrate in what follows that the approach may be effective in some situations. Suitable nonlinear problems allow for (3.61) to be used by simply neglecting the higher order terms.

To that end we must deal with the fact that, although neglecting the remainders in (3.61) provides a tractable estimate, it still requires the exact adjoint solution z. As we did for the linear adjoint, we seek an approximate adjoint solution in an enriched space V^+,

$$\begin{aligned} &\text{find } z^+ \in V^+ \text{ such that} \\ &\mathcal{B}'(u^h; v^+, z^+) = \mathcal{Q}'(u^h; v^+), \quad \forall v^+ \in V^+. \end{aligned} \tag{3.62}$$

Replacing z with the approximate adjoint z^+ in (3.61), and dropping the remainder terms, we obtain a computable error estimate

$$\mathcal{Q}(u) - \mathcal{Q}(u^h) \approx \eta^{\mathcal{R}}(u^h, z^+) := \mathcal{R}(u^h; z^+ - \pi^h z^+). \tag{3.63}$$

As error indicators, we propose to use the same procedure as for the linear case and break the global residual into element-wise contributions $\eta(u^h, z^+) =$

$\sum_{K\in\mathcal{T}_h}\eta_K$. Following that, adaptive mesh refinement can again proceed by marking elements based on a chosen strategy; element fraction or error fraction in our case.

Example: Nonlinear Burgers' equation. As prototype non-linear example, we choose the 1D Burgers' equation. Its relative simplicity makes it acceptable for the application of the simplified error estimation approach discussed above. In addition, it has been used as a test case on several occasions; in particular it is examined in the literature on *a posteriori* error estimation for differential equations with uncertainty [84, 89], which we will discuss in Chapter 4.

In the notation of (3.6) we can write the standard Burgers' equation by setting $a(x,u,\nabla u)=\mu\nabla u$ and $b(x,u,\nabla u)=-u\cdot\nabla u$, where μ represents the fluid viscosity. In one spatial dimension, this equates to

$$-\mu u_{xx}+uu_x=0,\quad x\in\Omega=(-1,1). \tag{3.64}$$

Typical boundary conditions are nonhomogeneous Dirichlet boundary conditions of the form,

$$u(-1)=u_-\qquad u(1)=u_+, \tag{3.65}$$

We wish to evaluate the performance of the estimator compared to the exact error; for that reason, we prefer to use the boundary conditions $u_-=\tanh(1/2\mu)$ and $u_+=-\tanh(1/2\mu)$, for which the exact solution reads,

$$u(x)=-\tanh(x/2\mu), \tag{3.66}$$

that will be used to compute errors in the numerical results below.

We will again make use of a lift function u^D to take care of boundary conditions and arrive at a weak formulation in the setting of homogeneous Dirichlet boundary conditions. Let $u^D \in H^1(\Omega)$ satisfy the boundary conditions (3.65), for example $u^D(x) = -\tanh(1/2\mu)x$, and let $U = V = H_0^1(\Omega)$, then $u - u^D = w \in V$. The weak formulation of (3.65) can be written as,

$$\begin{aligned} &\text{find } w \in V \text{ such that,} \\ &\mathcal{B}(w; v) = \mathcal{F}(v) \quad \forall v \in V, \end{aligned} \tag{3.67}$$

where

$$\mathcal{B}(w; v) = \int_\Omega \mu w_x v_x + w w_x v - w u^D v_x \, dx, \tag{3.68}$$

$$\mathcal{F}(v) = -\left(\int_\Omega \mu u^D_x v_x + u^D u^D_x v \, dx \right). \tag{3.69}$$

We also define the residual form $\mathcal{R}(w; v) = \mathcal{F}(v) - \mathcal{B}(w; v)$.

In practice, of course, we cannot solve (3.67) exactly, and instead seek the approximate solution in the finite element space V^h;

$$\begin{aligned} &\text{find } w^h \in V^h \text{ such that,} \\ &\mathcal{B}(w^h; v^h) = \mathcal{F}(v^h) \quad \forall v^h \in V^h. \end{aligned} \tag{3.70}$$

As mentioned previously, we will use Newton's method to solve for the solution to the nonlinear problem. Linearizing about the present iterative solution w^h_n, we solve the following error equation for the update to obtain the next iteration $w^h_{n+1} = w^h_n + dw$,

$$\mathcal{B}'(w^h_n; dw, v^h) = \mathcal{R}(w^h_n; v^h) \quad \forall v^h \in V^h, \tag{3.71}$$

where

$$\mathcal{B}'(u;\hat{u},v) = \int_\Omega \mu\hat{u}_x v_x + \hat{u}u_x v + u\hat{u}_x v - \hat{u}u^D v_x dx. \tag{3.72}$$

For our quantity of interest, we consider the kinetic energy,

$$\mathcal{Q}(u) = \frac{1}{2}\int_\Omega u^2 dx. \tag{3.73}$$

As discussed above, since (3.73) is a nonlinear functional of the solution, we must linearize the functional in order to define the adjoint problem,

$$\mathcal{Q}'(u;\hat{u}) = \int_\Omega u\hat{u}dx \quad \forall \hat{u} \in V. \tag{3.74}$$

With the linearized form of the operator (3.72) and functional (3.74), we define the discrete adjoint problem,

$$\begin{aligned} &\text{find } z^+ \in V^+ \text{ such that,} \\ &\mathcal{B}'(w^h; v^+, z^+) = \mathcal{Q}'(w^h; v^+) \quad \forall v^+ \in V^+. \end{aligned} \tag{3.75}$$

One can then obtain a computable error estimator for the 1D Burgers' equation using (3.63). In Figure 3.1 we show the convergence of the error in the quantity of interest for uniform h refinement. The *a posteriori* error estimator obtained by neglecting the nonlinear terms, as traditionally done in the literature, does provide a reasonable estimate of the exact error, both in magnitude and in terms of the rate of reduction.

To further investigate the nonlinear terms we make use of the following relationships,

$$\mathcal{B}''(u;\hat{u},\hat{\hat{u}},v) = \int_\Omega (\hat{\hat{u}}\hat{u}_x + \hat{\hat{u}}_x\hat{u})v dx \tag{3.76}$$

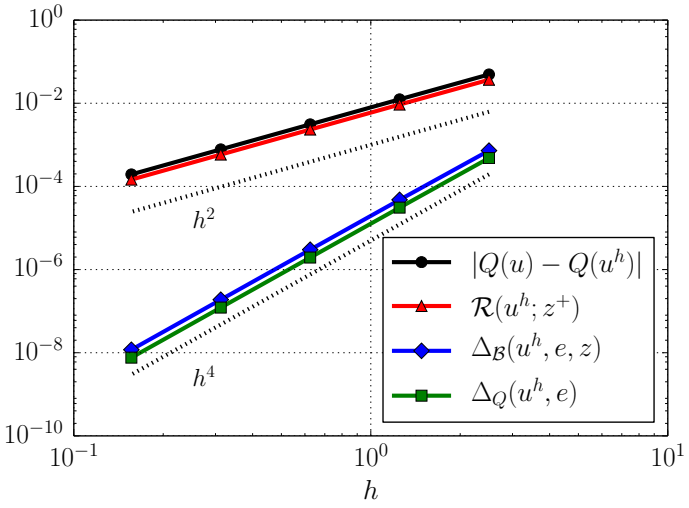

Figure 3.1: Convergence of error components for nonlinear Burgers' problem with uniform mesh refinement.

and

$$\mathcal{Q}''(u; \hat{u}, \hat{\hat{u}}) = \int_\Omega \hat{\hat{u}}\hat{u}dx \tag{3.77}$$

We can define the nonlinear terms from (3.61)

$$\Delta_{\mathcal{B}}(u^h, e, z) = -\int_0^1 \left(\int_\Omega e^2 z_x dx\right)(1-s)ds = -\frac{1}{2}\int_\Omega e^2 z_x dx, \tag{3.78}$$

$$\Delta_{\mathcal{Q}}(u^h, e) = \int_0^1 \left(\int_\Omega e^2 dx\right)(1-s)ds = \int_\Omega e^2 dx. \tag{3.79}$$

Making use of Theorem 3.1.6, specifically $\|e\|_{L^2(\Omega)} \sim h^2$ (where h is the element size), we can establish asymptotic convergence rates for the nonlinear terms above. The rate for $\Delta_{\mathcal{Q}} \sim h^4$ follows directly from the rate for $\|e\|_{L^2(\Omega)}$ and the fact that

$$\left|\Delta_{\mathcal{Q}}(u^h, e)\right| \leq \int_\Omega |e|^2 \, dx = \|e\|^2_{L^2(\Omega)}. \tag{3.80}$$

To estimate the rate for the nonlinear contribution of the operator, $\Delta_{\mathcal{B}}$, we require the additional assumption that z_x be continuous. Under this assumption, we may bound the nonlinear term $\Delta_{\mathcal{B}}$ by,

$$\left|\Delta_{\mathcal{B}}(u^h, e, z)\right| \leq \int_{\Omega} \left|e^2\right| |z_x| \, dx \leq \|e\|^2_{L^2(\Omega)} \|z_x\|_{L^\infty} , \tag{3.81}$$

Thus, provided $\|z_x\|_{L^\infty}$ is defined $\forall h$, we can expect $|\Delta_{\mathcal{B}}| \sim h^4$ as well. In Figure 3.1 we see that these rates are in fact observed in practice. The computation of $\Delta_{\mathcal{B},\mathcal{Q}}$ requires the exact adjoint z and the exact error in the primal solution e. Since we known the exact solution for the present problem, we could use it to compute $e = u - h^h$. However, to obtain a more practical estimate of the nonlinear terms we use a reference solution computed in an enriched space $v^{++} \in V^{++} \supset V^+$ in place of the exact solution. Likewise we obtain a reference adjoint solution $z^{++} \in V^{++}$.

As evidenced by the example above, the practice of neglecting the higher-order contributions to the error representation is valid for some problems. Using the residual term only as an error estimator tracks well with the exact error; the nonlinear terms are shown to be both higher-order and significantly smaller in magnitude than the residual term for the Burgers' problem in one dimension. We will demonstrate in the next section that this is not always the case and these terms may in fact be on the same order of the residual in terms of convergence rates and, more importantly, perhaps, in magnitude.

3.3 A case for improved estimates

While previous section suggests that neglecting the remainder terms in the error representation can lead to a meaningful error estimate, this is not always the case. The emphasis of this section is to show that in some problems $\Delta_{\mathcal{B}}$ and $\Delta_{\mathcal{Q}}$ are of the same order as the residual term and may thus have a significant impact on the usefulness of the *a posteriori* error estimate, if these terms were to be neglected.

Example: nonlinear diffusion (sub-optimal convergence) As motivation for investigating these terms we examine a nonlinear diffusion problem. We first show that the rate of convergence of the residual remainder term $\Delta_{\mathcal{R}}$ is of the same order as the residual term itself. Numerical results are then provided that corroborate this claim.

Consider the nonlinear diffusion problem in one spatial dimension given by,

$$-\nabla \cdot (A(u_x)u_x) = f, \quad x \in \Omega = (0,1), \tag{3.82}$$

with homogeneous Dirichlet boundary conditions,

$$u(0) = u(1) = 0. \tag{3.83}$$

Here the diffusion coefficient has a nonlinear dependence on the solution,

$$A(u_x) = 1 + \frac{1}{10}u_x^2, \tag{3.84}$$

and the forcing term in (3.82) is determined by the use of the manufactured solution,

$$u(x) = (x - x^2)\left[\exp\left(-100(x - 0.25)^2\right) + \frac{1}{2}\exp\left(-100(x - 0.75)^2\right)\right]. \quad (3.85)$$

The graphical representation of manufactured solution is shown in Figure 3.2. Let $U = V = H_0^1(\Omega)$, then the weak formulation of (3.82) can be written as,

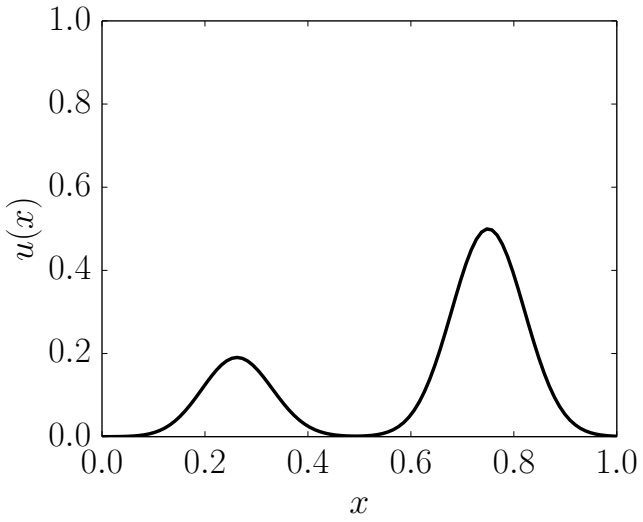

Figure 3.2: Manufactured solution for the nonlinear diffusion problem.

$$\begin{aligned} &\text{find } u \in U \text{ such that,} \\ &\mathcal{B}(u; v) = \mathcal{F}(v) \quad \forall v \in V, \end{aligned} \quad (3.86)$$

where

$$\mathcal{B}(u; v) = \int_\Omega A(u_x) u_x v_x dx, \quad (3.87)$$

$$\mathcal{F}(v) = \int_\Omega f v dx. \quad (3.88)$$

Again we will use Newton's method as in (3.71), with the linearized operator

$$\mathcal{B}'(u;w,v) = \int_\Omega \left(A'(u;w)u_x + A(u_x)w_x\right) v_x dx. \tag{3.89}$$

We consider the square fo teh L^2-norm as the quantity of interest, $Q(u) = \int_\Omega u^2 dx$. The error estimation procedure follows the standard procedure of neglecting the higher-order terms, as in the previous section; corresponding results are shown in Figure 3.3. Initially, the estimator $\mathcal{R}(u^h; z^+ - \pi^h z^+)$, and exact error $\mathcal{Q}(u) - \mathcal{Q}(u^h)$ show some pre-asymptotic variability. Eventually both stabilize and the estimate performs well in terms of tracking the trend of the error. However, the estimate consistently underestimates the true error by nearly an order of magnitude. Examining the previously omitted nonlinear terms explains why.

Since we consider the same quantity of interest as as in the Burgers' case, we know that $|\Delta_\mathcal{Q}| \sim h^4$. For the nonlinear residual term, we first note that

$$\mathcal{B}''(u;\hat{u},\hat{\hat{u}},v) = \frac{1}{5}\int_\Omega (\hat{\hat{u}}_x\hat{u}_x u_x + u_x\hat{u}_x\hat{\hat{u}}_x + u_x\hat{\hat{u}}_x\hat{u}_x)v_x dx, = \frac{3}{5}\int_\Omega (\hat{\hat{u}}_x\hat{u}_x u_x)v_x dx, \tag{3.90}$$

which means

$$\Delta_\mathcal{B}(u^h, e, z) = \frac{3}{5}\int_0^1 \left(\int_\Omega (u^h + se)_x\ e_x^2\ z_x dx\right)(1-s)ds. \tag{3.91}$$

We can again derive an estimate for the convergence rate of the nonlinear term by making the assumption that z is continuously differentiable. Additionally,

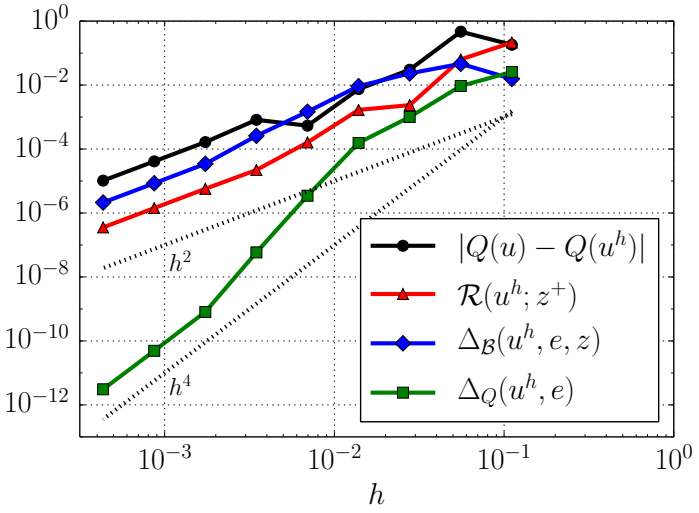

Figure 3.3: Convergence of error components for nonlinear diffusion problem with uniform mesh refinement.

we observe that for small h, $\left\|(u^h + se)_x\right\|_{L^2} \sim \left\|u^h_x\right\|_{L^2}$. Still, we can only go as far as to show

$$\left|\Delta_{\mathcal{B}}(u^h, e, z)\right| \leq \frac{3}{5}\int_0^1 \left\|(u^h + se)_x\right\|_{L^2} \|e_x\|^2 \|z_x\|_{L^\infty} (1-s)ds \sim h^2. \quad (3.92)$$

Where we used the fact that $\|e_x\|_{L^2} \sim h$. In contrast to the previous example, the rate of convergence is the same as that of the residual itself. The numerical results in Figure 3.3 support this claim. In fact, the nonlinear term not only exhibits the same rate of convergence, but the magnitude is surprisingly larger than that of the residual term. The effectivity index for the estimator $\eta^{\mathcal{R}}$ is only 0.035, while the nonlinear contribution is much closer to the exact error, yielding a ratio of $|\Delta_{\mathcal{B}}| \,/\, |\mathcal{E}| = 0.21$, where $\mathcal{E} = Q(u) - \mathcal{Q}(u^h)$. This would

suggest the development of alternative estimators that take into account the nonlinear terms.

While we do not expect the nonlinear contribution alone to be an accurate representation of the error in the quantity of interest, the previous example shows that an enhanced estimator taking into account the nonlinear terms would actually be more accurate than the traditional $\eta^{\mathcal{R}}$. In order to construct a *computable* estimator of this form we need to evaluate the functions e and z. For z, we can naturally use z^+ and for e, we propose $e^+ = u^+ - u^h$, where $u^+ \in V^+$ is the solution to the primal problem in the enriched space. With that we define the estimator,

$$\eta^{\Delta} = -\Delta_{\mathcal{B}}(u^h, e^+, z^+) + \Delta_{\mathcal{Q}}(u^h; e^+). \tag{3.93}$$

An alternative could be to combine the residual and nonlinear terms, namely

$$\eta^{\mathcal{B}'} = \mathcal{B}'(u^h; e^+, z^+) + \Delta_{\mathcal{Q}}(u^h; e^+). \tag{3.94}$$

This estimator attains an effectivity index $\left|\eta^{\mathcal{B}'}\right| / |\mathcal{E}| = 0.24$ for the previous example, somewhat better than either of the other two previous estimators.

Results from the nonlinear diffusion problem suggest that the nonlinear terms may need to be included in the estimator for some nonlinear problems, in order to obtain accurate estimates of the error in quantities of interest. Since the higher-order terms may significantly contribute to the overall error, one naturally wonders whether including those terms in refinement indicators may influence an adaptive refinement procedure. In the next section, we in-

vestigate the different indicators based on above estimates, with and without the nonlinear terms in the error representation.

3.4 Adaptive mesh refinement for nonlinear problems

In light of the previous section, it is worth considering the effect, if any, the nonlinear terms may have on mesh adaptivity. Since classical approaches generally assume that the nonlinear terms can be neglected in the *a posteriori* error estimation framework, their influence on adaptive refinement has never been studied, to our best knowledge, in detail and is the subject of the presentation below.

Our basic hypothesis is that the nonlinear terms may indicate mesh refinement in regions of the domain where nonlinear effects dominate prior to the residual term alone would do so. To analyze this concept we perform an adaptive study for Navier-Stokes flow past an obstacle in a channel. Three different refinement indicators are compared; the first being the classical indicator obtained by neglecting the nonlinear contributions. Then we consider indicators based on the nonlinear term only and the combination of the residual and nonlinear terms. At the end of this section numerical results are shown for refinement, as well as the estimators discussed above.

3.4.1 Model problem: Incompressible flow past an obstacle

We begin by defining the setting of our model problem, namely the simulation of a viscous flow past an obstacle. A square obstacle is placed in a

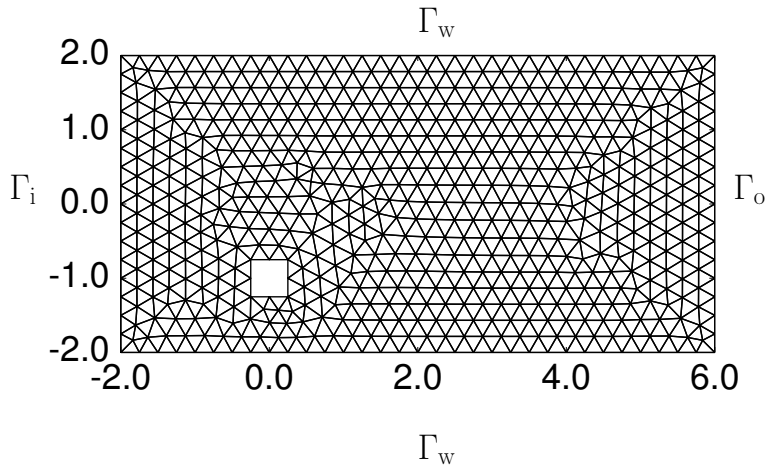

Figure 3.4: Computational domain and initial finite element mesh for Navier-Stokes flow past a square obstacle.

2D channel, as shown in Figure 3.4. The flow is governed by the incompressible Navier-Stokes equations,

$$\begin{cases} -\nu\Delta\boldsymbol{u} + \boldsymbol{u}\cdot\nabla\boldsymbol{u} + \nabla p &= \boldsymbol{0}, \\ \nabla\cdot\boldsymbol{u} &= 0, \end{cases} \qquad \text{in } \Omega, \tag{3.95}$$

and the boundary conditions:

$$\boldsymbol{u}(\boldsymbol{x}) = 6\begin{bmatrix} 1-\left(\frac{x_1}{2}\right)^2 \\ 0 \end{bmatrix}, \qquad \boldsymbol{x}\in\Gamma_{\mathrm{i}}, \tag{3.96}$$

$$\boldsymbol{u} = 0, \qquad \boldsymbol{x}\in\Gamma_{\mathrm{w}}\cup\Gamma_{\mathrm{sq}}, \tag{3.97}$$

$$(\nu\nabla\boldsymbol{u} - p\boldsymbol{I})\cdot\boldsymbol{n} = \boldsymbol{0}, \qquad \boldsymbol{x}\in\Gamma_{\mathrm{o}}, \tag{3.98}$$

where Γ_{i}, Γ_{o}, Γ_{w}, and Γ_{sq} are the inflow, outflow, wall, and obstacle boundaries, respectively. The viscosity ν will be chosen as the dimensionless value $\nu = 0.05$.

The initial finite element mesh used in all computational studies is also shown in Figure 3.4. We define the Reynolds number based on the diameter of the obstacle, 0.5, and the average inflow velocity

$$u_{\text{avg}} = \frac{6}{4}\int_{-2}^{2} 1 - \left(\frac{x_2}{2}\right)^2 dx = 4 \tag{3.99}$$

The Reynolds number for our particular flow is thus given by $Re = 40$. This value was selected small enough in order to obtain a stationary and laminar solution, yet large enough so that the convective term is not negligible.

As we did for the Stokes problem of Chapter 2, we use here a mixed formulation for the Navier-Stokes equations. Let $V = [H_0^1(\Omega)]^2$ and $Q = L_0^2(\Omega)$, and define the lift function $\boldsymbol{u}_D \in [H^1(\Omega)]^2$ that satisfies the inhomogeneous boundary condition on Γ, so that $V \ni \boldsymbol{w} = \boldsymbol{u} - \boldsymbol{u}_D$. Then, we can define the weak formulation of (3.95),

$$\begin{aligned} &\text{find } (\boldsymbol{w}, p) \in V \times Q \text{ such that} \\ &\mathcal{B}((\boldsymbol{w}, p); (\boldsymbol{v}, q)) = \mathcal{F}((\boldsymbol{v}, q)) \quad \forall (\boldsymbol{v}, q) \in V \times Q, \end{aligned} \tag{3.100}$$

where

$$\begin{aligned} \mathcal{B}((\boldsymbol{w}, p); (\boldsymbol{v}, q)) = a(\boldsymbol{w}; \boldsymbol{v}) &+ (\boldsymbol{w} \cdot \nabla \boldsymbol{u}^D + \boldsymbol{u}^D \cdot \nabla \boldsymbol{w}, v)_{L^2(\Omega)} \\ &+ b(\boldsymbol{v}, p) + b(\boldsymbol{w}, q) \end{aligned} \tag{3.101}$$

$$\mathcal{F}((\boldsymbol{v}, q)) = -a(\boldsymbol{u}_D; \boldsymbol{v}) - b(\boldsymbol{u}_D, q), \tag{3.102}$$

with

$$a(\boldsymbol{w}; \boldsymbol{v}) = \int_\Omega \nabla \boldsymbol{w} : \nabla \boldsymbol{v} + \boldsymbol{w} \cdot \nabla \boldsymbol{w}\ \boldsymbol{v}\ dx, \tag{3.103}$$

and

$$b(\boldsymbol{v}, q) = -\int_{\Omega} q\nabla \cdot v \; dx. \tag{3.104}$$

Let $V^h \subset V$ and $Q^h \subset Q$ be conforming finite element spaces. The finite dimensional formulation of (3.100) is given by,

$$\begin{aligned} &\text{find } (\boldsymbol{w}^h, p^h) \in V^h \times Q^h \text{ such that} \\ &\mathcal{B}((\boldsymbol{w}^h, p^h); (\boldsymbol{v}^h, q^h)) = \mathcal{F}((\boldsymbol{v}^h, q^h)) \quad \forall (\boldsymbol{v}^h, q^h) \in V^h \times Q^h. \end{aligned} \tag{3.105}$$

We will use analogous finite element approximation spaces as we did in Chapter 2, $\mathbb{P}_k/P_{k-1}$, to discretize (3.105). Again, to solve (3.105) numerically we will use Newton's method and the update equation (3.71) with

$$\begin{aligned} &\mathcal{B}'\left((\boldsymbol{u}, p); (\hat{\boldsymbol{u}}, \hat{p}), (v, q)\right) = \\ &\quad \int_{\Omega} \nabla \hat{\boldsymbol{u}} : \nabla \boldsymbol{v} + \left(\hat{\boldsymbol{u}} \cdot \nabla \boldsymbol{u} + \boldsymbol{u} \cdot \nabla \hat{\boldsymbol{u}}\right) \boldsymbol{v} \; dx \\ &\quad + \int_{\Omega} \left(\hat{\boldsymbol{u}} \cdot \nabla \boldsymbol{u}^D + \boldsymbol{u}^D \cdot \nabla \hat{\boldsymbol{u}}\right) \boldsymbol{v} \; dx + b(\hat{\boldsymbol{u}}, q), \end{aligned} \tag{3.106}$$

For the quantity of interest we will consider the pointwise value of the x-velocity at a point, $\boldsymbol{x}_0 = (1.0, -1.0)^T$, directly behind the obstacle. Borrowing from our treatment of pointwise quantities of interest in Section 2.3.4.3, we can estimate the quantity $u_x(\boldsymbol{x}_0)$ by the functional

$$\mathcal{Q}\left((\boldsymbol{u}, p)\right) = \int_{\Omega} \kappa_{\varepsilon}(\boldsymbol{x} - \boldsymbol{x}_0) \; u_1(\boldsymbol{x}) \; dx, \tag{3.107}$$

where κ_{ε} is given by (2.24), and we set $\varepsilon = 0.25$. Note that (4.42) is a linear functional of $(\boldsymbol{u}, p)$. We then define the linearized adjoint problem,

$$\begin{aligned} &\text{find } (\boldsymbol{z}_u, z_p) \in V \times Q \text{ such that} \\ &\mathcal{B}'\left((\boldsymbol{u}, p); (\boldsymbol{v}, q), (\boldsymbol{z}_u, \boldsymbol{z}_p)\right) = \mathcal{Q}\left((\boldsymbol{v}, q)\right), \quad \forall (\boldsymbol{v}, q) \in V \times Q. \end{aligned} \tag{3.108}$$

The finite dimensional counterpart to (3.108) is obtained in the enriched functions spaces V^+ and Q^+, defined in (2.66) and (2.67), respectively. That is,

$$\begin{aligned}&\text{find } (\boldsymbol{z}_u^+, z_p^+) \in V^+ \times Q^+ \text{ such that}\\ &\mathcal{B}'\Big((\boldsymbol{u}, p); (\boldsymbol{v}^+, q^+), (\boldsymbol{z}_u^+, \boldsymbol{z}_p^+))\Big) = \mathcal{Q}\left((\boldsymbol{v}^+, q^+)\right), \quad \forall (\boldsymbol{v}^+, q^+) \in V^+ \times Q^+.\end{aligned} \tag{3.109}$$

We also derive the nonlinear term $\Delta_{\mathcal{B}}\left((\boldsymbol{u}^h, p^h), (\boldsymbol{e}_u, e_p), (\boldsymbol{z}_u, z_p)\right)$, based on the second derivative of $\mathcal{B}$ since we will make use if it in defining the error indicators in the following section. First, note that,

$$\mathcal{B}''\Big((\boldsymbol{u}, p); (\hat{\boldsymbol{u}}, \hat{p}), (\hat{\hat{\boldsymbol{u}}}, \hat{\hat{p}}), (v, q))\Big) = \int_\Omega \left(\hat{\boldsymbol{u}} \cdot \nabla \hat{\hat{\boldsymbol{u}}} + \hat{\hat{\boldsymbol{u}}} \cdot \nabla \hat{\boldsymbol{u}}\right) \boldsymbol{v} \; dx. \tag{3.110}$$

Thus,

$$\Delta_{\mathcal{B}}\left((\boldsymbol{u}^h, p^h), (\boldsymbol{e}_u, e_p), (\boldsymbol{z}_u, z_p)\right) = \int_\Omega \boldsymbol{e}_u \cdot \nabla \boldsymbol{e}_u \; \boldsymbol{z}_u \; dx. \tag{3.111}$$

The exact error $\boldsymbol{e}_u$ and adjoint $\boldsymbol{z}_u$ are not available for the present problem, as they were in the simpler examples above. Instead, we will estimate the nonlinear term using the higher-order adjoint solution $\boldsymbol{z}_u^+$ and a higher-order primal solution $\boldsymbol{u}^+ \in V^+$; since this solution will only be used in the computation of the nonlinear term there is no concern regarding Galerkin orthogonality. Obtaining the enriched solution $\boldsymbol{u}^+$ represents a significant amount of additional computational work, just to obtain an estimate of the nonlinear error in $\boldsymbol{u}^h$ and it may not be practical to use this approach in practical engineering applications. However, since the present focus is on researching the effect of these features, it is reasonable in this case; should the inclusion of the nonlin-

ear term prove valuable, further research could focus on making the process more computationally efficient.

We may expect that the accuracy of the solution could influence the residual $\mathcal{R}$ and the nonlinear term $\Delta_{\mathcal{B}}$ differently in different regions of the domain. With the traditional estimator $\eta^{\mathcal{R}}$, we expect refinements to target the region near the quantity of interest as well as regions where the primal error is large, such as the singularities around the corners of the obstacle. The nonlinear terms may lead to similar results, but it is difficult to anticipate how the combination of both terms might impact the optimal mesh. In the next section, we define element indicators which should identify regions of the domain that are important for obtaining an accurate approximation of the quantity of interest.

3.4.2 Element error indicators

Before proposing two new indicators that incorporate the nonlinear effects, we first recall the definition of the traditional error indicators used in the study of linear problems. Motivated by the error estimator (3.63), we recall the definition of the error indicators defined in Section 2.2.4),

$$\eta_K^{\mathcal{R}} := \left| \int_K r_K^h((\boldsymbol{z}_u^+ - \pi^h \boldsymbol{z}_u^+, z_p^+ - \pi^h z_p^+)) \right. \\ \left. + \sum_{e \subset \partial K \cap \Gamma_{\text{int}}} \int_e j_K^h((\boldsymbol{z}_u^+ - \pi^h \boldsymbol{z}_u^+, z_p^+ - \pi^h z_p^+)) ds \right|, \tag{3.112}$$

where

$$
\begin{aligned}
&r_K^h((\boldsymbol{z}_u^+ - \pi^h \boldsymbol{z}_u^+, z_p^+ - \pi^h z_p^+)) \\
&\quad = \left(\nu \Delta \boldsymbol{u}^h - \boldsymbol{u}^h \cdot \nabla \boldsymbol{u}^h - \nabla p^h\right) \cdot (\boldsymbol{z}_u^+ - \pi^h \boldsymbol{z}_u^+) \\
&\qquad + (\nabla \cdot \boldsymbol{u}^h)(z_p^+ - \pi^h z_p^+),
\end{aligned} \tag{3.113}
$$

where the subscript K denotes the restriction to element K and

$$
j_K^h((\boldsymbol{z}_u^+ - \pi^h \boldsymbol{z}_u^+, z_p^+ - \pi^h z_p^+)) = \boldsymbol{n} \cdot [\![\nabla \boldsymbol{u}^h]\!](\boldsymbol{z}_u^+ - \pi^h \boldsymbol{z}_u^+) \tag{3.114}
$$

Using the higher-fidelity solutions $\boldsymbol{u}^+$ and $\boldsymbol{z}^+$, we define an error indicator based solely on $\Delta_{\mathcal{B}}$,

$$
\eta_K^{\Delta} := \left| \Delta_{\mathcal{B}} \left((\boldsymbol{u}^h, p^h), (\boldsymbol{e}_u^+, e_p^+), (\boldsymbol{z}_u^+, z_p^+) \right) + \Delta_{\mathcal{Q}} \left((\boldsymbol{u}^h, p^h), (\boldsymbol{e}_u^+, e_p^+) \right) \right| \tag{3.115}
$$

In all likelihood one would not devise a refinement procedure based on η_K^{Δ} alone. It may be useful in an alternating strategy where the element error indicators $\eta_K^{\mathcal{R}}$ *or* η_K^{Δ} are used based on the relative magnitude of the associated estimators $\eta^{\mathcal{R}}$ and η^{Δ}. In any case, we will still consider a refinement strategy based on η^{Δ} only in the numerical study.

Lastly, we define element error indicators that combine both $\eta_K^{\mathcal{R}}$ and η_K^{Δ}. We examine here two different forms, the first of which was the sum of the two previously defined indicators, namely

$$
\eta_K^{\mathcal{B}'(I)} := \eta_K^{\mathcal{R}} + \eta_K^{\Delta}. \tag{3.116}
$$

This form is appealing due to its simplicity, but it also eliminates any chance of cancellation between the two sources of error. A more direct approach is to

define the indicator using the full error representation (3.59) (recall that $\mathcal{Q}$ is linear so there is no $\Delta_{\mathcal{Q}}$ term),

$$\eta_K^{\mathcal{B}'(II)} := \left| \mathcal{B}'((\boldsymbol{u}^h, p^h); (\boldsymbol{e}_u^+, e_p^+), (\boldsymbol{z}_u^+, z_p^+)) + \Delta_{\mathcal{Q}} \left((\boldsymbol{u}^h, p^h), (\boldsymbol{e}_u^+, e_p^+) \right) \right|. \quad (3.117)$$

In contrast to $\eta_K^{\mathcal{B}'(I)}$, this form of the indicator may result in some cancellation of errors within an element. Preliminary investigation showed little difference between the two forms of the final indicator. So, from here on we only consider $\eta_K^{\mathcal{B}'(II)}$ and we drop the extra identifier, referring to it by simply $\eta_K^{\mathcal{B}'}$.

We have proposed two new element indicators to consider in addition to the classical one used in the literature. Previous examples suggest that the inclusion of the nonlinear term in the error estimation procedure may lead to better results; we expect refinement procedures based on element indicators that also take these terms into consideration to be superior to the standard refinement indicator $\eta^{\mathcal{R}}$. Convergence studies for all of these indicators are evaluated in the next section.

3.4.3 Numerical results

We begin our numerical study of the Navier-Stokes flow past an obstacle by examining the performance of the error estimates defined at the end of Section 3.3.

Since an exact solution is not available, we use a reference solution u^*, computed on the mesh in Figure 3.5, as a replacement for the exact solution. This allows us to compute effectivity indices and to assess the performance of

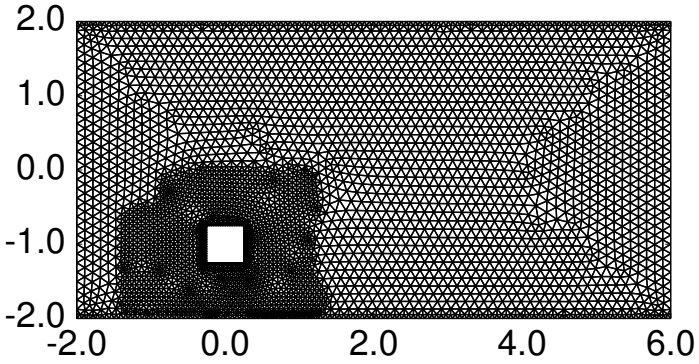

Figure 3.5: Reference mesh used to compute u^*.

each of the error estimators relative to the reference error $\mathcal{E}^* = \mathcal{Q}((\boldsymbol{u}^*, p^*)) - \mathcal{Q}((\boldsymbol{u}^h, p^h))$.

Based on the solution on the initial mesh shown in Figure 3.4, we first compute the approximations $(\boldsymbol{u}^h, p^h)$ and then perform one level of p-refinement to obtain the adjoint solutions $(\boldsymbol{z}_u^+, z_p^+)$; recall that $\boldsymbol{u}^+$ will also be needed to compute $\boldsymbol{e}_u^+ = \boldsymbol{u}^+ - \boldsymbol{u}^h$. The three estimators and their effectivities are shown in Table 3.1. As we expected, both of the estimators that contain residual information perform much better than using $\Delta_{\mathcal{B}}$ only. The best estimator is the one that combines residual information and the nonlinear terms; though the improvement isn't significant enough to warrant the additional computational cost to obtain the solution $\boldsymbol{u}^+$.

	η	$\frac{\lvert\eta\rvert}{\lvert\mathcal{E}^*\rvert}$
$\eta^{\mathcal{R}}$	0.342	1.308
η^{Δ}	0.0496	0.189
$\eta^{\mathcal{B}'}$	0.297	1.135

Table 3.1: Error estimates and associated effectivity indices for the flow past an obstacle at $Re = 40$. ($\mathcal{E}^* = 0.344$)

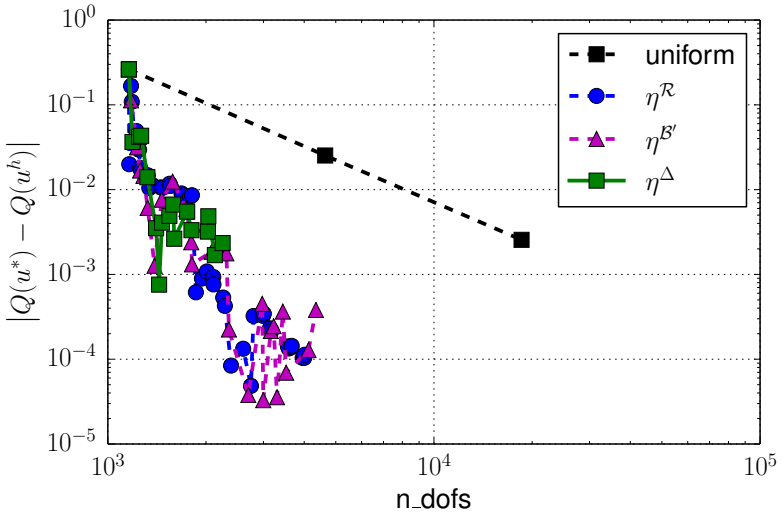

Figure 3.6: Convergence of reference error for refinement strategies using three different element error indicators.

Starting from the same initial mesh, we perform three refinement studies with respect to each of the indicators given in Section 3.4.2. Firstly, we examine the convergence in the reference error, $\mathcal{E}^*$, for each strategy, see Figure 3.6[2]. Adaptive refinement with any of the element error indicators clearly outperforms uniform h refinement. Interestingly, all of the adaptive strategies

[2]The error fraction element marking strategy and smoothing procedure, described in Section 2.2.4, are used in all cases.

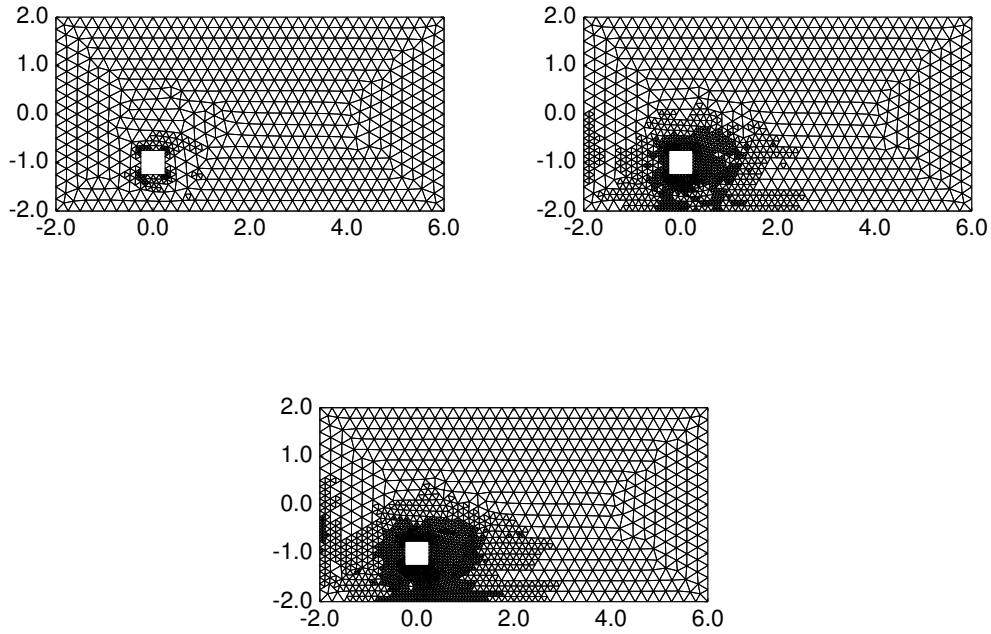

Figure 3.7: Sequence of meshes for adaptive refinement of Navier-Stokes flow past an obstacle using the element error indicator $\eta_K^{\mathcal{R}}$.

demonstrate roughly the same convergence behavior; examining the actual refinement patterns obtained for each strategy provides further insight as to why.

Figure 3.7 shows a sequence of three of the adapted meshes for the traditional indicators $\eta_K^{\mathcal{R}}$. Observe that the refinement is focused around the edges of the obstacle and coarsens smoothly as elements get further from obstacle; the inlet boundary is also marked for refinement. By comparison, looking at Figure 3.8, we see that refinement using the indicator $\eta^{\mathcal{B}'}$ is even more fo-

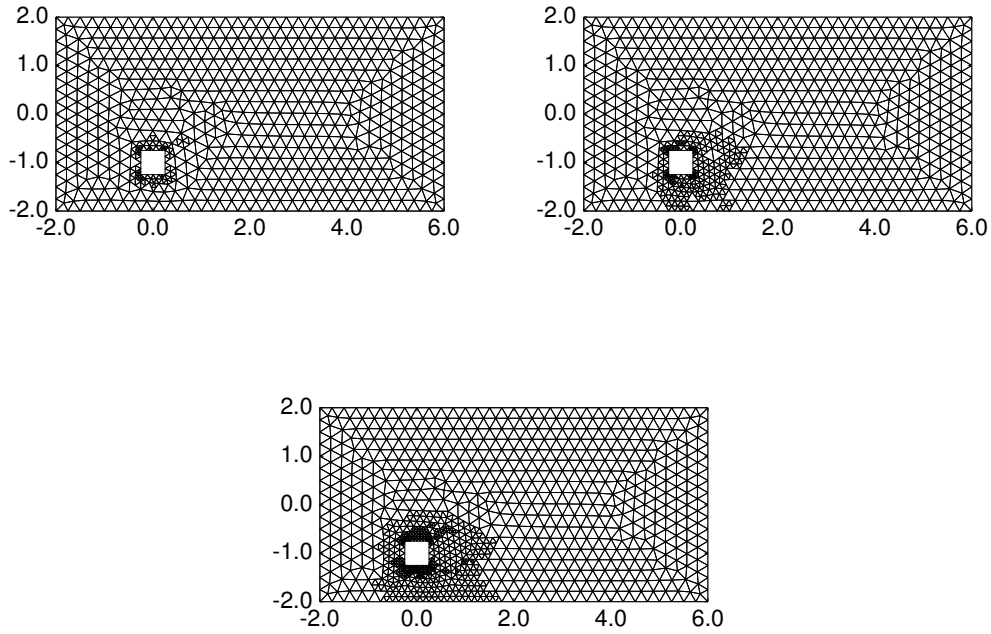

Figure 3.8: Sequence of meshes for adaptive refinement of Navier-Stokes flow past an obstacle using the element error indicator $\eta_K^{\mathcal{B}'}$.

cused on the edges of the obstacle, and in particular the leading edge. The inlet boundary remains unrefined in this case, and refinements do not transition as smoothly as the residual estimator. These differences suggest that the higher-order nonlinear terms identify the leading edge of the obstacle as more influential on the evaluation of the quantity of interest. One would expect that using the indicator comprised of only the nonlinear contribution would focus almost entirely on the obstacle and more so on the leading edge. Figure 3.9 shows that to be the case and the majority of the domain is left unrefined

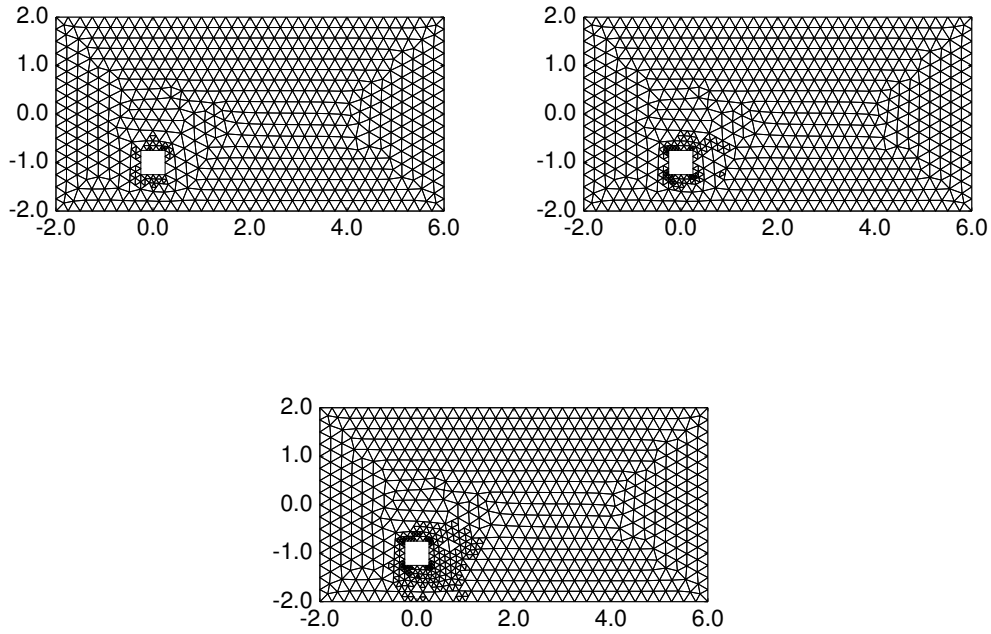

Figure 3.9: Sequence of meshes for adaptive refinement of Navier-Stokes flow past an obstacle using the element error indicator η_K^{Δ}.

using this element indicator.

3.5 Concluding remarks

Overall the numerical results for *a posteriori* error estimatin in the case of nonlinear problems provide a mixed picture. On the one hand, both Burgers' equation in 1D and Navier-Stokes equations in the case of flow past an obstacle demonstrate that the nonlinear contributions have little effect on error estimation or adaptive refinement and using the residual error estimator

is generally sufficient for both. On the other hand, as exemplified by the rather simple nonlinear diffusion problem, it is easy to show that the nonlinear terms can actually be of comparable order to the residual term, or even dominate in this case. However, in terms of mesh adaptation, no significant difference in the refinement pattern was found between $\eta_K^{\mathcal{R}}$ and $\eta_K^{\mathcal{B}'}$ for the Navier-Stokes problem.

We hope we have presented enough theoretical and numerical justification for pursuing efforts in investigating goal-oriented error estimation for nonlinear problems; the nonlinear diffusion example suggests for instance that there may be problems for which one should be careful when neglecting the 'higher-order' terms in the error analysis. One objective of ongoing research is to find or design a model problem in which the element indicators that include the nonlinear contributions lead to a very different refinement pattern from the one that the standard residual based indicators would provide.

Nonetheless, the extension of classical theorems, namely Theorem 3.1.2 and Theorem 3.1.5, to the case of nonlinear problems also suggests that, provided the approximate solution is *close enough* to the exact solution, these problems will essentially behave as they do in the linear case. We believe that the Burgers' and Navier-Stokes problems that we considered in this chapter fall within that category of problems.

One conclusion from this study is that the classical estimator and adaptive approach based on the residual seems adequate for the simulation of a flow past an obstacle at low to moderate Reynolds numbers. We are thus confi-

dent to move forward in this work and extend the classical goal-oriented error estimates to linear and nonlinear problems with uncertain data.

Chapter 4

Goal-oriented error estimation in the presence of uncertainty

In engineering applications, uncertainties generally arise from a lack of knowledge with respect to the governing differential equations or through the data of the problem, such as boundary conditions, material properties, or external forcing on the system. To account for these uncertainties in a computational model requires careful mathematical analysis and tailored solution techniques.

In the area of goal-oriented error estimation for boundary-value problems with uncertain data, some progress has been made in recent years [3, 33, 32, 44, 84, 91, 92]. However the approaches that have been proposed so far do not provide separate estimates of the error contributions due to physical discretization and the uncertainty representation. The work of the present chapter aims to add this ability to existing goal-oriented error estimation techniques.

We begin the chapter by addressing the solution methodology we will use for solutions of boundary-value problems with uncertain data. In Section 4.2, we introduce a model problem and review established results for

goal-oriented error estimation in Section 4.3. The proposed error estimation and decomposition is developed in Section 4.4, and associated adaptive refinement strategies are presented in Section 4.5. We conclude in Section 4.6 with comments on preliminary work and extension of the methodology to the case of quantities of interest defined with respect to statistical measures.

4.1 Boundary value problems with uncertain data

The notion of randomness in the modeling of physical systems is far from new; though, the advance of computational resources has made it more accessible in practice. In contrast to the mathematical study of stochastic partial differential equations, used for example to model financial transactions, we consider here situations more commonly found in engineering applications. The behavior of a given system in generally modeled in terms of an initial or boundary-value problem. Unfortunately, the complete description of the system and its environment is often lacking, meaning that some of the physical projections of the system or boundary values may be unknown, or poorly described. In that respect we will view the initial and boundary-value problems as problems parameterized by random variables

We start by reviewing relevant concepts of probability theory. In Section 4.1.2 we present the model boundary-value problems with uncertain data. The approximation method used here to describe the uncertainty in the solution is discussed in Section 4.1.3.

4.1.1 Probability foundations

We introduce a probability space, $\{\Theta, \Sigma, P\}$, where Θ is the sample space of random events, Σ is a σ-algebra, and P is the probability measure on Σ, meaning $P(\Theta) = 1$. A random variable on the probability space is defined as a P-measurable function of Θ. We will use the notation $\boldsymbol{\xi} : \Theta \to \Xi \subset \mathbb{R}^n$ for scalar and vector-valued random variables.

It is useful to define the probability density of $\boldsymbol{\xi}$ so that integration with respect to the measure P can be translated into integration with respect to the Lebesgue measure on Ξ. We first define the distribution of the random variable $\boldsymbol{\xi}$ as the push-forward of the measure P by the map $\boldsymbol{\xi}$,

$$\mu_\xi(S) = P\left[\boldsymbol{\xi} \in S\right], \quad S \in \mathcal{B}(\Xi) \tag{4.1}$$

which is a probability measure on $\mathcal{B}(\Xi)$, the Borel σ-algebra. The probability density function (pdf), denoted $p_\xi(\boldsymbol{\xi})$, is a special case of the Radon-Nikodym theorem that relates the two measures [**?**, 50, 77, 84, 133]

Theorem 4.1.1. *(Radon-Nikodym) Let λ be the Lebesgue measure on $\mathcal{B}(\Xi)$. If μ_ξ is absolutely continuous with respect to λ, i.e. $\lambda(S) = 0$ implies $\mu_\xi(S) = 0$ for any $S \in \Sigma$, then there exists a measurable function p_ξ such that for all $S \in \Sigma$,*

$$\mu_\xi(S) = \int_S p_\xi(\boldsymbol{\xi}) d\boldsymbol{\xi}, \tag{4.2}$$

where the notational convention $d\boldsymbol{\xi}$ is used in place of the more precise $\lambda(d\boldsymbol{\xi})$ for the Lebesgue measure.

Useful theoretical results can be established for specific classes of functions. Let the space of square-integrable functions on Θ be represented by $L^2(\Xi)$. For this class of functions, Cameron and Martin [36] proposed the use of a Fourier-like expansion, known as homogeneous chaos [125], to represent random variables. They established the convergence of these expansions based on the number of terms, or basis functions, in the expansion. Their result focused on random variables with Gaussian measure in particular, but subsequent works have generalized the result to any $L^2(\Xi)$ random variable [55].

Let $\alpha = (\alpha_1, \ldots, \alpha_n) \in \mathbb{N}^n$ be a multi-index and $\Psi_\alpha(\boldsymbol{\xi})$ (multivariate) polynomials

$$\Psi_\alpha(\boldsymbol{\xi}) = \psi_{\alpha_1}(\xi_1) \cdots \psi_{\alpha_n}(\xi_n), \tag{4.3}$$

where the univariate polynomial $\psi_{\alpha_i}(\xi_i)$ is the orthonormal polynomial of degree α_i, orthogonal with respect to the probability distribution of ξ_i [61, 62, 47]. That is, for $\alpha, \beta \in \mathbb{N}^n$

$$\int_\Omega \Psi_\alpha(\boldsymbol{\xi}) \Psi_\beta(\boldsymbol{\xi}) p_{\boldsymbol{\xi}}(\boldsymbol{\xi}) d\boldsymbol{\xi} = \delta_{\alpha\beta}, \tag{4.4}$$

where

$$\delta_{\alpha\beta} = \begin{cases} 1, & \alpha_i = \beta_i, i = 1, \ldots, n \\ 0, & \text{otherwise.} \end{cases} \tag{4.5}$$

Theorem 4.1.2. *(Generalized Cameron-Martin) Let $\mathcal{F}_\infty$ be the σ-algebra generated from the set of random variables $\{\xi_m\}_{m \in \mathbb{N}}$. For any $Z \in L^2(\Theta, \mathcal{F}_\infty, P)$ the generalized polynomial chaos expansion,*

$$Z^N = \sum_{\alpha \in \mathbb{N}^n} z_\alpha \Psi_\alpha(\boldsymbol{\xi}), \tag{4.6}$$

where the coefficients are given by,

$$z_\alpha = \langle Z, \Psi_\alpha \rangle \,, \tag{4.7}$$

converges to Z in mean square sense.

For uniform random variables used here, the corresponding basis functions are Legendre polynomials. The Legendre polynomials can be defined based on a recursion relation. Let $P_0(x) = 1$ and $P_1(x) = x$, then the $(n+1)$th-degree Legendre polynomial is given by,

$$(n+1)P_{n+1}(x) = (2n+1)xP_n(x) - nP_{n-1}(x). \tag{4.8}$$

The correct choice of basis polynomials for random variables with other common distributions are given by the Askey scheme and a thorough discussion can be found in [128].

The use of L^2 convergent series for representing random variables is collectively referred to as generalized polynomial chaos (gPC). The generalization of the methodology has led to an increase in the popularity of the method, which is now employed for in the literature on the solution of boundary-value problems with uncertain data.

4.1.2 Uncertainty representation in differential equations

We now turn our attention to the solution of boundary-value problems with uncertain parameters; in particular, we focus on second-order nonlinear operators. The uncertain parameters are represented directly by, or as a

function of, the value of the random variable $\boldsymbol{\xi}$. Various coefficients in the operator, source terms, or boundary conditions may be functions of the same set of parameters.

We thus assume the following abstract model problem holds P-almost everywhere,

$$\mathcal{A}(\boldsymbol{x}, \boldsymbol{\xi}; u) = f(\boldsymbol{x}, \boldsymbol{\xi}), \quad \forall \boldsymbol{x} \in \Omega. \tag{4.9}$$

Here $\mathcal{A}$ is a non-linear, second-order differential operator, $u = u(\boldsymbol{x}, \boldsymbol{\xi})$ is the solution of the differential equation (4.9), and $f = f(\boldsymbol{x}, \boldsymbol{\xi})$ represents the forcing term. Furthermore, we assume that $\mathcal{A}$, f, and appropriate boundary conditions on $\partial\Omega$ are defined so that (4.9) is well-posed. We present a number of examples for $\mathcal{A}$ and f in the numerical experiments that follow.

Although uncertainties in (4.9) imply that u is a random process, as mentioned previously, we interpret (4.9) for the moment as a collection of differential equations parameterized by $\boldsymbol{\xi}$. Let V_Ω represent a Hilbert space on Ω. Then, we assume (4.9) can be recast in the variational formulation,

$$\text{find } u(\cdot, \boldsymbol{\xi}) \in V_\Omega \text{ s.t.} \quad B_{\boldsymbol{\xi}}(u; v) = F_{\boldsymbol{\xi}}(v) \quad \forall v \in V_\Omega, \tag{4.10}$$

where $B_{\boldsymbol{\xi}}(\cdot;\cdot)$ is differentiable and semi-linear.

Let $V_\Omega^h \subset V_\Omega$ represent a finite element subspace consisting of piecewise continuous functions constructed from polynomials of degree p, on a suitable partition of Ω with maximal element diameter h. The semi-discrete weak formulation of (4.10) is,

$$\text{find } u^h(\cdot, \boldsymbol{\xi}) \in V_\Omega^h \text{ s.t.} \quad B_{\boldsymbol{\xi}}(u^h; v) = F_{\boldsymbol{\xi}}(v) \quad \forall v \in V_\Omega^h. \tag{4.11}$$

The subscript $_{\boldsymbol{\xi}}$ is used to emphasize the fact that the form of A and F depend on the specific value of the parameters.

Remark 4.1.1. We should emphasize the fact that Theorem 2.1.1 applies to operators $B_{\boldsymbol{\xi}}$ and $F_{\boldsymbol{\xi}}$ for a fixed $\boldsymbol{\xi}$. That is, in order to establish well-posedness of (2.3) for all $\boldsymbol{\xi}$ one must show that $B_{\boldsymbol{\xi}}$ and $F_{\boldsymbol{\xi}}$ satisfy the assumptions of Theorem 2.1.1 *for all* $\boldsymbol{\xi} \in \Xi$.

At this point the solution of (4.11) represents a semi-discrete solution, being continuously dependent on the random variable $\boldsymbol{\xi}$. To discretize the solution in terms of the random variable, many authors have proposed the use of generalized polynomial chaos [67, 68, 128, 123, 122, 121, 42], led by the seminal work of Ghanem and Spanos [68]. While truncated generalized polynomial chaos expansions are provable convergent, one must still approximate the coefficients in the expansion; in the next section we discuss some methodologies for the computation of the coefficients.

4.1.3 Non-intrusive response surface approximation

In the study of generalized polynomial chaos, numerous methods of computing the coefficients of the expansion have been proposed, and generally fall into two categories: intrusive and non-intrusive.

Non-intrusive approaches attempt to estimate the coefficients of a generalized polynomial chaos expansion by solving the deterministic problem at a set of realizations of $\boldsymbol{\xi}$. As a result existing simulation codes can usually be used directly. In contrast, intrusive approaches, such as those based on

Galerkin methods, solve a system of equations for the entire set of expansion coefficients together; typically this requires the use of specially designed solvers.

When existing simulation codes exist for the underlying deterministic problems, non-intrusive approaches are desirable since the code can be reused with limited modification. Moreover, the set of independent realizations can usually be run in parallel, making non-intrusive approaches more efficient. For this reason, we will focus on non-intrusive approaches in the present work.

The error estimates and decomposition strategy introduced in the next section are rather general and can be utilized with most intrusive or non-intrusive surrogate methods for uncertainty quantification [33, 32, 42]. However, for completeness, we detail the pseudo-spectral projection method [84] used in the present work.

In order to represent the solution u of (4.11) by its generalized polynomial chaos expansion it remains to calculate the coefficients. The coefficients are determined by the projection of the solution onto the basis. That is

$$u_i(\boldsymbol{x}) = \langle u(\boldsymbol{x}, \cdot), \Psi_i \rangle \,, \tag{4.12}$$

where Ψ_i are the orthogonal polynomials associated with the distribution of $\boldsymbol{\xi}$. Using the pdf we can write (4.12) as,

$$u_i(\boldsymbol{x}) = \int_{\Xi} u(\boldsymbol{x}, \boldsymbol{\xi}) \Psi_i(\boldsymbol{\xi}) p_{\xi}(\boldsymbol{\xi}) d\boldsymbol{\xi}. \tag{4.13}$$

As discussed previously, non-intrusive approaches aim to compute the

coefficients of the expansion based on independent realizations of the deterministic solution $u(\boldsymbol{x}, \boldsymbol{\xi})$. One can use sampling-based methods, such as Monte Carlo or Latin hypercube sampling, to estimate the integral in (4.13). In high-dimensional parameter spaces sampling may be preferred, since convergence is based on the number of samples and not the dimension of the space. In our case, the dimension will remain relatively low so that we can rely on direct numerical integration using quadrature techniques. Even in a high number of dimensions authors have proposed the use of sparse representations to make the process more efficient [5, 42, 59, 65, 98, 99, 117].

Using basic quadrature formula we can approximate the integration in (4.13) by,

$$u_i(\boldsymbol{x}) \approx \sum_{k=1}^{m} u(\boldsymbol{x}, \boldsymbol{\xi}^k)\Psi_i(\boldsymbol{\xi}^k)w^k, \tag{4.14}$$

where $\{\boldsymbol{\xi}^k\}$ and $\{w^k\}$ are quadrature points and weights, respectively. It has been shown in [43] that using a Gaussian quadrature rule yields a geometric convergence rate. It does however require a number of quadrature points $m(N)$ that scales exponentially with the dimension of Ξ. Thus the fully discretized solution to (4.11) can be written as,

$$u^{h,N}(\boldsymbol{x}, \boldsymbol{\xi}) = \sum_{i=0}^{N} u_i^h(\boldsymbol{x})\Phi_i(\boldsymbol{\xi}), \tag{4.15}$$

where $u_i^h(\boldsymbol{x}) \in V_\Omega^h \subset V_\Omega, \forall i = 1, \ldots, N$ are computed independently by (4.14). To reiterate, the error estimation and decomposition strategy developed in the subsequent section is applicable to any solution technique that results in an expansion of the form (4.15), where the coefficients may be computed

independently (as in non-intrusive methods) or concurrently (as in spectral Galerkin methods).

We remark than many surrogate methods, e.g. spectral Galerkin and stochastic collocation, use the imposed distribution of the random parameters to determine a stochastic basis with certain desirable attributes, such as orthogonality with respect to the joint distribution and analytic formulas for computing the first- or second-order moments. Unfortunately, these features do not generally hold for other probabilistic quantities of the solution and in this paper we will *not* assume that the basis is orthogonal with respect to the joint distribution of the parameters.

4.2 Error in 'deterministic' QoI

The term 'deterministic' QoI is used here to refer to a straightforward extension of the types of QoI discussed in the previous chapters, that is, functionals that represent a feature of the solution in the physical domain. The focus of the present section is on obtaining accurate representations of the response in these 'deterministic' QoI over the entire range of uncertain parameters; in that way, the quantity of interest can be though of as global in parameter space. This is in contrast to the local nature of the QoI in the physical domain. So, in general a 'deterministic' QoI can be thought of as a local feature in the physical domain, measured by its global dependence in parameter space.

We will consider the most general case of a nonlinear problem, c.f.

Section 3.1; of course, the results that follow are applicable to the linear case as well. For an approximate representation in parameter space we will consider the form discussed in the previous chapter, namely (4.15). This is by no means a strict requirement, and we make a note to highlight the situations in which we rely on this fact. The main condition required for the results of this section is that the approximate representations of the solution, both primal and adjoint, are obtained as functions of the uncertain parameters, such that they can be evaluated at any value in parameter space. This is in contrast to a purely sampling-based method, such as Monte Carlo, where random samples of the solution are obtained without constructing a global functional representation. One could choose to construct a kernel-density type of representation from these random samples, and then the present framework would again be applicable.

Notice that the error in the quantity of interest discussed in Chapters 2 and 3, in particular equation (2.25), represents error from discretization in the physical domain only; that is, for any value of the parameters, (2.35) can be used to estimate the *discretization error at* $\boldsymbol{\xi} \in \Xi$. We are interested in the error in the response surface for the quantity of interest, $\mathcal{Q}(u^{h,N}(\cdot, \boldsymbol{\xi}))$. If $\mathcal{Q}$ and v are measurable functions on Ξ, then the quantity of interest $\mathcal{Q}(v)$ is also measurable by the Doob-Dynkin lemma [110], and thus it makes sense to talk about the norm of $\mathcal{Q}(u(\cdot, \boldsymbol{\xi}))$ on Ξ. So we will consider the error in the quantity of interest as,

$$\left\| \mathcal{Q}(u(\cdot, \boldsymbol{\xi})) - \mathcal{Q}(u^{h,N}(\cdot, \boldsymbol{\xi})) \right\|. \tag{4.16}$$

Below we choose to consider the weighted $L^2(\Xi)$ norm,

$$\|v\|_{L^2(\Xi)} = \left[\int_\Xi \left(v(\boldsymbol{\xi})\right)^2 \rho(\boldsymbol{\xi}) d\boldsymbol{\xi}\right]^{1/2}.$$

However, the main result of this section, Theorem 4.3.2, does not depend on this choice directly and, provided u is sufficiently regular, alternative choices of the norm lead to analogous results.

For L^2-measurable solutions, the L^2-norm is not only the natural choice, but it also implies the control of the mean and variance of the quantity of interest.

Lemma 4.2.1. *For any $L^2(\Xi)$-measurable function v,*

$$|E[v]| \leq \|v\|_{L^2(\Xi)} \tag{4.17}$$

Proof.

$$\begin{aligned} |E[v]| &= \int_\Xi |v| \rho d\boldsymbol{\xi} \\ &\leq \left(\int_\Xi |v|^2 \rho d\boldsymbol{\xi}\right)^{1/2} \left(\int_\Xi |1|^2 \rho d\boldsymbol{\xi}\right)^{1/2} \\ &= \|v\|_{L^2(\Xi)} \end{aligned}$$

□

Lemma 4.2.2. *For any $L^2(\Xi)$-measurable function v,*

$$E\left[(v - E[v])^2\right] \leq \|v\|^2_{L^2(\Xi)} \tag{4.18}$$

Proof.

$$
\begin{aligned}
E\left[(v - E[v])^2\right] &= \int_{\Xi} (v - E[v])^2 \rho d\boldsymbol{\xi} \\
&= \int_{\Xi} v^2 - 2vE[v] + E[v]^2 \rho d\boldsymbol{\xi} \\
&= \int_{\Xi} v^2 \rho d\boldsymbol{\xi} - E[v]^2 \\
&\leq \int_{\Xi} v^2 \rho d\boldsymbol{\xi} \\
&= \|v\|^2_{L^2(\Xi)}
\end{aligned}
$$

□

With this definition of the quantity of interest and the error in the quantity of interest, we now turn our attention to the extension of the goal-oriented error estimation framework to the case of boundary-value problems with uncertainty.

4.3 Total approximation error

In this section we focus on the basic extension of the deterministic goal-oriented error estimation methodology to account for uncertainty. Since the solution approach used here relies on independent solutions of the problem the results for the deterministic setting are readably applicable.

Using the notation from Section 4.1, and the discrete solution $u^{h,N}$, we can extend the results from Section 3.2 to the present context. For each value of the parameters, $\boldsymbol{\xi}$ we have already established the approximation

$u^{h,N}(\cdot, \boldsymbol{\xi}) \in V_\Omega$. For the adjoint solution, an alternative linearized adjoint equation can be defined using $u^{h,N}$ in place of u^h,

$$\text{find } \hat{z}(\cdot, \boldsymbol{\xi}) \in V_\Omega \text{ s.t.} \quad B'_{\boldsymbol{\xi}}(u^{h,N}; v, \hat{z}) = \mathcal{Q}(v) \quad \forall v \in V_\Omega. \tag{4.19}$$

Assuming $B_{\boldsymbol{\xi}}$ is continuously differentiable in a subset of V_Ω containing $u(\cdot, \boldsymbol{\xi})$ and $u^{h,N}(\cdot, \boldsymbol{\xi})$, then (4.19) is well-posed and it is straight-forward to show an analogous error representation to (3.61).

Lemma 4.3.1. *Assume $B_{\boldsymbol{\xi}}$ to be continuously differentiable, for any $\boldsymbol{\xi} \in \Xi$, in a subset of V_Ω that contains $u, u^h, u^{h,N}$ given by* (4.10)*,* (4.11)*, and* (4.15)*, respectively. Let $\hat{z} \in V_\Omega$ be the solution to* (4.19)*. Then, the error in the linear quantity of interest $\mathcal{Q}$ at $\boldsymbol{\xi} \in \Xi$ is given by,*

$$\mathcal{Q}(u(\cdot, \boldsymbol{\xi})) - \mathcal{Q}(u^{h,N}(\cdot, \boldsymbol{\xi})) = \mathcal{R}_{\boldsymbol{\xi}}(u^{h,N}; \hat{z}) - \Delta_{\mathcal{R}}(\boldsymbol{\xi}; u^{h,N}, e^{h,N}, \hat{z}), \tag{4.20}$$

where $e^{h,N} = u - u^{h,N}$ and $\Delta_{\mathcal{R}}$ is as defined in (3.53)*.*

Again, one cannot generally solve the adjoint equation exactly and must rely on approximation of the adjoint solution $\hat{z}^+ \in V_\Omega^+$ in an enriched function space. Furthermore, calculating the norm of (3.61) requires numerical integration and the solution $\hat{z}^+$ at each quadrature point. Instead of solving for the adjoint solution at each quadrature point we resort to the same type of surrogate approximation as for the primal solution (4.15), and assume that the adjoint solution is approximated by a surrogate model

$$\hat{z}^{+,M}(\boldsymbol{x}, \boldsymbol{\xi}) = \sum_{i=0}^{M} \hat{z}_i^+(\boldsymbol{x}) \Phi_i(\boldsymbol{\xi}), \tag{4.21}$$

where $z_i^+(\boldsymbol{x}) \in V_\Omega^+ \subset V_\Omega, \forall i = 1, \ldots, N$ and each $\Phi_i(\boldsymbol{\xi})$ represents a basis function for a subset of $L^2(\Xi)$. In general the expansion order M used in (4.21) may be different from that used for the primal surrogate, (4.15). We will take $M = N$ for reasons to be discussed in the following section. Substitution of (4.21) into the error representation (4.20) makes quadrature more feasible and leads to a computable error estimate of the total approximation error–that due to both physical discretization and the surrogate approximation–which we present in the following theorem.

Theorem 4.3.2. *Let the conditions of Lemma 4.3.1 hold and let $z^{+,N}$ be an approximation of the adjoint solution according to* (4.21)*. The error estimate*

$$\eta = \left\| \mathcal{R}_{\boldsymbol{\xi}}(u^{h,N}; \hat{z}^{+,N}) \right\|_{L^2(\Xi)}, \tag{4.22}$$

for (4.16) *satisfies the bound,*

$$\begin{aligned} &\left| \left\| \mathcal{Q}(u(\cdot, \boldsymbol{\xi})) - \mathcal{Q}(u^{h,N}(\cdot, \boldsymbol{\xi})) \right\|_{L^2(\Xi)} - \eta \right| \\ &\qquad \leq \mathcal{O}\left(\left\| \left\| e^{h,N} \right\|_{V_\Omega} \left\| \hat{z} - \hat{z}^{+,N} \right\|_{V_\Omega} \right\|_{L^2(\Xi)} \right) + \mathcal{O}\left(\left\| \left\| e^{h,N} \right\|_{V_\Omega}^2 \right\|_{L^2(\Xi)} \right). \end{aligned} \tag{4.23}$$

Proof. First note that by Lemma 4.3.1, adding and subtracting the surrogate model of the adjoint in (4.20) yields

$$\begin{aligned} \mathcal{Q}(u(\cdot, \boldsymbol{\xi})) - \mathcal{Q}(u^{h,N}(\cdot, \boldsymbol{\xi})) &= \mathcal{R}_{\boldsymbol{\xi}}(u^{h,N}; \hat{z}^{+,N}) \\ &\quad + \mathcal{R}_{\boldsymbol{\xi}}(u^{h,N}; \hat{z} - \hat{z}^{+,N}) - \Delta_{\mathcal{R}}(\boldsymbol{\xi}; u^{h,N}, e^{h,N}, \hat{z}). \end{aligned} \tag{4.24}$$

By the reverse triangle inequality and using the estimate (4.22), we have

$$\begin{aligned}\Big|\big\|\mathcal{Q}(u(\cdot,\boldsymbol{\xi})) - \mathcal{Q}(u^{h,N}(\cdot,\boldsymbol{\xi}))\big\|_{L^2(\Xi)} - \eta\Big| \\ \leq \big\|\mathcal{Q}(u(\cdot,\boldsymbol{\xi})) - \mathcal{Q}(u^{h,N}(\cdot,\boldsymbol{\xi})) - \mathcal{R}_{\boldsymbol{\xi}}(u^{h,N};\hat{z}^{+,N})\big\|_{L^2(\Xi)}\,.\end{aligned}$$

Rearranging (4.24) and substituting into the previous equation leads to,

$$\begin{aligned}\Big|\big\|\mathcal{Q}(u(\cdot,\boldsymbol{\xi})) - \mathcal{Q}(u^{h,N}(\cdot,\boldsymbol{\xi}))\big\|_{L^2(\Xi)} - \eta\Big| \\ \leq \big\|\mathcal{R}_{\boldsymbol{\xi}}(u^{h,N};\hat{z}-\hat{z}^{+,N}) - \Delta_{\mathcal{R}}(\boldsymbol{\xi};u^{h,N},e^{h,N},\hat{z})\big\|_{L^2(\Xi)}\,.\end{aligned}$$

Recalling the definition of the residual and the linearization (3.52), we can rewrite the first term on the right-hand side and apply the triangle inequality,

$$\begin{aligned}\Big|\big\|\mathcal{Q}(u(\cdot,\boldsymbol{\xi})) - \mathcal{Q}(u^{h,N}(\cdot,\boldsymbol{\xi}))\big\|_{L^2(\Xi)} - \eta\Big| \\ \leq \big\|B'_{\boldsymbol{\xi}}(u^{h,N};e^{h,N},\hat{z}-\hat{z}^{+,N})\big\|_{L^2(\Xi)} \\ + \big\|\Delta_{\mathcal{R}}(\boldsymbol{\xi};u^{h,N},e^{h,N},\hat{z}-\hat{z}^{+,N})\big\|_{L^2(\Xi)} \\ + \big\|\Delta_{\mathcal{R}}(\boldsymbol{\xi};u^{h,N},e^{h,N},\hat{z})\big\|_{L^2(\Xi)}\end{aligned}$$

The two $\Delta_{\mathcal{R}}$ terms correspond to linearization errors and would disappear for linear problems. These terms are also *at least* quadratic in the error $e^{h,N}$– the first one actually being cubic in $e^{h,N}$ and $\hat{z}-\hat{z}^{+,N}$–and may usually be neglected compared to the residual.

Finally, using the continuity of $B'_{\boldsymbol{\xi}}$ on $V_\Omega \times V_\Omega$, the remaining term can be bounded by a term quadratic in $e^{h,N}$ and $\hat{z}-\hat{z}^{+,N}$. □

4.4 Error decomposition

The error estimate (4.22) contains finite element discretization error as well as the error due to the approximation in parameter space. To efficiently

control approximation error through adaptivity we seek to separate the errors due to the physical discretization and the errors due to the discretization in stochastic space, and then to use those indicators to drive adaptive refinement. As mentioned previously most methods to date [84, 91, 92, 3, 33, 32, 121] do not provide separate indicators. In this section we propose a decomposition of the resulting error estimate into separate error estimates for each approximation space.

In order to obtain separate error estimates for each space, we consider an alternative representation of the total error. Since, u^h can be computed at specific points $\boldsymbol{\xi}$, it can be used to separate the error into contributions from each space,

$$\begin{aligned}\mathcal{Q}(u(\cdot,\boldsymbol{\xi})) - \mathcal{Q}\left(u^{h,N}(\cdot,\boldsymbol{\xi})\right) = & \underbrace{\mathcal{Q}(u(\cdot,\boldsymbol{\xi})) - \mathcal{Q}\left(u^{h}(\cdot,\boldsymbol{\xi})\right)}_{\text{error due to physical discretization}} \\ & + \underbrace{\mathcal{Q}\left(u^{h}(\cdot,\boldsymbol{\xi})\right) - \mathcal{Q}\left(u^{h,N}(\cdot,\boldsymbol{\xi})\right)}_{\text{error due to surrogate approximation}}.\end{aligned} \tag{4.25}$$

Since we are interested in the $L^2(\Xi)$ norm of the error in this work, we have the following bound on the total error:

$$\begin{aligned}\left\|\mathcal{Q}(u(\cdot,\boldsymbol{\xi})) - \mathcal{Q}\left(u^{h,N}(\cdot,\boldsymbol{\xi})\right)\right\|_{L^2(\Xi)} \leq & \left\|\mathcal{Q}(u(\cdot,\boldsymbol{\xi})) - \mathcal{Q}\left(u^{h}(\cdot,\boldsymbol{\xi})\right)\right\|_{L^2(\Xi)} \\ & + \left\|\mathcal{Q}\left(u^{h}(\cdot,\boldsymbol{\xi})\right) - \mathcal{Q}\left(u^{h,N}(\cdot,\boldsymbol{\xi})\right)\right\|_{L^2(\Xi)}\end{aligned} \tag{4.26}$$

4.4.1 Estimation of error term due to physical discretization

The first term on the right-hand side of (4.25) corresponds to that introduced in (2.34) and can be approximated by (2.35). Notice that calcu-

lating the norm of (2.35) would require integration of u^h over the parameter domain. In practice these integrals can be approximated using quadrature or Monte Carlo sampling. Either approach requires the solution $u^h(\cdot, \boldsymbol{\xi}_j)$ at each integration point $\boldsymbol{\xi}_j$. We can eliminate the need for additional solutions by constructing a surrogate approximation of the physical discretization error estimate (2.35) with the same expansion order $M = N$ as that used for the surrogate solution $u^{h,N}$,

$$\mathcal{R}_{\boldsymbol{\xi}}(u^h; z^+) \approx \sum_{i=0}^{N} \left[\mathcal{R}_{\boldsymbol{\xi}}(u^h; z^+)\right]_i \Phi_i(\boldsymbol{\xi}) := \mathcal{E}^{\Omega}(\boldsymbol{\xi}). \tag{4.27}$$

With the same expansion order for $u^{h,N}, z^{+,N}$ and $\mathcal{E}^{\Omega}$ the coefficients of all three responses can be computed at the same time, eliminating the need for additional solutions of the governing equations. This is also the reason for choosing $M = N$ in the adjoint surrogate, (4.21). Using (4.27) the norm of the physical discretization error can be approximated rather efficiently by,

$$\left\| \mathcal{Q}(u(\cdot, \boldsymbol{\xi})) - \mathcal{Q}\left(u^h(\cdot, \boldsymbol{\xi})\right) \right\|_{L^2(\Xi)} \approx \left[\sum_{j=1}^{m} \left| \mathcal{E}^{\Omega}(\boldsymbol{\xi}_j) \right|^2 w_j \right]^{1/2}.$$

Despite the fact that the stochastic approximation of the physical discretization error, $\mathcal{E}^{\Omega}$, is of comparable accuracy to the forward solution, it is fairly straightforward to show that the error in $\mathcal{E}^{\Omega}$ is actually comparable to the error in $\mathcal{R}_{\boldsymbol{\xi}}(u^{h,N}; \hat{z}^{+,N})$. This is due to the fact that the value of $\mathcal{E}^{\Omega}$ is on the order of the physical discretization error in the quantity of interest. Therefore, the error in $\mathcal{E}^{\Omega}$ is the *product* of the physical and stochastic errors, rather than the sum. This is consistent with the error in $\mathcal{R}_{\boldsymbol{\xi}}(u^{h,N}; \hat{z}^{+,N})$ given in Theorem 4.3.2.

4.4.2 Estimation of error term due to surrogate approximation

On the other hand, the error due to the surrogate approximation can be computed directly for a given value of $\boldsymbol{\xi}$ using the semi-discrete solution and the surrogate approximation. Again, this would require a potentially large number of additional solutions to the forward problem.

While the error surrogate (4.27) can not be used directly in the computation of the error in the surrogate approximation we can still avoid the need for additional solutions of u^h. By writing the surrogate approximation error as,

$$\mathcal{Q}\left(u^h(\cdot,\boldsymbol{\xi})\right) - \mathcal{Q}\left(u^{h,N}(\cdot,\boldsymbol{\xi})\right) = \\ \left[\mathcal{Q}(u(\cdot,\boldsymbol{\xi})) - \mathcal{Q}\left(u^{h,N}(\cdot,\boldsymbol{\xi})\right)\right] - \left[\mathcal{Q}(u(\cdot,\boldsymbol{\xi})) - \mathcal{Q}\left(u^{h}(\cdot,\boldsymbol{\xi})\right)\right].$$

Replacing the first term on the right-hand side with the estimate (4.22), and second term with the physical discretization error surrogate (4.27), the surrogate approximation error can be estimated by

$$\mathcal{Q}\left(u^h(\cdot,\boldsymbol{\xi})\right) - \mathcal{Q}\left(u^{h,N}(\cdot,\boldsymbol{\xi})\right) \approx \mathcal{R}_{\boldsymbol{\xi}}(u^{h,N};\hat{z}^{+,N}) - \mathcal{E}^{\Omega}. \tag{4.28}$$

Using (4.28) to estimate the norm would still require a large number of residual evaluations. Even though residual calculations are usually much cheaper than fully solving the governing equation, we choose to construct another surrogate model for the total approximation error,

$$\mathcal{R}_{\boldsymbol{\xi}}(u^{h,N};\hat{z}^{+,N}) \approx \sum_{i=0}^{M} \left[\mathcal{R}_{\boldsymbol{\xi}}(u^{h,N};\hat{z}^{+,N})\right]_i \Phi_i(\boldsymbol{\xi}) := \mathcal{E}(\boldsymbol{\xi}),$$

with a higher-order $M > N$. Substituting this result into (4.28) leads to

$$\mathcal{Q}\left(u^h(\cdot,\boldsymbol{\xi})\right) - \mathcal{Q}\left(u^{h,N}(\cdot,\boldsymbol{\xi})\right) \approx \mathcal{E} - \mathcal{E}^{\Omega} := \mathcal{E}^{\Xi},$$

and estimating the norm of the surrogate approximation error then only requires evaluations of the surrogate models for the respective error terms,

$$\left\|\mathcal{Q}\left(u^h(\cdot,\boldsymbol{\xi})\right) - \mathcal{Q}\left(u^{h,N}(\cdot,\boldsymbol{\xi})\right)\right\|_{L^2(\Xi)} \approx \left\|\mathcal{E}^{\Xi}\right\|_{L^2(\Xi)}.$$

4.4.3 Estimator performance: manufactured solution

To investigate the performance of the proposed total error estimator we first apply the methodology to a problem with a manufactured solution. We consider a convection diffusion problem where the convective term is driven by two uncertain parameters. Given $\xi_1, \xi_2 \sim U(0,1)$, the problem consists in solving for u such that,

$$\begin{aligned} -\nabla\cdot(2\nabla u) + \begin{bmatrix} 10\sin\left(\frac{\pi}{2}\xi_1\right) \\ 10\cos\left(\pi\xi_2\right) \end{bmatrix} \cdot \nabla u &= f(\boldsymbol{\xi}) \quad \text{in } \Omega = (0,1)^2 \\ u &= 0 \qquad \text{on } \partial D \end{aligned} \tag{4.29}$$

where f is chosen so that

$$u(\boldsymbol{x},\boldsymbol{\xi}) = 400\Big[\xi_1(x_1 - x_1^2)e^{-\frac{20}{\xi_1}(x_1-\xi_1)^2}\Big]\Big[\xi_2(x_2 - x_2^2)e^{-\frac{20}{\xi_2}(x_2-\xi_2)^2}\Big] \tag{4.30}$$

The quantity of interest we consider here is the average solution in portion of the domain, $\omega = [0.5, 1]^2$,

$$\mathcal{Q}(u(\cdot,\boldsymbol{\xi})) = \frac{1}{4}\int_{\omega} u(\boldsymbol{x},\boldsymbol{\xi})\; d\boldsymbol{x} \tag{4.31}$$

which we approximate by introducing a smooth kernel

$$q(\boldsymbol{x}) = \Big[1 + \tanh[1000(x_1 - 0.5)]\Big]\Big[1 + \tanh[1000(x_2 - 0.5)]\Big],$$

$$\mathcal{Q}(u(\cdot, \boldsymbol{\xi})) \approx \int_\Omega q(\boldsymbol{x})\ u(\boldsymbol{x}, \boldsymbol{\xi})\ d\boldsymbol{x}. \tag{4.32}$$

Starting from a linear expansion in both parameters, we successively increase the expansion order to evaluate the performance of the estimator. Computed estimates and effectivities are shown in Table 4.1. Overall the

Table 4.1: Computed error estimates and effectivity indices for the manufactured convection-diffusion problem.

$\|\mathcal{E}\|_{L^2(\Xi)}$	$\frac{\|\mathcal{E}\|_{L^2(\Xi)}}{\|\mathcal{Q}(u)-\mathcal{Q}(u^{h,N})\|_{L^2(\Xi)}}$
4.34727e-01	.851
1.95149e-01	.782
4.25596e-02	.921
2.85842e-02	.949
8.41438e-03	.998
7.25161e-03	.987

results are promising. Clearly the error estimates captures the overall error of the surrogate approximation rather well. The effectivity indices are all reasonably close to one, especially after the initial very coarse estimates.

4.5 Adaptivity and refinement strategies

One advantage of using goal-oriented a posteriori error estimation is to adaptively refine the approximate solution with respect to the quantity of interest. The use of adaptive refinement techniques has become popular in

the finite element community; due to the so-called curse of dimensionality and overall computational cost associated with complex systems, we believe that adaptive techniques for uncertainty quantification are essential.

Decomposing the error estimate into indicators for physical discretization error and surrogate approximation error allows one to choose which approximation space should be refined. It also allows one to utilize adaptive finite element methods or adaptive response surface models for the physical discretization and surrogate approximation, respectively.

The overall procedure is summarized in Algorithm 1. It essentially describes the different calculations involved in the computation of the error estimates and provides the criterion for refinement of the finite element solution or surrogate model.

When refinement of the finite element solution is suggested a number of refinement techniques may be employed, e.g. uniform or adaptive mesh refinement. In the first example below we use adaptive mesh refinement based on the error in the quantity of interest. Refinement of the surrogate model may also be performed using various approaches and may depend on the particular surrogate method used. In Algorithm 2, we present a procedure for adapting a multi-element surrogate model. We make use of this approach in the numerical examples of the following section. This procedure could easily be used within Algorithm 1 when refining the surrogate model; however, we will assume the physical discretization is fixed and focus only on the refinement in parameter space.

Algorithm 1: General adaptive refinement in both D and Ξ.

1 Compute $\{u_i^h\}_{i=1}^N$, $\{\hat{z}_i^+\}_{i=1}^N$ and construct $u^{h,N}$ and $\hat{z}^{+,N}$;
2 Compute $\{\mathcal{R}_{\boldsymbol{\xi}}(u_i^h; \hat{z}_i^+)\}_{i=1}^N$ and form $\mathcal{E}^\Omega$;
3 Compute $\{\mathcal{R}_{\boldsymbol{\xi}}(u_i^{h,N}; z_i^{+,N}\}_{i=1}^M$ and construct $\mathcal{E}$;
4 Compute $\|\mathcal{E}\|_{L^2(\Xi)}$;
5 **if** $\|\mathcal{E}\|_{L^2(\Xi)} > TOL$ **then**
6 | Compute $\left\|\mathcal{E}^\Omega\right\|_{L^2(\Xi)}$;
7 | Compute $\left\|\mathcal{E}^\Xi\right\|_{L^2(\Xi)} = \left\|\mathcal{E} - \mathcal{E}^\Omega\right\|_{L^2(\Xi)}$;
8 | **if** $\left\|\mathcal{E}^\Omega\right\|_{L^2(\Xi)} > \left\|\mathcal{E}^\Xi\right\|_{L^2(\Xi)}$ **then**
9 | | Refine finite element solution(s) ;
10 | **else**
11 | | Refine surrogate model ;
12 | **end**
13 | Goto 1
14 **end**

Let $\Xi = \cup_i^{n_{\text{elem}}} \Xi_i$ represent a partition of the domain into n_{elem} rectangular elements, Ξ_i, and $\mathcal{E}^{\Xi_i}$ be the local surrogate contribution on element Ξ_i. We introduce the refinement indicator in each element as

$$\lambda_i = \frac{\left\|\mathcal{E}^{\Xi_i}\right\|_{L^2(\Xi_i)}}{\max\{\|\mathcal{E}^{\Xi_i}\|_{L^2(\Xi_i)}\}}.$$

If $\lambda_i \geq \gamma$, where γ is a user-chosen tolerance between 0 and 1, i.e. $0 \leq \gamma \leq 1$, then element Ξ_i is marked for refinement.

For each marked element we first generate candidate sub-elements $\Xi_i = \cup_k \Xi_{i_k}$ by bisecting Ξ_i in each parameter direction. The parent surrogate model is used to estimate $\left\|\mathcal{E}^{\Xi_i}\right\|_{L^2(\Xi_{i_k})}$. We introduce another indicator,

$$\lambda_{i_k} = \frac{\left\|\mathcal{E}^{\Xi_i}\right\|_{L^2(\Xi_{i_k})}}{\|\mathcal{E}^{\Xi_i}\|_{L^2(\Xi_i)}},$$

for the candidate elements. A second user-chosen tolerance, $0 \leq \theta \leq 1$, is used to select h or p refinement for each element; if $\lambda_{i_k} \geq \theta$, we choose to retain the candidate Ξ_{i_k}'s (h-refinement), otherwise the surrogate order of approximation is increased on Ξ_i and the candidate elements are discarded (p-refinement).

Algorithm 2: Adaptive refinement in Ξ.

while $\|\mathcal{E}\|_{L^2(\Xi)} > \left\|\mathcal{E}^{\Omega}\right\|_{L^2(\Xi)}$ **do**
  for $i = 1 \cdots n_{elem}$ **do**
    Construct $\mathcal{E}^{\Xi_i}$;
    Compute $\left\|\mathcal{E}^{\Xi_i}\right\|_{L^2(\Xi_i)}$;
    if $\left\|\mathcal{E}^{\Xi_i}\right\|_{L^2(\Xi_i)} \geq \gamma \max\{\left\|\mathcal{E}^{\Xi_i}\right\|_{L^2(\Xi_i)}\}$ **then**
      Partition Ξ_i into 2^n candidate Ξ_{i_k}'s by bisection in each stochastic direction and compute $\left\|\mathcal{E}^{\Xi_i}\right\|_{L^2(\Xi_{i_k})}$;
      if $\left\|\mathcal{E}^{\Xi_i}\right\|_{L^2(\Xi_{i_k})} > \theta \left\|\mathcal{E}^{\Xi_i}\right\|_{L^2(\Xi_i)}$ **then**
        Retain Ξ_{i_k} and construct new surrogate models $\mathcal{E}^{\Xi_{i_k}}$;
      else
        Discard Ξ_{i_k} and increase surrogate approximation order of $\mathcal{E}^{\Xi_i}$. [1]
      end
    end
  end
end

For problems with a large number of parameters, uniformly increasing the polynomial expansion order in dimensions is impractical. We will use Algorithm 2 with θ large enough to force p-refinement of the surrogate model and anisotropically refine the surrogate approximation. To describe the exact

[1] One can choose to uniformly increase the expansion order or perform an anisotropic refinement which we demonstrate in Section 4.5.3

procedure we first need a generalization of the definition of a set of multi-indices. Let

$$\mathcal{I}_{\mathcal{N}} = \{\alpha \in \mathbb{N}^n : \alpha_j \leq N_j, j = 1, \ldots, n\}, \tag{4.33}$$

where $\mathcal{N} = (N_1, \ldots, N_n)$ represents the maximum polynomial order in each direction. Higher-order expansions of the error will now be obtained using $\mathcal{M} = \mathcal{N} + \mathbf{1} = \{N_1 + 1, \ldots, N_n + 1\}$.

Since the expansion of the error estimate is represented by a higher-order ($M > N$) expansion, refinement can be driven by the higher-order terms. Specifically the relative magnitude of the higher-order coefficients–those that are not included in the expansion of the solution–will be used to determine the directions in which the polynomial degree of approximation should be increased. Adding polynomials associated with the largest contributions to the error accounts for the most important directions first, hence reducing the overall approximation error in a greedy way. Algorithm 3 presents the detailed refinement strategy.

4.5.1 Laminar flow past a cylinder

We begin by examining the solution of steady-state Navier-Stokes flow around a cylinder in a channel. In this example, the inlet velocity profile and fluid viscosity are treated as uncertain parameters and the quantity of interest is the x-velocity at a point behind the cylinder. We adaptively refine a response surface model of the solution using the refinement strategy detailed in Algorithm 1 and demonstrate that the error decomposition prevents over-

Algorithm 3: Anisotropic p refinement in Ξ.

Construct $\mathcal{E}(\boldsymbol{\xi}) = \sum_{\alpha \in \mathcal{I}_{\mathcal{M}}} \mathcal{R}_{\boldsymbol{\xi}}(u_\alpha^{h,N}, \hat{z}_\alpha^{+,N}) \Phi_\alpha(\boldsymbol{\xi})$;
Set $\beta^* = \sum_{\alpha \in \mathcal{I}_{\mathcal{M}} \setminus \mathcal{I}_{\mathcal{N}}} |\mathcal{R}_{\boldsymbol{\xi}}(u_\alpha^{h,N}, \hat{z}_\alpha^{+,N})|$.;
For $\alpha \in \mathcal{I}_{\mathcal{M}} \setminus \mathcal{I}_{\mathcal{N}}$, sort $|\mathcal{R}_{\boldsymbol{\xi}}(u_\alpha^{h,N}, \hat{z}_\alpha^{+,N})|$ in decending order giving index $\mathcal{I}_\alpha$.;
Given $0 \leq \eta \leq 1$, set $\beta = 0$ and $i = 0$;
while $\beta < \eta \beta^*$ **do**
    Set $i = i + 1$ and $\alpha^* = \mathcal{I}_\alpha(i)$;
    Set $\beta = \beta + |\mathcal{R}_{\boldsymbol{\xi}}(u_{\alpha^*}^{h,N}, \hat{z}_{\alpha^*}^{+,N})|$;
    for $j = 1 \to n$ **do**
        if $\alpha_j^* > N_j$ **then**
            Increase polynomial order of approximation in component j, $N_j \leftarrow N_j + 1$;
        end
    end
end

refinement in one space.

The Navier-Stokes equations are given by the system of equations

$$\mathcal{A}(\boldsymbol{x}, \boldsymbol{\xi}; \boldsymbol{u}) = \begin{cases} -\nu(\boldsymbol{\xi}) \Delta \boldsymbol{u} + \boldsymbol{u} \cdot \nabla \boldsymbol{u} + \nabla p &= \boldsymbol{0}, \\ \nabla \cdot \boldsymbol{u} &= 0, \end{cases} \qquad \text{in } \Omega, \tag{4.34}$$

supplemented with the boundary conditions:

$$\boldsymbol{u}(\boldsymbol{x}, \boldsymbol{\xi}) = \boldsymbol{u}_i(\boldsymbol{x}, \boldsymbol{\xi}) \qquad \boldsymbol{x} \in \Gamma_i, \tag{4.35}$$

$$\boldsymbol{u} = 0, \qquad \boldsymbol{x} \in \Gamma_{\mathrm{w}} \cup \Gamma_{\mathrm{cyl}}, \tag{4.36}$$

$$(\nu(\boldsymbol{\xi}) \nabla \boldsymbol{u} - p \boldsymbol{I}) \cdot \boldsymbol{n} = \boldsymbol{0}, \qquad \boldsymbol{x} \in \Gamma_{\mathrm{o}}, \tag{4.37}$$

where domain Ω and boundary $\partial\Omega$ are shown in Figure 4.1, along with the initial mesh in physical space. The inlet velocity $\boldsymbol{u}_i$ is defined as

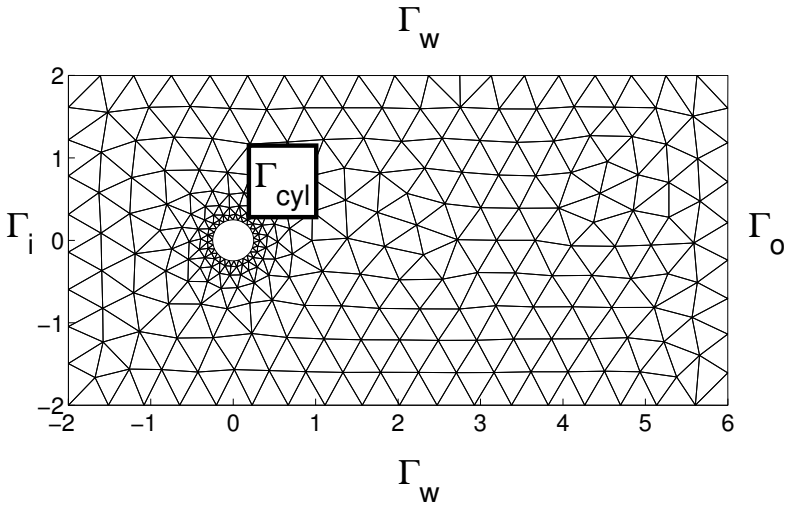

Figure 4.1: Initial finite element mesh of the physical domain and identification of boundaries.

$$\boldsymbol{u}_i(\boldsymbol{x}, \boldsymbol{\xi}) = \begin{bmatrix} u_{i_x}(\boldsymbol{x}, \boldsymbol{\xi}) \\ 0 \end{bmatrix}, \tag{4.38}$$

with u_{i_x} given by the parabolic profile

$$u_{i_x}(\boldsymbol{x}, \boldsymbol{\xi}) = U_i(\boldsymbol{\xi}) \left(1 - \left(\frac{x_1}{2}\right)^2\right).$$

We suppose that the kinematic viscosity ν and the magnitude of the maximum value U_i of the inlet velocity are parameterized by uniformly distributed random variables such that

$$\begin{cases} \nu(\boldsymbol{\xi}) = \nu(\xi_1) = \xi_1 \sim \mathcal{U}(0.01, 0.1) \\ U_i(\boldsymbol{\xi}) = U_i(\xi_2) = \xi_2 \sim \mathcal{U}(3/8, 9/8) \end{cases}. \tag{4.39}$$

These parameter distributions correspond to the range of Reynolds numbers Re,

$$1.25 \leq \mathrm{Re}(\boldsymbol{\xi}) \leq 37.5,$$

when the Reynolds number is defined with respect to the diameter of the cylinder, $\Omega_{\text{cyl}} = 0.5$, and the average value of the inflow velocity, $1 \leq u_{\text{avg}} \leq 3$,

$$u_{\text{avg}}(\boldsymbol{\xi}) = \frac{U_i(\boldsymbol{\xi})}{4} \int_{-2}^{2} 1 - \left(\frac{x_2}{2}\right)^2 dx = \frac{2}{3} U_i(\boldsymbol{\xi}).$$

For these values of the Reynolds number, the flow remains laminar and the steady-state symmetric solution is known to be stable. The weak formulation of 4.34 was derived in Section 3.4.1.

The quantity of interest is chosen to be the horizontal component u_x of the velocity u_x evaluated at the point $\boldsymbol{x}_0 = (1, 0)^T$ downstream of the cylinder, i.e.

$$\mathcal{Q}\left(\boldsymbol{u}(\cdot, \boldsymbol{\xi})\right) = u_x\left(\boldsymbol{x}_0, \boldsymbol{\xi}\right) = \int_{\Omega} u_x(\boldsymbol{x}, \boldsymbol{\xi}) \delta(\boldsymbol{x}, \boldsymbol{x}_0) dx = \int_{\Omega} \left(\boldsymbol{u}(\boldsymbol{x}, \boldsymbol{\xi}) \cdot \boldsymbol{e}_x\right) \delta(\boldsymbol{x}, \boldsymbol{x}_0) d\boldsymbol{x}, \tag{4.40}$$

where $\boldsymbol{e}_x = (1, 0)^T$ is the unit vector in the x-direction. Since the above functional is unbounded in V_Ω, we slightly modify its definition by considering the following kernel function q,

$$q(\boldsymbol{x}, \boldsymbol{x}_0) = \frac{10}{\pi} \exp\left(-10 \left|\boldsymbol{x} - \boldsymbol{x}_0\right|^2\right), \tag{4.41}$$

so that the modified quantity of interest, i.e.

$$\tilde{\mathcal{Q}}\left(\boldsymbol{u}(\cdot, \boldsymbol{\xi})\right) = \int_{\Omega} (\boldsymbol{u}(\boldsymbol{x}, \boldsymbol{\xi}) \cdot \boldsymbol{e}_x) q(\boldsymbol{x}, \boldsymbol{x}_0) \, dx, \tag{4.42}$$

is a bounded functional. We will neglect the error due to this approximation in our analysis, i.e. we shall consider that $\tilde{\mathcal{Q}}(\boldsymbol{u}(\cdot, \boldsymbol{\xi})) \simeq \mathcal{Q}(\boldsymbol{u}(\cdot, \boldsymbol{\xi}))$. The nominal value of the norm of the quantity of interest has been computed as $\|\mathcal{Q}\|_{L^2(\Xi)} =$

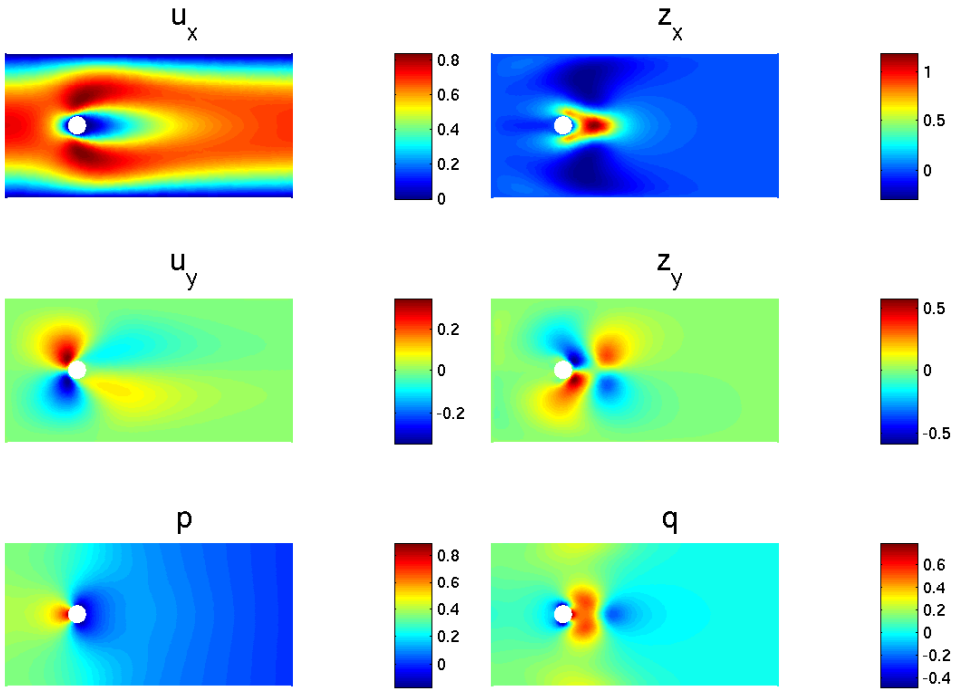

Figure 4.2: Average solution fields for Navier-Stokes flow past a cylinder: (left) primal solution; (right) adjoint solution.

0.11972; this estimate was computed using the final adapted mesh, shown in Figure 4.4, and a 10th order expansion for the surrogate solution. Figure 4.2 shows the average forward and adjoint solution fields over the range of parameter values, obtained on the initial mesh.

Beginning with the physical mesh in Figure 4.1 and polynomial degree $N = 1$ in parameter space, four simulation studies were performed.

1. The proposed error decomposition and Algorithm 1 were used to determine which approximation space to refine. Adaptive h refinement is used when refining the physical mesh. For error indicators on the phys-

ical mesh we use standard approaches that rely on integration of the element residual [14, 16], such as those prescribed in Chapter 2. Since these indicators are actually functions of the parameter, the mean of the error indicators is used and elements are marked for refinement if the error indicator is within $\alpha = 10\%$ of the maximum error indicator over the entire mesh. When the surrogate model is selected for refinement the expansion order is increased by one.

2. Adaptive h-refinement of the physical discretization only. The same error indicators and marking strategy as those prescribed in 1.

3. Adaptive p-refinement of the surrogate model only by successively increasing expansion order.

4. Simultaneous refinement of both spaces was performed; adaptive h-refinement on Ω *and* increasing the polynomial order of the surrogate approximation at each adaptive step.

Figure 4.3 shows the convergence of the relative error estimate $\frac{\|\mathcal{E}\|_{L^2(\Xi)}}{\|\mathcal{Q}\|_{L^2(\Xi)}}$ versus the total number of degrees of freedom used for each approach. The sequence of physical meshes obtained during the adaptive procedure are shown in Figure 4.4.

As one might expect, improving the approximation in physical space only leads to little or no reduction in the overall error. Clearly the most significant source of error is the discretization in parameter space. Accordingly,

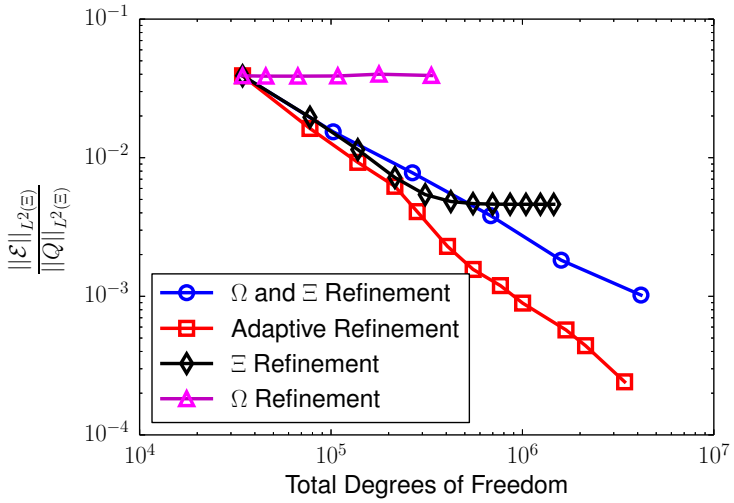

Figure 4.3: Convergence of the relative error $\frac{\|\mathcal{E}\|_{L^2(\Xi)}}{\|\mathcal{Q}\|_{L^2(\Xi)}}$ versus total number of degrees of freedom (physical and surrogate) for each refinement strategy.

an initial reduction is seen as a result of improving the approximation in parameter space, but once the error $\left\|\mathcal{E}^{\Xi}\right\|_{L^2(\Xi)}$ is reduced below the level of the physical discretization error $\left\|\mathcal{E}^{\Omega}\right\|_{L^2(\Xi)}$, no further reduction in the total error can be expected. The response surface for the quantity of interest is shown in Figure 4.5; the surface is smooth, but it is evident that a high degree polynomial is necessary to precisely capture the curvature.

Figure 4.3 clearly shows that the adaptive procedure we propose is more efficient that simultaneously refining both the physical mesh and the surrogate model. Since we are able to identify the greater source of error, we can refine each approximation space individually and allocate degrees of freedom more efficiently. This leads to significant savings during later refinement iterations.

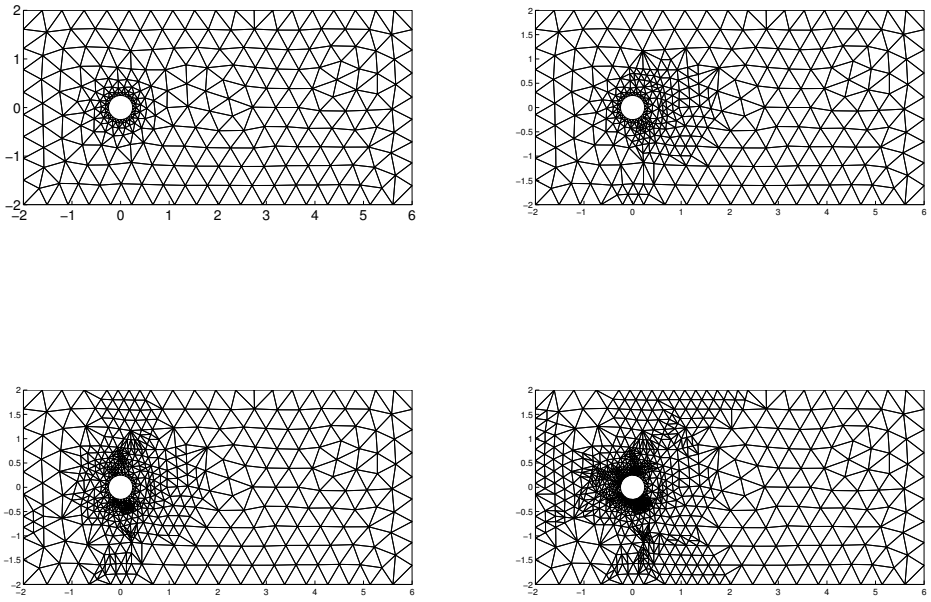

Figure 4.4: Sequence of physical meshes obtained from adaptive refinement procedure: (top left) initial physical mesh, (top right) physical mesh after first adaptive h-refinement, (bottom left) physical mesh after 2 stages of adaptive h-refinement, (bottom right) final physical mesh after 3 stages of adaptive h-refinement.

4.5.2 h-refinement: discontinuous convection

To demonstrate the advantages of h-refinement in parameter space, we consider an example where the quantity of interest is a discontinuous function on the parameter space. Attempting to capture responses with steep gradients or discontinuities using global spectral approximations result in the well-known Gibb's phenomenon, producing spurious oscillations. As a result, many au-

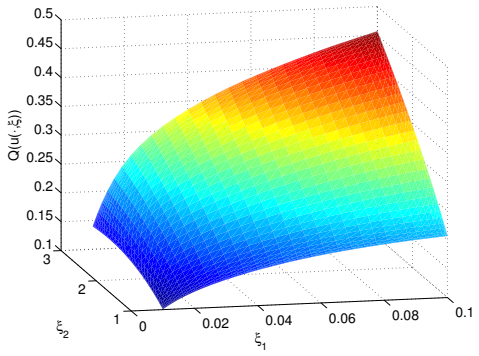

Figure 4.5: Approximate response surface for the quantity of interest (4.42), computed at the final stage of adaptive refinement.

thors have proposed changing the expansion basis to reduce the effect of the oscillatory behavior. Among the bases used are piecewise polynomials and multiwavelet bases [123, 91, 92, 83, 82]. Wan and Karniadakis [123, 121] use a multi-element generalized polynomial chaos approach, where the decision to add elements is based on the contribution of higher-order terms to the solution variance. In addition to this type of h-refinement they adapt the order of the local expansions, i.e. p-refinement, and achieve similar convergence results as spectral hp methods used for spatial discretization. Multiwavelet approaches of Le Maître et al. [83, 82] rely on a similar type of refinement indicator to perform h-refinement in stochastic space and showed convergence rates superior to Monte Carlo sampling approaches in estimating the mean and variance of the solution. Mathelin and Le Maître [91, 92] later proposed a refinement criterion based on goal-oriented *a posteriori* error estimates. They propose adaptive refinement strategies for both physical and stochastic spaces based on these error estimates and show promising results for flow problems with

uncertainties. However, to guide physical refinement they rely on an estimate of the discretization error using the expansion of the fully discretized solution, which may be corrupted by a coarse approximation in stochastic space. Furthermore, while the total error estimate is in terms of the quantity of interest, the indicator used for adaptive refinement is based on the solution itself and not the quantity of interest. In contrast, the error estimates proposed in this work are given with respect to quantities of interest and also provide the contributions from each space.

We consider here the convection-diffusion problem,

$$\mathcal{A}(\boldsymbol{x}, \boldsymbol{\xi}; u) = -2\Delta u + \boldsymbol{b}(\boldsymbol{\xi}) \cdot \nabla u = f(\boldsymbol{x}, \boldsymbol{\xi}), \quad \forall \boldsymbol{x} \in \Omega = (0,1)^2, \tag{4.43}$$

where uncertainty is present in the convection and source terms. The discontinuity arises from the definition of the velocity term,

$$\boldsymbol{b}(\boldsymbol{\xi}) = \begin{bmatrix} \sin\left(\frac{3\pi}{2}\xi_1\right) \\ 4\lfloor \xi_2 - \xi_1 \rfloor \end{bmatrix} \tag{4.44}$$

where

$$\lfloor \xi_2 - \xi_1 \rfloor = \begin{cases} 0 & \xi_1 \leq \xi_2 \\ -1 & \xi_1 > \xi_2 \end{cases}. \tag{4.45}$$

The x and y components of the velocity term are shown in Figure 4.6. Discontinuities are easily captured when element boundaries coincide with discontinuities of the solution. To make the response more difficult to model and to avoid partitioning directly along the discontinuity we have chosen the discontinuity to lie on the line $\xi_1 = \xi_2$, while the element boundaries are oriented along each axis of ξ_i. The source term is chosen so that the exact solution is,

$$u(\boldsymbol{x}, \boldsymbol{\xi}) = 40 \sin\left(\frac{3\pi}{2}\xi_1\right) (\lfloor \xi_2 - \xi_1 \rfloor)\, x_1(1-x_1)x_2(1-x_2). \tag{4.46}$$

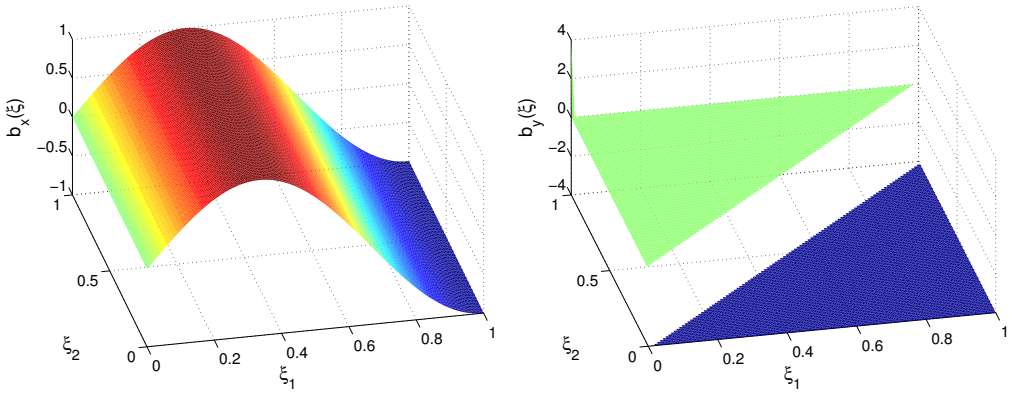

Figure 4.6: Dependence of the convection velocity (4.44) over parameter space: (left) x component $b_x(\boldsymbol{\xi})$, (right) y component $b_y(\boldsymbol{\xi})$.

We choose as a quantity of interest the solution at the point $\boldsymbol{x}_0 = (0.33, 0.33)^T$, which will again be approximated using the kernel function

$$q(\boldsymbol{x}, \boldsymbol{x}_0) = \frac{100}{\pi} \exp\left(-100\,|\boldsymbol{x} - \boldsymbol{x}_0|^2\right), \tag{4.47}$$

that is,

$$\mathcal{Q}(u(\cdot, \boldsymbol{\xi})) = u\,(\boldsymbol{x}_0, \boldsymbol{\xi}) \approx \int_\Omega q(\boldsymbol{x}, \boldsymbol{x}_0)\; u(\boldsymbol{x}, \boldsymbol{\xi})\; d\boldsymbol{x}. \tag{4.48}$$

We assume that the two parameters are uniformly distributed, with $\xi_1 \sim \mathcal{U}(0, 1)$ and $\xi_2 \sim \mathcal{U}(0, 1)$. Figure 4.7 shows the true response for the quantity of interest over parameter space. Notice that on one side of the discontinuity the response is actually zero while the other region shows a smooth non-linear dependence. We will also restrict the expansion order of the surrogate model to linear polynomials; in addition to refinement along the discontinuity, the non-linear behavior of the solution will require local refinement away from the discontinuity to obtain an accurate solution.

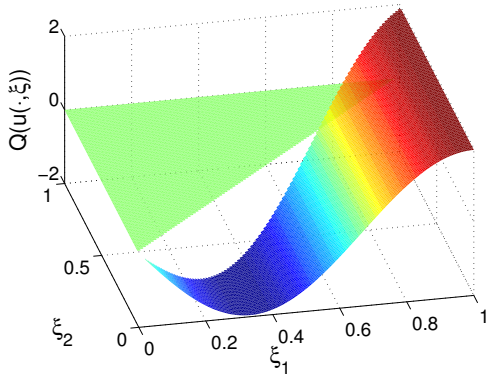

Figure 4.7: Exact response surface for the quantity of interest $\mathcal{Q}$ in (4.48).

The spatial discretization error for this quantity of interest is approximately $\left\|\mathcal{E}^{\Omega}\right\|_{L^2(\Xi)} \sim 10^{-4}$. Since this error is very small, we focus on adaptive refinement of the parametric approximation. To start, one element was used in parameter space and the spectral expansions were formed with $N = 1$. Three simulation studies were performed.

1. Our proposed h-refinement strategy (Algorithm 2) with $\gamma = 0.75$ and $\theta = 0.25$.

2. Standard uniform h-refinement in parameter space.

3. Global surrogate approximation with p-refinement.

Convergence results for each algorithm are shown in Figure 4.8.

From Figure 4.8 we can see that the adaptive refinement leads to a higher convergence rate after an initial pre-asymptotic region. Interestingly the uniform p-refinement does not perform much worse than uniform h-

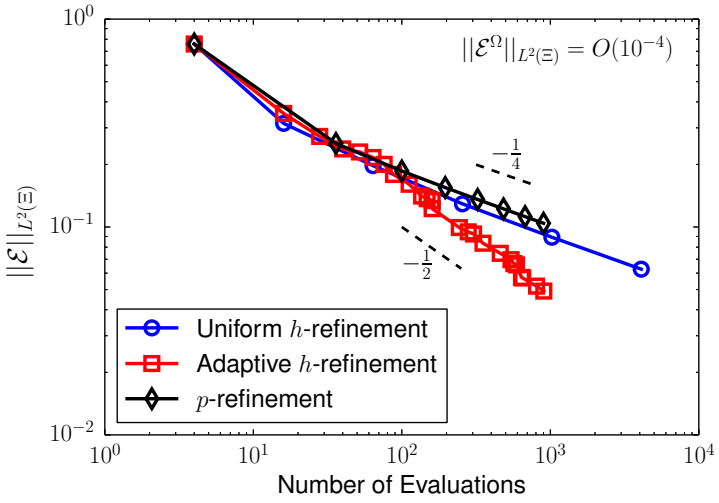

Figure 4.8: Convergence of error estimate $\|\mathcal{E}\|_{L^2(\Xi)}$ versus the number of evaluations of the governing equations for uniform h-refinement, adaptive h-refinement, and p-refinement strategies.

refinement for this quantity of interest. The asymptotic rates for both uniform h-refinement and p-refinement agree with the expected theoretical results. Due to the discontinuity in the response surface, the quantity of interest belongs to a fractional Sobolev space less than one-half, i.e. $\mathcal{Q}(u(\cdot, \boldsymbol{\xi})) \in H^{1/2-\varepsilon}(\Xi)$ where $0 < \varepsilon \leq \frac{1}{2}$. According to [121], the spectral projection w^p of a function $w \in H^s(\Xi)$ converges with the rate

$$\|w^p - w\|_{L^2(\Xi)} \leq CN^{-s} \left(n_{\text{elem}}\right)^{-s/n} |w|_{H^s(\Xi)}, \tag{4.49}$$

where n_{elem} is the number of elements in the decomposition of Ξ (assuming a uniform rectangular decomposition), C is a constant independent of N and

n_{elem}, and $|\cdot|_{H^s(\Xi)}$ is the $H^s(\Xi)$ semi-norm, defined as

$$|w|_{H^m(\Xi)} = \left(\sum_{|\alpha|=s} \int_{\Xi} |\partial_{\xi} w|^2 \, d\boldsymbol{\xi} \right)^{1/2}.$$

Finally, N is the polynomial degree of the projection (assumed the same over each element of the decomposition) and n is the dimension of $\Xi \subset \mathbb{R}^n$.

Since the number of evaluations n_{eval} is proportional to the number of elements, $n_{\text{eval}} \propto n_{\text{elem}}$, we expect the rate of convergence for uniform h-refinement to follow $\|\mathcal{E}\|_{L^2(\Xi)} \sim (n_{\text{eval}})^{-s/n}$, or $\|\mathcal{E}\|_{L^2(\Xi)} \sim (n_{\text{eval}})^{-1/4}$ for this example. Similarly, the number of evaluations required for a surrogate model of degree N, namely $n_{\text{eval}} = (N+1)^n$, suggests the same convergence rate for p-refinement, $\|\mathcal{E}\|_{L^2(\Xi)} \sim (n_{\text{eval}})^{-1/4}$.

We have included a comparison of the total error plotted as a function of $\boldsymbol{\xi}$ after the final refinement step using p-refinement, and our proposed h-refinement strategy in Figure 4.9. Notice the oscillatory behavior in the case of the global approach. Clearly the multi-element approach does a better job of identifying the discontinuity, and localizes it to smaller elements along the discontinuity. This can be seen more clearly in Figure 4.10 which shows the progression of the mesh over parameter space at various stages of the adaptive process. Recall that all elements have linear surrogate approximations; as a result, the region below $\xi_1 = \xi_2$ requires some refinement in order to accurately capture the nonlinear response, which is also evident in Figure 4.10.

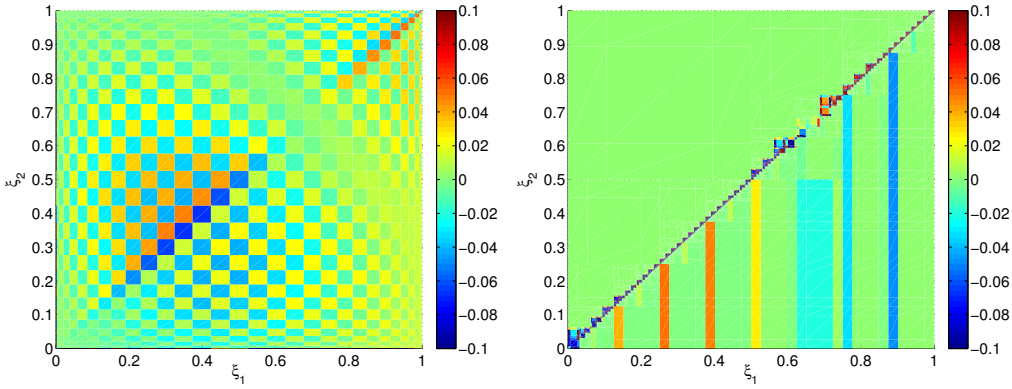

Figure 4.9: Distribution of errors for final stage of p-refinement strategy (left) and adaptive h-refinement (right). Colorbar indicates magnitude of error estimator $\mathcal{E}(\boldsymbol{\xi})$.

4.5.3 Anisotropic p-refinement: diffusion with 10 parameters

Finally, we demonstrate the use of the error estimate to perform anisotropic p-refinement in parameter space. To make the example more informative a problem is chosen such that the influence of different directions in parameter space varies by orders of magnitude. Consider the following diffusion problem:

$$\mathcal{A}(\boldsymbol{x}, \boldsymbol{\xi}; u) = -\nabla \cdot (K(\boldsymbol{x}, \boldsymbol{\xi}) \nabla u) = 0, \qquad \forall \boldsymbol{x} \in \Omega = (0, 1), \tag{4.50}$$

subject to the physical boundary conditions:

$$u(0, \boldsymbol{\xi}) = 1, \quad u(1, \boldsymbol{\xi}) = 0. \tag{4.51}$$

Furthermore assume that the log random diffusivity satisfies

$$K(x, \boldsymbol{\xi}) = \bar{K} + \sigma_a \sum_{k=1}^{d} \sqrt{\lambda_k} \varphi_k(x) \xi_k, \tag{4.52}$$

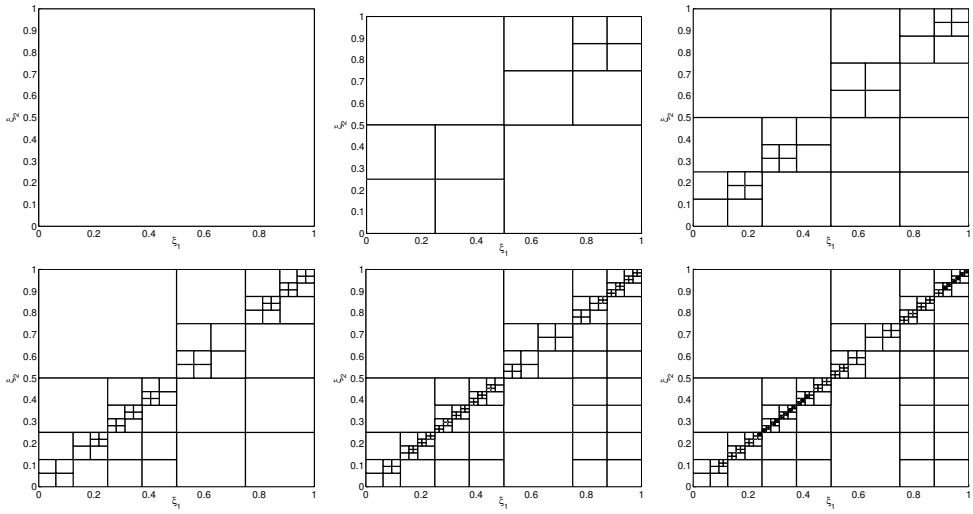

Figure 4.10: Progression of the mesh over parameter space at various stages of the adaptive procedure: (top left) initial mesh (one element), (top middle) at iteration 5, (top right) at iteration 10, (bottom left) at iteration 15, (bottom middle) at iteration 20, (bottom right) final mesh over parameter space after 25 iterations of the adaptive h-refinement.

where $\{\lambda_k\}_{k=1}^d$ and $\{\varphi_k(x)\}_{k=1}^d$ are, respectively, the eigenvalues and eigenfunctions of the covariance kernel

$$C_a(x_1, x_2) = \exp\left[-\frac{(x_1 - x_2)^2}{2l_c}\right] \tag{4.53}$$

The variability of the diffusivity field (4.52) is controlled by σ_a and the correlation length l_c which determines the decay of the eigenvalues λ_k. Here we set $d = 10$, $\sigma_a = 0.1$, $l_c = 0.5$, $\bar{K} = 0$ and $\xi_k \in [-1, 1]$, $k = 1, \ldots, d$ to be independent and uniformly distributed random variables. The square-root of the eigenvalues associated with these parameter choices are shown in Figure 4.11.

Clearly the first few dimensions are the most important and will re-

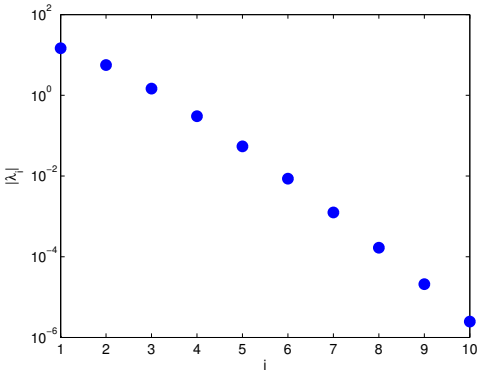

Figure 4.11: Magnitude of the square root of the first ten eigenvalues of the covariance kernel (4.53) with chosen parameters.

quire a higher polynomial degree to capture the predominant behavior of the response. Moreover, we expect the influence of the subsequent terms in the expansion to decrease rapidly.

Our quantity of interest is the average value of the solution over the physical domain for which

$$\mathcal{Q}(u(\cdot, \boldsymbol{\xi})) = (1, u(\cdot, \boldsymbol{\xi}))_{L^2(\Omega)} \,. \tag{4.54}$$

Uniformly increasing the polynomial degree of the expansion in all stochastic directions is impractical in 10 dimensions. We will use Algorithm 3 and set $\eta = 0.75$, which means that we increase the space until the cumulative errors reach 75% of the total error. Other choices of η required different numbers of refinement steps, but gave similar results. A comparison of the adaptive refinement strategy (Algorithm 3) to isotropic refinement is shown in Figure 4.12. As in the previous example, we keep the physical discretization

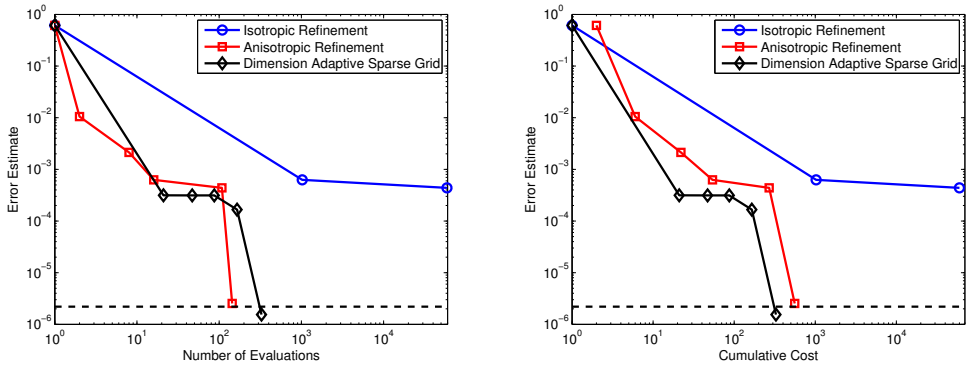

Figure 4.12: Comparison of p-adaptive refinement strategies: isotropic, anisotropic refinement, and a dimension adaptive sparse grid approximation.

fixed with 500 uniform elements, which gives a physical discretization error of $\left\|\mathcal{E}^{\Omega}\right\|_{L^2(\Xi)} = 2.2026\text{E-}06$ and corresponds to the dotted line in Figure 4.12. We terminate the anisotropic refinement when the error estimate reaches this threshold. We also compare these results with a dimensional adaptive sparse grid approximation [58, 76], which is a state-of-the-art technique for such problems. The error estimate reported in Figure 4.12 is an estimate of the L^2-norm of the error, which we compute using the surrogate approximation and the exact QoI at 10,000 random samples. The same 10,000 samples are used for all of the surrogate approximations for all levels of refinement.

We see that the anisotropic refinement case is comparable to the adaptive sparse grid in terms of producing a response surface with comparable accuracy and partial differential equation evaluations. On the right-side of Figure 4.12, we plot the cumulative cost required to achieve each surrogate approximation. This cumulative cost includes the cost in constructing the

Table 4.2: Expansion orders obtained from adaptation.

	isotropic	anisotropic					
iter	N_i	N_1	N_2	N_3	N_4	N_5	$N_6 - N_{10}$
1	0	0	0	0	0	0	0
2	1	0	1	0	0	0	0
3	2	1	1	1	0	0	0
4		1	1	1	1	0	0
5		2	2	2	1	1	0
6		2	3	2	1	1	0

surrogate at all previous levels of refinement as well as the cost in solving the adjoint problems. We see that the anisotropic refinement is still reasonably competitive with the adaptive sparse grid case. We also see that the error in both the anisotropic pseudospectral approximation and the sparse grid stagnate around 3E-4 before dropping rapidly. This is most likely due to the fact that a higher-order term is required to resolve the QoI below this level.

The sequence of polynomial orders corresponding to the iterations shown in Figure 4.12 are provided in Table 4.2. The proposed indicator reasonably identifies the first few terms of the expansion as the most important ones and can be used to adapt the polynomial order accordingly. Interestingly, it identifies the second variable as the most significant, rather than the first, for this particular quantity of interest. When compared with isotropic p refinement one sees significant computational savings in terms of the number of solutions of the partial differential equation.

4.6 Concluding remarks

In this chapter, we have developed *a posteriori* error estimates for second-order differential equations with uncertain parameters. Error was defined in terms of specific quantities of interest represented as functionals of the solution. A novel decomposition of the error estimate into contributions from physical and stochastic approximation spaces was proposed and shown to properly identify which approximation space should be refined; this was demonstrated on flow past a cylinder within a channel at low to moderate Reynolds numbers. Adaptive refinement strategies were also developed that took advantage of the indicator for the error in the stochastic approximation. Adaptive mesh refinement in stochastic space using the error estimator proved to be superior to uniform refinement. Finally, anisotropic p-refinement was performed to significantly reduce the computational cost needed to obtain an accurate solution for a diffusion problem in a 10-dimensional parameter space. The work of this chapter has been published as an ICES report [30] and presented in a manuscript submitted to the SIAM/ASA Journal on Uncertainty Quantification [31].

When modeling a system with uncertainty, one is often more concerned with the probability of extreme events rather than the average behavior. Extreme events, beyond the typical range of operating conditions for the system, can have dangerous consequences. Probabilities of events can be calculated through the use of targeted sampling techniques; however, sampling a surrogate model instead of a full model is usually much more efficient. In this case,

the accuracy of computed probabilities strongly depends on the local accuracy of the surrogate model near the event threshold.

Recently Butler and Wildey [34] have started to investigate adaptive procedures for this specific class of problems. In their work, they propose the use of two adaptive surrogate models, where a higher fidelity model is used near the region defining the random event of interest, and a low-fidelity model is used elsewhere. Instead of a two-stage approach, we could envision an adaptive technique that constructs a single surrogate model that is also accurate in the region of the event. By altering the definition of the quantity of interest to incorporate the location of the random event in parameter space, we may define a *statistical quantity of interest* (sQoI),

$$\mathcal{S}(u) = \int_{\Xi} \kappa_{\Xi}(u; \boldsymbol{\xi})\ p_{\xi}(\boldsymbol{\xi}) d\boldsymbol{\xi}, \tag{4.55}$$

where, κ_{Ξ} is in general a nonlinear function of the solution u. A vast number of quantities of interest can be described in the form (4.55). For example, to represent the probability of failure corresponding to the physical quantity of interest exceeding a predefined tolerance TOL, given by the event $S = \{\mathcal{Q}(u(\cdot, \boldsymbol{\xi}) > \text{TOL}\}$, we could define the kernel as $\kappa_{\Xi}(u; \boldsymbol{\xi}) = \mathbf{1}_S$, where $\mathbf{1}_S$ is the indicator function for event S. This choice of a statistical quantity of interest clearly depends on the solution u in a complex nonlinear manner; the results of Chapter 3 may need to be revisited in this context. Possible future work would be to assess the accuracy of statistical quantities of interest using the *a posteriori* error estimation and to adaptively construct surrogate models that best predict statistical features of the solution defined as sQoI.

Chapter 5

Efficient Bayesian model selection for RANS

In the previous chapters we focused on goal-oriented error estimation for nonlinear problems and differential equations with uncertain coefficients; we conclude this work with a practical engineering problem that incorporates these two concepts.

Having obtained reasonable results for benchmark fluid flow problems we now turn our attention to the simulation of turbulent flows. Even in the absence of uncertainty, computational costs associated with the direct simulation of turbulence are prohibitively expensive for scenarios of engineering interest. As a result, one often resorts to reduced modeling in order to make simulations more tractable. Simplified models of turbulence are often constructed based on the Reynolds averaged Navier-Stokes (RANS) [49, 105, 126] and the introduction of closure models to capture the turbulent behavior of the flow; the accuracy of these models usually depends on the value of their parameters, making them an excellent candidate for application of the present work.

Uncertainty in the RANS model parameters is a known issue in the turbulence community, but quantifying the effect of this uncertainty is seldom

analyzed in the computational fluid dynamics literature [104]. We nevertheless cite the works [40, 104] on the application of Bayesian uncertainty quantification to turbulence modeling. Our study is based on the work of Oliver and Moser [104] in which they compare four turbulence models: Baldwin-Lomax [13, 126], Spalart-Allmaras [2, 113, 103], Chien $k - \varepsilon$ [41, 126], and the so-called $v^2 - f$ model [49, 103]; and four different uncertainty models: independent homogeneous, correlated homogeneous, correlated inhomogeneous, and an additive Reynolds stress error model. The authors used Bayesian inference to obtain posterior distributions for the parameters in the RANS model as well as the parameters of the uncertainty models. Bayesian inference requires a large number of model simulations; replacing the full simulation with an accurate surrogate model may lead to considerable computational savings.

We begin the chapter with a review of the RANS equations and the Spalart-Allmaras turbulence model. In Section 5.2 we describe the details of the specific flow scenario and the construction of the adaptive surrogate model for the RANS equations. Section 5.3 contains a summary of Bayesian model comparison and use of surrogate models to reduce the computational cost. Finally, in Section 5.4, we examine the results of our Bayesian model comparison and compare them to the study performed by Oliver and Moser [104].

5.1 RANS equations and the Spalart-Allmaras turbulence model

We begin with a brief review of the Reynolds averaged Navier-Stokes equations for incompressible flows. The RANS equations are obtained by averaging the time-dependent Navier Stokes equations. The averaged equations are not only more computationally manageable, often average properties of turbulent flows are sufficient in engineering practice.

The RANS equations are derived from the Navier-Stokes equations (3.95) using the Reynolds decomposition of the velocity, $\boldsymbol{u} = U + \boldsymbol{u}'$, where $U = \overline{\boldsymbol{u}}$ is the time-averaged velocity, and $\boldsymbol{u}'$ is the fluctuation about the mean; the mean of the fluctuation is therefore equal to zero. Substituting this decomposition into the Navier-Stokes equations and taking the time average we obtain the RANS equations,

$$\begin{aligned} \frac{DU_i}{Dt} &= -\frac{1}{\rho}\frac{\partial P}{\partial x_i} + \frac{\partial}{\partial x_j}\left(\nu\frac{\partial U_i}{\partial x_j} - \overline{\boldsymbol{u}_i'\boldsymbol{u}_j'}\right) \\ \frac{\partial U_i}{\partial x_i} &= 0, \end{aligned} \tag{5.1}$$

where $P = \overline{p}$ represents the mean pressure. These equations are not closed because the Reynolds stress $r_{ij} := \overline{\boldsymbol{u}_i'\boldsymbol{u}_j'}$ is generally not known in terms of the mean velocity. To close the equations, one needs to propose a model for r_{ij}. A common approach is to model the Reynolds stress using the eddy viscosity assumption. That is, we model the Reynolds stress by the viscosity term,

$$r_{ij} = -\nu_T\left(\frac{\partial U_i}{\partial x_j} + \frac{\partial U_j}{\partial x_i}\right) \tag{5.2}$$

where the "eddy viscosity" ν_T, can be written in terms of a turbulent length and time scale. Modeling the turbulence effects as a viscosity makes sense because turbulence transports momentum in a similar manner to viscosity [49, 97, 105].

Numerous researchers have proposed closure models based on the eddy viscosity assumption, [2, 13, 41, 48, 49, 113], many of which are examined in the study by Oliver and Moser [104]. Here we will focus on one of the most commonly used models, the eddy viscosity transport model of Spalart and Allmaras [113]. The form considered in [104] has actually been modified from the original model of Spalart-Allmaras; we shall also use the modified version of the model, as described below.

The modifications are twofold; firstly, since we do not wish to model the transition to turbulence, the terms associated with laminar suppression and trip are omitted; secondly, the production term is modified in order to avoid negative values of the production. Starting from the eddy viscosity assumption (5.2) the Spalart-Allmaras model introduces a working variable $\tilde{\nu}$ such that

$$\nu_T = \tilde{\nu} f_{v1}, \tag{5.3}$$

where

$$f_{v1} = \frac{\chi^3}{\chi^3 + c_{v1}^3}, \qquad \chi = \frac{\tilde{\nu}}{\nu}, \tag{5.4}$$

and ν is the kinematic viscosity. The working variable is taken to be governed

by the transport equation

$$\frac{D\tilde{\nu}}{Dt} = c_{b1}\tilde{S}\tilde{\nu} - c_{w1}f_w\left(\frac{\tilde{\nu}}{d}\right)^2 + \frac{1}{\sigma_{\mathrm{SA}}}\left[\frac{\partial}{\partial x_j}\left((\nu+\tilde{\nu})\frac{\partial\tilde{\nu}}{\partial x_j}\right) + c_{b2}\frac{\partial\tilde{\nu}}{\partial x_j}\frac{\partial\tilde{\nu}}{\partial x_j}\right], \quad (5.5)$$

where d is the distance to the nearest wall, and $c_{w1} = c_{b1}/\kappa^2 + (1+c_{b2})/\sigma_{\mathrm{SA}}$. The modified vorticity $\tilde{S}$ is used to eliminate negative production and is given by,

$$\tilde{S} = \begin{cases} S + \bar{S} & \bar{S} \geq -c_{v2}S \\ S + \frac{S(c_{v2}^2 S + c_{v3}\bar{S})}{(c_{v3}-2c_{v2})S - \bar{S}} & \bar{S} < -c_{v2}S, \end{cases} \quad (5.6)$$

which is positive for all nonzero S and is C^1 continuous [2, 103]. In (5.6), S is the magnitude of the vorticity and,

$$\bar{S} = \frac{\tilde{\nu}}{\kappa^2 d^2} f_{v2}, \qquad f_{v2} = 1 - \frac{\chi}{1+\chi f_{v1}}. \quad (5.7)$$

The remaining undefined terms are given by the relationships below

$$f_w = g\left(\frac{1+c_{w3}^6}{g^6 + c_{w3}^6}\right)^{1/6}, \quad g = r + c_{w2}(r^6 - r), \quad r = \frac{\tilde{\nu}}{\tilde{S}\kappa^2 d^2}, \quad (5.8)$$

and the parameter values suggested by Spalart and Allmaras are given in Table 5.1.

5.2 Physical model and surrogate construction

In [104], the full RANS simulation is used as the forward map to propagate uncertainties in the parameters to the output quantity of interest. Here, we will construct an anisotropic polynomial expansion, using the refinement strategies proposed in Chapter 4, perform an uncertainty analysis using the surrogate model in place of the full simulation, and compare the conclusions with those obtained in [104].

Parameter	Standard value
c_{b1}	0.1355
σ_{SA}	2/3
c_{b2}	0.622
κ	0.41
c_{w2}	0.3
c_{w3}	2
c_{v1}	7.1
c_{v2}	0.7
c_{v3}	0.9

Table 5.1: Standard parameter values for the Spalart-Allmaras turbulence model [104].

5.2.1 Physical model

We investigate the prediction of the centerline velocity in a fully-developed, incompressible channel flow at $Re_\tau = 5000$. We first elaborate on the details of the implementation and discretization of the governing equations used in [104], from which we develop our adaptive surrogate models.

We consider here a 2D channel. The turbulence is assumed non-homogeneous in the y-direction (wall normal direction) and homogeneous in the x-direction, reducing the complexity of the RANS equations significantly. Derivatives of statistical variables are all assumed to vanish with respect to x and t, except the mean pressure gradient in the x-direction, as it serves as the driving force for the flow [49]. Thus, U is only a function of y and the mean

flow equations reduce to

$$0 = -\frac{1}{\rho}\frac{\partial P}{\partial x} + \frac{\partial}{\partial y}\left(\nu\frac{\partial U}{\partial y} - \overline{\boldsymbol{u}_x'\boldsymbol{u}_y'}\right) \tag{5.9}$$

$$0 = -\frac{1}{\rho}\frac{\partial P}{\partial y} - \frac{\partial}{\partial y}\left(-\overline{\boldsymbol{u}_y'\boldsymbol{u}_y'}\right). \tag{5.10}$$

Using the fact that $\partial_x(\overline{\boldsymbol{u}_y'\boldsymbol{u}_y'}) = 0$, we can differentiate the second equation with respect to x to show that $\partial_y\partial_x P = 0$ and, thus, the gradient of P is constant [49]. To simplify the presentation we set $1/\rho\frac{\partial P}{\partial x} = 1$ and control the dynamics of the flow purely through the Reynolds number. Combining this simplified form of the RANS equations with the Spalart-Allmaras turbulence model we arrive at the strong form of the equations for our problem. Let $D = (0, H)$, where H represents the half height of the channel,

$$1 = \frac{\partial}{\partial y}\left((\nu + \nu_T)\frac{\partial U}{\partial y}\right), \quad y \in D, \tag{5.11}$$

$$\begin{aligned} 0 = {} & c_{b1}\tilde{S}\tilde{\nu} - c_{w1}f_w\left(\frac{\tilde{\nu}}{y}\right)^2 \\ & + \frac{1}{\sigma_{\mathrm{SA}}}\frac{\partial}{\partial y}\left[\left((\nu + \tilde{\nu})\frac{\partial \tilde{\nu}}{\partial y}\right) + c_{b2}\left(\frac{\partial \tilde{\nu}}{\partial y}\right)^2\right], \quad y \in D. \end{aligned} \tag{5.12}$$

The RANS momentum equation is the first equation (5.11) and governs the behavior of the flow variable U; equation (5.12) is the transport equation for the Spalart-Allmaras working variable $\tilde{\nu}$. The equations are supplemented with the following boundary conditions:

$$\partial_y U(H) = 0, U(0) = 0, \qquad \tilde{\nu}(0) = 0, \partial_y\tilde{\nu}(H) = 0, \tag{5.13}$$

which amount to symmetry boundary conditions at the center of the channel ($\partial_y U(H) = 0$ and $\partial_y\tilde{\nu}(H) = 0$) and no slip conditions at the walls. We indeed

assume that the eddy viscosity is also symmetric across the channel and zero at the wall.

The weak formulations of equations (5.11) and (5.12) are derived in the typical manner of multiplying by a test function and integrating by parts. Let $\mathcal{V} = V \times V$ where $V = \{v \in H^1(D) | v(0) = 0\}$. Then the weak formulation of the problem is,

$$\begin{aligned} &\text{find } (U, \tilde{\nu}) \in \mathcal{V} \text{ such that,} \\ &\mathcal{B}\left((U, \tilde{\nu}); (v_u, v_{\tilde{\nu}})\right) = \mathcal{F}\left((v_U, v_{\tilde{\nu}})\right), \qquad \forall (v_U, v_{\tilde{\nu}}) \in \mathcal{V}, \end{aligned} \tag{5.14}$$

where

$$\mathcal{F}\left((v_U, v_{\tilde{\nu}})\right) = \int_0^H v_U dy \tag{5.15}$$

$$\mathcal{B}\left((U, \tilde{\nu}); (v_U, v_{\tilde{\nu}})\right) = \mathcal{B}_m\left((U, \tilde{\nu}); (v_U, v_{\tilde{\nu}})\right) + \mathcal{B}_t\left((U, \tilde{\nu}); (v_U, v_{\tilde{\nu}})\right), \tag{5.16}$$

and

$$\mathcal{B}_m\left((U, \tilde{\nu}); (v_U, v_{\tilde{\nu}})\right) = -\int_0^H \left((\nu + \nu_T)\frac{\partial U}{\partial y}\right) \frac{\partial v_U}{\partial y}\, dy, \tag{5.17}$$

$$\begin{aligned} \mathcal{B}_t\left((U, \tilde{\nu}); (v_U, v_{\tilde{\nu}})\right) = \int_0^H &\left[c_{b1}\tilde{S}\tilde{\nu} - c_{w1} f_w \left(\frac{\tilde{\nu}}{y}\right)^2\right] v_{\tilde{\nu}} \\ &- \frac{1}{\sigma_{\mathrm{SA}}}\left[\left((\nu + \tilde{\nu})\frac{\partial \tilde{\nu}}{\partial y}\right) + c_{b2}\left(\frac{\partial \tilde{\nu}}{\partial y}\right)^2\right] \frac{\partial v_{\tilde{\nu}}}{\partial y}\, dy. \end{aligned} \tag{5.18}$$

We obtain a computable system of equations using Newton's method, as in Chapter 3, i.e. by linearizing (5.14) about an approximate state $(U^h, \tilde{\nu}^h)$. We recall that the same $\mathcal{B}'$ will also be used to define the adjoint problem below.

In [104], Oliver and Moser use the entire velocity profile to calibrate their models, and the pointwise quantity of the centerline velocity as their

prediction quantity. As a representative of the full profile we will use the average of the mean flow velocity U over the entire domain as our quantity of interest,

$$\mathcal{Q}\left((U,\tilde{\nu})\right) = \int_0^H U \; dy. \tag{5.19}$$

Since the velocity profile is expected to reach the maximum at the centerline of the channel, the centerline velocity will contribute more to the quantity of interest than any other point in the channel. The adjoint problem is thus given by:

$$\begin{aligned} &\text{find } (z_U, z_{\tilde{\nu}}) \in \mathcal{V} \text{ such that} \\ &\mathcal{B}'\left((U,\tilde{\nu});(z_U,z_{\tilde{\nu}}),(v_U,v_{\tilde{\nu}})\right) = \mathcal{Q}\left((v_U,v_{\tilde{\nu}})\right), \qquad \forall (v_U,v_{\tilde{\nu}}) \in \mathcal{V}. \end{aligned} \tag{5.20}$$

The above equations will be solved using a standard continuous finite element discretization on D. We use piecewise linear approximations for U and $\tilde{\nu}$ and quadratic functions for their adjoints, z_U and $z_{\tilde{\nu}}$, respectively.

The equations presented in this section make up the necessary components of a goal-oriented error estimation and adaptivity framework. However, since we also wish to investigate the effect of uncertainty in the RANS turbulence model parameters, we should consider these equations as parameterized by a random variable ξ as we did in Chapter 4. We discuss the characterizations of the uncertain parameters in the subsequent section.

5.2.2 Models of parameter uncertainty

As we discussed previously, the Spalart-Allmaras turbulence model (5.3) and (5.5) involve many parameters, often assumed constant, whose values are

fixed as provided in Table 5.1.

In the present work, we will consider a subset of the model parameters to be random. In the study performed in [104], the authors considered seven parameters for calibration: $\kappa, c_{b1}, \sigma_{\mathrm{SA}}, c_{b2}, c_{v1}, c_{w2}, c_{w3}$. Ultimately we will fix c_{w3} and consider the remaining six parameters to be random variables; this change was motivated following a private communication from the authors concerning the poor calibration of c_{w3} and the adverse effects on the quality of the predictive models as a result. Initially, we will treat only κ as a random variable. Then we will model two parameters, κ and c_{v1} as random variables before proceeding with the full set of uncertain parameters. This will allow us to test the proposed surrogate models on simpler cases before applying the methodology to the full model.

We will model all parameters as uniform distributions between 0.5 and 1.5 times the nominal values listed in Table 5.1. This is in contrast to [104] where they used Gaussian distributions for the parameters. This discrepancy in the two analyses is purely due to the limitations of the available software for the construction of the adaptive surrogates; currently we are only able to construct surrogates based on uniformly distributed random variables. The option of choosing non-uniform distributions will be added to the software in a future effort. For the time being, our preliminary results compare favorably despite the differences in parameter distributions.

5.2.3 Adaptive surrogate model

As a first step in verifying our surrogate model for the RANS simulations, all parameters are set to their nominal value, except κ, which we model as a uniformly distributed random variable, $\kappa \sim \mathcal{U}(0.205, 0.615)$. The one parameter model is rather crude but allows for a comparison to the approximate distribution of the quantity of interest one would obtain using the exact forward model.

First, we introduce the non-dimensional variables, $U^+ = U/u_*$, $y_+ = yu_*/\nu$, where $u_* = \sqrt{\tau_w/\rho}$ is the friction velocity and τ_w is the wall shear stress. The log-law states that the non-dimensional velocity is governed by the relationship,

$$U^+ = \frac{1}{\kappa}\log(y_+) + B, \tag{5.21}$$

where κ is the von Karman constant and B is an integration constant. While this law does not hold throughout the channel, it does approximate the velocity well away from the wall where the magnitude of the velocity is small relative to the velocity far from the wall. Hence, in estimating our quantity of interest, i.e. the average velocity over width of the channel, it captures the basic dependence on the model parameter κ. Using the log-law an estimate of the distribution of $\mathcal{Q}((U, \tilde{\nu}))$ in terms of κ is obtained from the integral of (5.21),

$$\mathcal{Q}((U, \tilde{\nu})) \approx \int_0^H U^+ \, dy = \int_0^H \frac{1}{\kappa}\log(y_+) + BH, \tag{5.22}$$

$$= \frac{1}{\kappa} I + BH. \tag{5.23}$$

For the prediction scenario of $Re_\tau = u_* H/\nu = 5000$ and a channel half-height $H = 1$ the constants I and B were estimated from numerical results of the full model simulation and computed to be $I = 7.9385$ and $B = 4.4078$. Given the probability distribution for κ, p_κ, we can perform a standard change of variables to obtain the distribution of p_Q,

$$p_{\mathcal{Q}}(\mathcal{Q})\ d\mathcal{Q} = p_\kappa(\kappa)\ d\kappa \tag{5.24}$$

$$= p_\kappa \left(\frac{I}{\mathcal{Q} - B} \right) \left(\frac{I}{\mathcal{Q} - B} \right)^2\ d\mathcal{Q} \tag{5.25}$$

Figure 5.1 shows the distribution of samples obtained from the adapted surrogate model with a twelfth-order expansion in the κ parameter and the estimated theoretical distribution. We observe an excellent agreement between the two approaches, which suggests that the surrogate model accurately captures the forward distribution of the quantity of interest over the range of κ.

Next, we extend the analysis to a two-parameter model, with both κ and c_{v1} being uniformly distributed random variables. The same distribution as before is assumed for κ and we assume $c_{v1} \sim \mathcal{U}(3.55, 10.65)$. A kernel density estimate of the distribution obtained from the two-parameter Spalart-Allmaras model is shown in Figure 5.2 along with the distribution obtained from a surrogate with twelfth-order expansion in both variables. The overall accuracy, computed with the error estimates proposed in Chapter 4, also suggests an adequate resolution of the model with an estimate of $\left\| \mathcal{Q}(u) - \mathcal{Q}(u^{h,N}) \right\|_{L^2(\Xi)} \approx \eta = 1.316793e-04$.

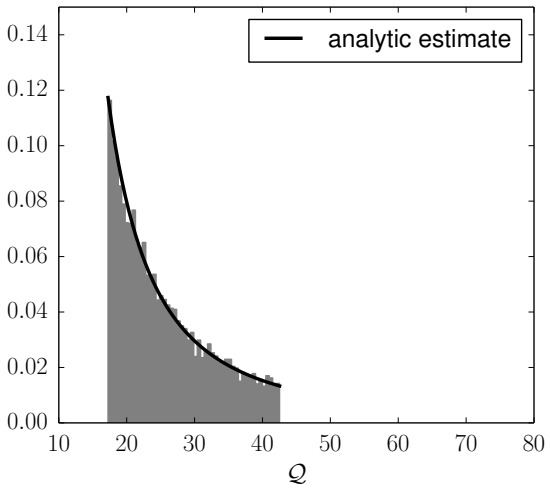

Figure 5.1: Histogram for samples of the average velocity from the one parameter (κ) Spalart-Allmaras turbulence model.

Finally, we construct a surrogate using all six uncertain model parameters. We employ the adaptive methodology developed in Chapter 4, to guide the construction of an anisotropic surrogate model. While we do not have an estimate of the exact distribution for the quantity of interest generated by the full forward model, we can sample from the parameter distribution and run the forward model to obtain samples of the quantity of interest. Comparing the full model distribution with the surrogate distribution over the range of the parameters, see Figure 5.3, we observe good agreement between kernel density estimates obtained from the full and surrogate models. The posterior obtained using the surrogate model is slightly narrow, which can be attributed to the uniform distribution of the parameters compared to the Gaussian distribution

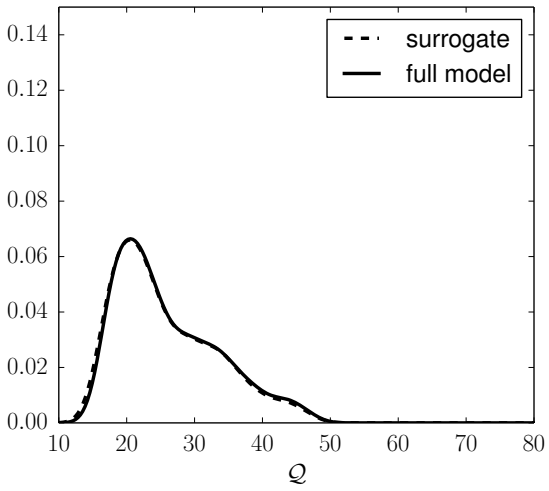

Figure 5.2: Kernel density estimates of the average velocity from the two-parameter (κ, c_{v1}) Spalart-Allmaras turbulence model.

used for the full model simulation.

Figure 5.4 shows the convergence of the error estimate for the surrogate model. Compared to uniform, or isotropic p-refinement, the anisotropic refinement of the surrogate model leads to significant improvement of the error for an equal number of forward model evaluations, roughly two orders of magnitude reduction. In Table 5.2 we show the progression of the expansion order for the six parameters in the model. We can see that the initial refinements are associated with the κ and c_{v1} parameters, demonstrating that their values have the greatest influence on the quantity of interest. This is in agreement with [104], where they showed that the posteriors were maximized near the nominal values, indicating that deviations from these values were not consis-

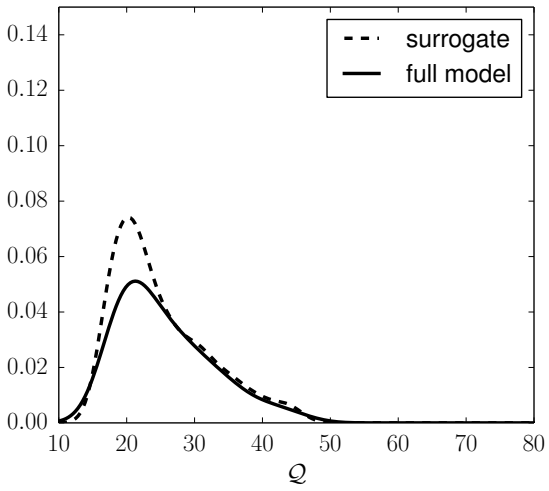

Figure 5.3: Kernel density estimates of the average velocity from the six-parameter Spalart-Allmaras turbulence model.

tent with the observed data. Following initial refinement of κ and c_{v1} we see continued increase in the expansion order for κ, which we would expect to see since it has a significant impact on the flow velocity away from the wall where the velocity is higher and thus contributes more significantly to the average. Refinements are suggested for all model parameters, though c_{b2} is only modeled linearly, suggesting that the gradient of the working variable $\tilde{\nu}$ does not have a notable impact on the average velocity. Ultimately, we expected to see a greater expansion order for c_{v1} than the other model parameters besides κ. We believe that the positive correlation between κ and c_{v1}, seen in the posterior distributions discussed in [104], contributed to refinement of only one of the two parameters being sufficient to accurately estimate the quantity of

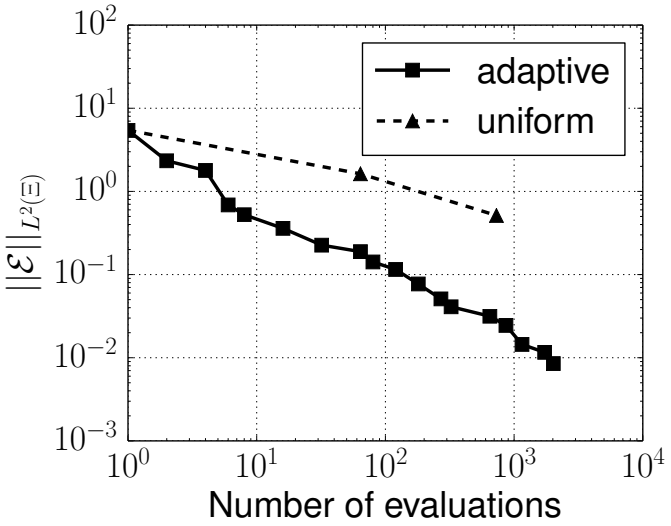

Figure 5.4: Convergence of error estimate for adaptive surrogate of Spalart-Allmaras turbulence model with six uncertain parameters.

interest.

5.3 Efficient Bayesian inference using surrogates

Recently, there has been increased popularity in the use of Bayesian inference techniques for uncertainty quantification [80, 85, 90, 89, 87, 115]. When calibrating an approximate model to experimental data, instead of the one best parameter value provided by traditional deterministic calibration methodologies, Bayesian techniques allow for a probabilistic description of calibration parameters. However, the additional information that one gains about the parameters in this process often comes with a substantial increase in computational cost. One proposal to mitigate the additional cost is through the

iteration	κ	c_{b1}	σ_{SA}	c_{b2}	c_{v1}	c_{w2}
1	0	0	0	0	0	0
2	1	0	0	0	0	0
3	1	0	0	0	1	0
4	2	0	0	0	1	0
5	3	0	0	0	1	0
6	3	0	1	0	1	0
7	3	1	1	0	1	0
8	3	1	1	0	1	1
9	4	1	1	0	1	1
10	4	2	1	0	1	1
11	4	2	2	0	1	1
12	4	2	2	0	2	1
13	5	2	2	0	2	1
14	5	2	2	1	2	1
15	5	2	3	1	2	1
16	5	3	3	1	2	1
17	5	3	3	1	2	2
18	6	3	3	1	2	2

Table 5.2: Expansion orders for parameters in adaptive surrogate of Spalart-Allmaras turbulence model.

use of approximate response surface models, or surrogates [80, 85, 90, 89, 87], similar to those constructed in the previous Chapter.

In this section we briefly review the elements of Bayesian inference and model selection and discuss some recent advances in efficient calibration using surrogate models.

5.3.1 Overview of Bayesian inference

Baye's theorem is a fundamental result of statistics and probability. Relatively recently, it has been adapted toward parameter identification for

complex mathematical models. The advantage of Bayesian inference for model calibration is that it provides for a distribution of probable parameter values instead of the one best fitting parameter value obtained from traditional optimization procedures. Bayesian parameter identification can be interpreted as an update of the degree of belief in the parameters.

The solution of the Bayesian calibration procedure is the posterior pdf, or the conditional distribution of the model parameters given the observed data. Let $\boldsymbol{q} \in \mathbb{R}^n$ represent the vector of calibration data, or observations, and let $\boldsymbol{\xi} \in \Xi = \mathbb{R}^m$ be the random variable representing the model parameters we wish to calibrate. The prior distribution of the parameters is denoted by $p(\boldsymbol{\xi})$ and encapsulates the prior knowledge one has about the parameters independent of the calibration data. Bayes theorem then states that the posterior distribution, $p(\boldsymbol{\xi}|\boldsymbol{q})$ is proportional to the prior times the likelihood $L(\boldsymbol{\xi}, \boldsymbol{q})$ of observing the data [35, 78],

$$p(\boldsymbol{\xi}|\boldsymbol{q}) = \frac{L(\boldsymbol{\xi}|\boldsymbol{q})\ p(\boldsymbol{\xi})}{p(\boldsymbol{q})}. \tag{5.26}$$

More specifically, the likelihood is defined by the conditional distribution of the data as a function of the parameters $L(\boldsymbol{\xi}|\boldsymbol{q}) = p(\boldsymbol{q}|\boldsymbol{\xi})$, but to emphasize the dependence on the value of the parameters it is often written in the former notation. The denominator in Bayes theorem acts as a normalization constant and using the law of total probability can be expressed as,

$$p(\boldsymbol{q}) = \int_{\Xi} p(\boldsymbol{q}|\boldsymbol{\xi}) p(\boldsymbol{\xi}) d\boldsymbol{\xi}. \tag{5.27}$$

This quantity plays a crucial role in model comparison as we will see in the following section on model selection.

Perhaps the most critical component of the Bayesian framework is the likelihood function. Ideally the likelihood is determined by the measurement process, or any other process contributing to uncertainty in the calibration data. For example, if the measurement error is additive, meaning the observations take the form,

$$\boldsymbol{q} = M(\boldsymbol{\xi}) + \boldsymbol{\varepsilon}, \tag{5.28}$$

where $M(\boldsymbol{\xi})$ is the predicted value of $\boldsymbol{q}$ using the model with parameters $\boldsymbol{\xi}$ and $\boldsymbol{\varepsilon} \in \mathbb{R}^n$ is the error model with distribution $p_{\boldsymbol{\varepsilon}}$, then the likelihood is given by

$$L(\boldsymbol{\xi}|\boldsymbol{q}) = p_{\boldsymbol{\varepsilon}}\left(\boldsymbol{q} - M(\boldsymbol{\xi})\right). \tag{5.29}$$

In practice, while one might have a decent estimate of the uncertainty in measurements, it is often difficult to fully characterize the distribution of experimental uncertainty. For this reason, it can be beneficial to use a model selection procedure to determine the best choice of uncertainty model.

5.3.2 Bayesian model selection

We resort here to a Bayesian model selection procedure that quantitatively compares a set of models to decide which uncertainty description most likely matches the data. We will only consider the methodology to select the most probable model among a class of uncertainty models, but one can just as well employ the technique to decide between models governing the physical

response of a system, such as different RANS closure models, or a combination of physical and uncertainty models [104].

In the Bayesian model comparison procedure, the respective models are evaluated on the basis of the model posterior plausibility. Given a set of models $\mathcal{M} = \{M_1, M_2, \ldots, M_n\}$, model plausibility quantifies the relative probability with which model M_i actually generates the observed data [77]. Again, we let $\boldsymbol{q}$ represent the calibration data and employ Baye's theorem to define the plausibility for model M_i by

$$p(M_i|\boldsymbol{q}, \mathcal{M}) = Cp(\boldsymbol{q}|M_i, \mathcal{M})\ p(M_i|\mathcal{M}), \tag{5.30}$$

where C is a normalization constant similar to that in (5.26), $p(\boldsymbol{q}|M_i, \mathcal{M})$ acts like a likelihood for model M_i, and $p(M_i|\mathcal{M})$ is the prior model plausibility. The likelihood of the model is given by the evidence, which is simply the normalization constant discussed in the previous section, conditioned on model M_i,

$$E(M_i|\boldsymbol{q}, \mathcal{M}) := p(\boldsymbol{q}|M_i, \mathcal{M}) = \int_{\Xi} p(\boldsymbol{q}|\xi, M_i, \mathcal{M}) p(\xi|M_i, \mathcal{M})\ d\xi, \tag{5.31}$$

and it measures the probability of observing data $\boldsymbol{q}$ given the model M_i. The evidence is used to compare models relative to one another and to identify the model that is most likely capable of reproducing the data. In regards to the prior plausibility, one often chooses a uniform plausibility across the collection of models; if all models are equally likely candidates, then the natural choice for the prior is simply $p(M_i|\mathcal{M}) = 1/n$ for each model.

We have explicitly left $\mathcal{M}$ in the conditional distributions above since the whole process is strictly conditional on the original set of models. In other words, only the models included in the set $\mathcal{M}$ are evaluated, thus any conclusions or observations resulting from the quantitative analysis are limited by the quality of the models under consideration; the process can not be used to identify a *truth* model unless it is present in $\mathcal{M}$.

5.3.3 Computational considerations

To this point, we have ignored the computational costs associated with Bayesian inference, when in fact, it is often the primary complaint of its opponents. Computational costs are driven up by the need for repeated sampling of the forward model, often requiring the solution of initial and/or boundary-value problems. This suggests two obvious avenues to improve efficiency: better sampling techniques or a reduced forward model.

Without question the most popular sampling technique for Bayesian inference is the Markov Chain Monte Carlo (MCMC) method. MCMC involves the process of generating a proposal value for the calibration parameters ξ, in the most straightforward case, from the prior distribution, and accepting or rejecting the sample as a representative of the posterior based on specific criteria. The process is repeated as many times as necessary until the desired number of posterior samples are obtained. Since some samples will be rejected, a number of model solves will result in wasted computations. An improved rejection rate can lead to more efficient samplers; numerous variants of the ba-

sic MCMC algorithm have been developed with this in mind, beginning with the seminal works of Metropolis et al. [93], Hastings [73], and Geman and Geman [64]. Popular modern techniques include delayed rejection methods [72] and importance sampling [66], among others. A detailed discussion of MCMC is beyond the scope of the present work, see [24, 35, 63, 70, 78] and the references therein for a more in depth description of the Metroplis-Hastings and Gibbs sampling procedures, as well as other modern techniques.

For sampling posterior distributions in the present work, we rely on the open-source statistical library QUESO [107]. Specifically, we make use of the Hybrid Gibbs Transitional Markov Chain Monte Carlo method [39] implemented in the package. In addition to being a rather efficient technique, this choice is motivated by the fact that it is also the sampler used in [104]. Furthermore, the fact that it is written in C++ makes it an obvious candidate for easy interfacing with the other computational codes used in this work (libMesh, GRINS, agnos[1], etc.).

Instead of emphasizing efficient sampling techniques, we propose here to address the issue related to the cost of the forward model; indeed, reducing the cost of the forward model has the added advantage that it can be used with any of the state of the art sampling techniques to achieve even greater efficiency. However, since MCMC relies on the acceptance and rejection of repeated samples of the model, it is crucial to ensure that the accuracy of the

[1]agnos is a C++ library for adaptive surrogate construction based on the methodology of Chapter 4 and was developed solely by the author for the purpose of this work.

surrogate approximation is adequate to produce results of comparable quality to the full simulation. Thus, the addition of error estimates and solution verification for surrogate models is even more appealing.

In the last few years the use of surrogate models in Bayesian inference has received a fair amount of attention [85, 87, 88, 89, 90]. Marzouk and Xiu [89] provide a detailed error analysis for the stochastic collocation method assuming Gaussian errors; we will examine their results in more detail below. Ma and Zabaras [87] adopt a similar approach, using the adaptive hierarchical sparse grid collocation method for the surrogate approximation, but they omit a thorough theoretical error analysis. Alternatively, Marzouk et al. [88, 89], introduce a Karhunen-Loève expansion based on the prior distribution of parameters, arguing that this representation captures variation in the field more adequately than directly applying a generalized polynomial chaos approximation to the uncertain variables. Unlike [89] though, a relationship between the projection of the Karhunen-Loève expansion and the resulting posterior error is not provided. Li and Marzouk [85] extend the theoretical foundations from [89] to an optimization technique for minimizing the error in the posterior probability. The theoretical results of Marzouk and Xiu provide an opportunity for the natural extension of our results presented in Chapter 4; we can efficiently set a tolerance on how accurate the surrogate should be in order to guarantee final accuracy of the posterior distribution of the parameters relative to the complete forward model. Moreover, the proposed adaptive refinement schemes have the capability of constructing a sufficiently accurate

surrogate model in an efficient manner.

We briefly review the applicable results from Marzouk and Xiu [89]. As indicated above, the basic idea is to replace the forward model with the surrogate in the Bayesian calibration process, thus resulting in an approximate posterior

$$\tilde{p}^N(\xi) = \frac{\tilde{L}^N(\xi|q)p(\xi)}{\int \tilde{L}^N(\xi|q)p(\xi)}, \tag{5.32}$$

where $p(\xi)$ is the prior density and $\tilde{L}^N$ is the approximate likelihood obtained from replacing the forward model M with the surrogate model $\tilde{M}^N$. The superscript N refers here to the expansion order of the surrogate approximation while the symbol $\tilde{}$ denotes the use of the pseudo-spectral polynomial chaos expansion, $\tilde{M}^N(\xi) = \sum_{k\in\mathcal{I}_N} M_k^m \Psi_k(\xi)$, where the coefficients M_k^m are obtained using quadrature (see Chapter 4). Since $\tilde{M}^N$ can be evaluated with minimal computational cost compared to the numerical solution of a partial differential equation, we will be able to sample the posterior distribution with a high level of accuracy [89].

Remark 5.3.1. The posterior $\tilde{p}^N$ is the posterior distribution of the parameters under the assumption that the predictions of the observed data were generated from the surrogate model. For this reason it is vital that the surrogate being evaluated is accurate to the desired level of sampling error.

The authors in [89] also make use of the *exact* expansion of the model output and associated likelihood,

$$M^N(\xi) = \sum_{k\in\mathcal{I}_N} M_k \Psi_k(\xi), \tag{5.33}$$

$$p^N(\xi|q) = \frac{L^N(\xi|q)p(\xi)}{\int L^N(\xi|q)p(\xi)}. \tag{5.34}$$

In contrast to the surrogate expansion, the exact expansion contains the exact coefficients resulting from the projection of the full model onto the basis Ψ_k, and it allows for the application of some additional theoretical results used below.

They also suggest the use of the Kullback-Leibler divergence to quantify the difference between the approximate posterior $\tilde{p}$ and the exact posterior p,

$$D_{\mathrm{KL}}(\tilde{p}||p) = \int \tilde{p}(\xi) \log\left(\frac{\tilde{p}(\xi)}{p(\xi)}\right) d\xi. \tag{5.35}$$

Provided that the observational errors are independent and identically distributed (iid) with a Gaussian distribution, they demonstrate a series of results for the exact projection M^N, which we restate here without proof. First they establish a bound on the difference in the model evidence $E^N := E(M^N|q)$ and $E := E(M|q)$ as defined in (5.31), and thus prove that the convergence of the polynomial chaos expansions implies convergence of the Kullback-Leibler divergence.

Lemma 5.3.1. *Assume that the observational error $\boldsymbol{\varepsilon} \in \mathbb{R}^n$ in (5.29) are iid Gaussian distributed. If M^N converges to M as*

$$\left\|M - M^N\right\|_{L^2(\Xi)} \leq CN^{-\alpha}, \tag{5.36}$$

where C is a constant independent of N and $\alpha > 0$ depends on the regularity of M, then the following relationship holds for the evidence $E^N = \int L^N(\xi)d\xi$,

$$\left|E^N - E\right| \leq C_1 \prod_i^n \left\|M_i - M_i^N\right\|_{L^2(\Xi)}, \tag{5.37}$$

Moreover, the posterior probability p^N converges to p in the sense that the Kullback-Leibler divergence converges to zero,

$$D_{KL}(p^N||p) \to 0, \qquad N \to \infty. \tag{5.38}$$

Making use of the *a priori* convergence estimates for polynomial chaos expansion, Marzouk and Xiu establish two additional relationships for E and E^N.

Lemma 5.3.2. *Assume the convergence of M^N is in the form* (5.36)*. Then, for sufficiently large N,*

$$\left|\frac{E}{E^N} - 1\right| \leq \frac{C_E N^{-\alpha n}}{1 - C_E N^{-\alpha n}} \sim N^{-\alpha n}, \tag{5.39}$$

$$\left|\log\left(\frac{E}{E^N}\right)\right| \leq \left|\log\left(1 - C_E N^{-\alpha n}\right)\right| \sim N^{-\alpha n}, \tag{5.40}$$

where $C_E = C_1/E$ is independent of N with C_1 given in (5.37)*.*

The first major theoretical result in [89] follows from the previous two lemmas and provides an estimate of the convergence rate for the Kullback-Leibler divergence between the posterior for the exact expansion p^N and the true posterior p.

Theorem 5.3.3. *Assume that the observational error is iid Gaussian and the generalized polynomial chaos M^N of the forward model converges to M, then*

for sufficiently large N

$$D_{KL}(p^N||p) \leq \frac{C_2}{2\sigma^2 E}\left(1+\left|\frac{E}{E^N}-1\right|\right)\sum_i^n \left\|M_i^N - M_i\right\|_{L^2(\Xi)} + \left|\log\left(\frac{E}{E^N}\right)\right| \tag{5.41}$$

$$\sim N^{-\alpha} \tag{5.42}$$

In order to extend the result to the approximate posterior $\tilde{p}^N$, they make use of the following relationship,

$$D_{\mathrm{KL}}(\tilde{p}^N||p) = \int \tilde{p}^N(\xi)\log\left(\frac{\tilde{p}^N(\xi)}{p(\xi)}\right)d\xi \tag{5.43}$$

$$= \int \tilde{p}^N(\xi)\log\left(\frac{\tilde{p}^N(\xi)}{p^N(\xi)}\right)d\xi + \int \tilde{p}^N(\xi)\log\left(\frac{p^N(\xi)}{p(\xi)}\right)d\xi \tag{5.44}$$

$$= D_{\mathrm{KL}}(\tilde{p}^N||p^N) + D_{\mathrm{KL}}(p^N||p) + \int (\tilde{p}^N(\xi)-p^N(\xi))\log\left(\frac{p^N(\xi)}{p(\xi)}\right)d\xi \tag{5.45}$$

The final result guarantees the convergence of the surrogate posterior to the true posterior.

Theorem 5.3.4. *If the convergence of p^N is in the form* (5.36) *and $\tilde{M}^N$ converges to M^N as the number of quadrature points goes to infinity, i.e.*

$$\lim_{m(N)\to\infty} \tilde{p}^N(\xi) = p^N(\xi), \quad \forall\xi, \tag{5.46}$$

then the surrogate posterior density $\tilde{p}^N$ converges to the true density p in the following sense,

$$D_{KL}(\tilde{p}^N||p) \to 0, \quad N\to\infty, \quad m(N)\to\infty. \tag{5.47}$$

Unfortunately, above results cannot be directly applied to the case at hand. Indeed, only one of the error models examined in [104] satisfies the independent assumption. Moreover, another issue lies in the fact that the approximation error is defined with respect to the expansion of the observables used in the calibration process. In our case the quantity of interest used to define the error estimates is not the same quantity for which observable data is available. If we were to use experimental data for $\mathcal{Q}$ in the calibration process *and* employ the independence assumption, then the results of Marzouk and Xiu would be applicable. Future works will aim to extend the theoretical results to the present setting, but for the sake of the current discussion, we will limit ourselves to the comparison of our numerical results for the surrogate posterior with those obtained by Oliver and Moser [104].

5.4 Numerical results

Equipped with the Bayesian techniques reviewed in the previous section, we now return to the channel flow problem detailed in Section 5.2. As we eluded to in the Bayesian discussion, identifying the proper uncertainty model, or likelihood function, is often a difficult task. Since our quantity of interest is a function of the mean flow properties, one may argue that a model based entirely on the uncertainty in the mean flow may be sufficient. However, if one wishes to predict quantities beyond this relatively simple case, a more complex uncertainty model may be necessary.

In the present study, the calibration data are obtained from direct nu-

merical simulation (DNS) of the flow, while our computational model relies on the eddy viscosity assumption and the Spalart-Allmaras turbulence model. In essence, the uncertainty results from the approximation of the Reynolds stress tensor [104].

We will encompass both scenarios by considering three uncertainty models in terms of the mean flow velocity, as well as an uncertainty model that is based directly on the Reynolds stress.

5.4.1 Calibration data

Specifically, we use the same calibration data as Oliver and Moser [104], which was obtained from the DNS of Jaminez et al. [74, 45]. Mean velocity measurements were taken at $Re_\tau = 944$ and $Re_\tau = 2003$. The uncertainty in the observations from the direct simulation is the result of calculating the sample mean rather than the true mean. The authors of [75] provide an estimate of the variance in the error, however the covariance between data points in the profile is not provided. To minimize the impact of the correlation between measurement points, Oliver and Moser [104] downsample the data and use points that are farther apart; we will do the same and assume the data points are independent.

Since the simulation of the channel flow is dependent on the Reynolds number Re_τ, we will construct two surrogate models, one for each flow scenario. Technically, one could attempt to construct a projection of the mean velocity whose coefficients are dependent on the Reynolds number, in addition to the

location in the channel. We choose not to do this here because of the interface required between the channel simulation code and the code used to perform the goal-oriented adaptivity of the surrogate model. This does however increase the computational burden of our approach.

For all error models we will use the same surrogate construction for the approximate forward models. As we did in the examination of the forward model, we will perform a series of three studies, starting with only κ being uncertain, adding c_{v1} as an uncertain parameter, followed by including all six uncertain parameters used in Section 5.2.2. These sets of parameters are naturally augmented with the calibration parameters for the uncertainty models considered. In all cases we will use the same two surrogate models for the forward model simulations ($Re_\tau = 944$ and $Re_\tau = 2003$). In the one- and two-parameter cases, we use twelfth-order expansions for the uncertain turbulence model parameters, resulting in computed error of $\eta_{944} = 1.441803 \times 10^{-2}$ and $\eta_{2003} = 1.655369 \times 10^{-2}$, for the one-uncertain-parameter case, and $\eta_{944} = 2.489478 \times 10^{-2}$, $\eta_{2003} = 1.655369 \times 10^{-2}$, for the models with two uncertain parameters. When modeling six uncertain parameters we will use the final expansion order in Table 5.2, $\mathcal{N} = (6, 3, 3, 1, 2, 2)$, which yields error estimates $\eta_{944} = 1.388788 \times 10^{-2}$ and $\eta_{2003} = 1.878746 \times 10^{-2}$.

5.4.2 Multiplicative error models

We begin with a class of relatively simple models based on the mean velocity. We suppose that the error is multiplicative in terms of the velocity.

Thus, the observed data is taken to be governed by the equation,

$$\langle u \rangle^+ (z;\xi) = (1 + \boldsymbol{\varepsilon}(z;\xi))U^+(z;\xi), \tag{5.48}$$

where $z = y/H$ is the non-dimensionalized wall-normal coordinate, $U^+ = U/u_*$ is the non-dimensionalized velocity, and $\langle u \rangle^+$ is the prediction of the true non-dimensionalized velocity. We assume a zero-mean Gaussian field for the error term $\boldsymbol{\varepsilon} = \boldsymbol{\varepsilon}(z) = \boldsymbol{\varepsilon}(z;\xi)$. The choice of the covariance of $\boldsymbol{\varepsilon}$ distinguishes the three uncertainty models governed by (5.48).

5.4.2.1 Independent homogeneous covariance

First, we will adopt the belief that the data points provided in the DNS calibration data are independent. The covariance of $\boldsymbol{\varepsilon}$ is thus,

$$\langle \boldsymbol{\varepsilon}(z)\boldsymbol{\varepsilon}(z') \rangle = \sigma^2 \delta(z - z'), \tag{5.49}$$

where the standard deviation σ will be treated as an unknown parameter in the calibration process, in addition to the turbulence model parameters.

It is unreasonable to expect that the error along the mean velocity profile generated by DNS is spatially independent. Subsequent models will introduce spatial correlations in the velocity. Nonetheless, its simplicity makes it an attractive model to consider.

Using the surrogate models to evaluate $\tilde{U}^+$ instead of the full channel flow simulation, U^+, we define the likelihood for the uncertainty model

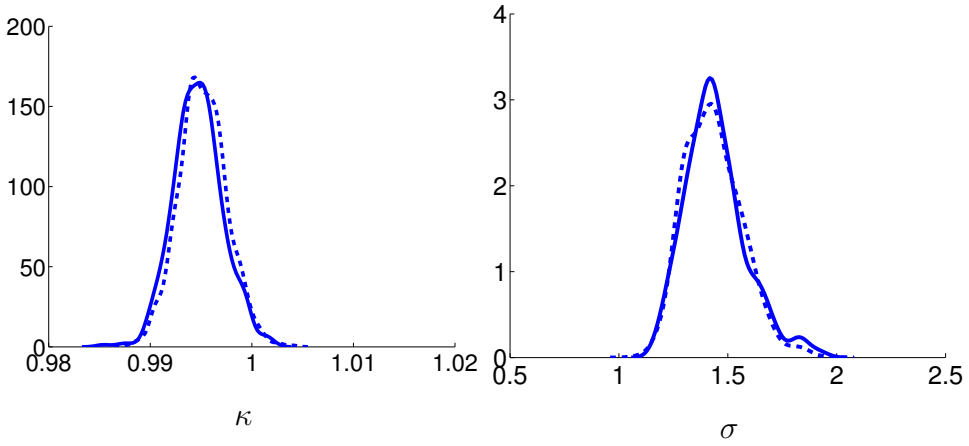

Figure 5.5: Posterior probability densities for the multiplicative error model with independent homogeneous covariance for the SA turbulence model with uncertain κ. Full model (solid line) and surrogate model (dashed), where 1 indicates nominal value.

in (5.48) with covariance (5.49) as

$$L_{Re_\tau}(\xi|q) = \prod_i^n p_{\varepsilon_i}\left(\frac{q_i}{\tilde{U}_i^+(z;\xi)} - 1\right), \tag{5.50}$$

where $\xi = \{\kappa, \sigma\}$. Kernel density estimates of the posterior densities resulting from the Bayesian calibration are shown in Figure 5.5. We see excellent agreement between the posteriors obtained from the full model simulation and our surrogate model. Moving on, we do the same analysis for the model with two uncertain parameters to obtain the densities in Figure 5.6. Again, the posterior distributions obtained from the full model and the surrogate model match rather well.

Finally we turn to the Spalart-Allmaras turbulence model with six uncertain parameters, using the surrogates with anisotropic expansion order

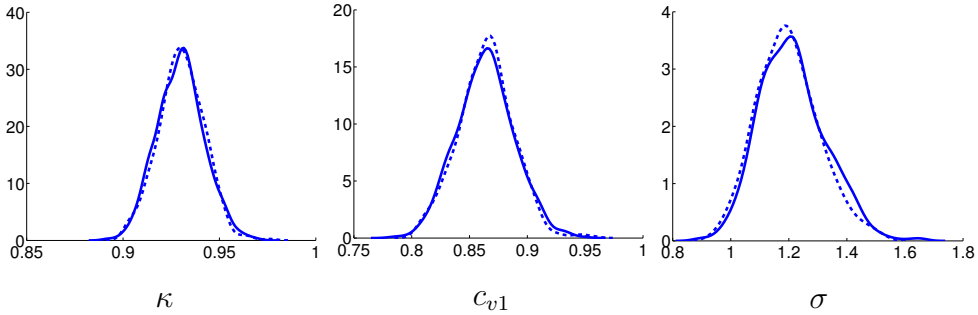

Figure 5.6: Posterior probability densities for the multiplicative error model with independent homogeneous covariance for the SA turbulence model with uncertain κ and c_{v1}. Full model (solid line) and surrogate model (dashed), where 1 indicates nominal value.

$\mathcal{N} = (6, 3, 3, 1, 2, 2)$. The posterior distributions in Figure 5.7 again appear to be well modeled using the surrogate model. Results for the full set of parameters are rather promising. While some minor differences are observed in the posterior distributions, overall the agreement is quite good. We can attribute what differences that do exist to the choice of prior distributions; since the uniform priors are more restrictive we see posteriors that are limited to the support of the prior as in the case of c_{b2} and c_{w2}.

5.4.2.2 Correlated homogeneous covariance

A straightforward extension of the independent multiplicative model proposed in the previous section is to add spatial correlation into the definition of the covariance for $\boldsymbol{\varepsilon}$. If we assume a homogeneous correlation length, we can write the covariance of $\boldsymbol{\varepsilon}$ as

$$\langle \boldsymbol{\varepsilon}(z)\boldsymbol{\varepsilon}(z')\rangle = \sigma^2 \exp\left(-1/2\frac{(z-z')^2}{l^2}\right), \tag{5.51}$$

where now both σ and the correlation length l are additional calibration parameters. Combined with the multiplicative form (5.48) this represents a complete characterization of the uncertainty in the mean flow velocity. While undoubtedly more reasonable than independent errors, a homogeneous correlation length still seems improbable; generally the accuracy of the turbulence models near the wall considerably differs from that in the region far from the wall.

We again examine the three sets of uncertain parameters starting with just κ and the additional parameters introduced by the covariance function, σ and l. Posterior probability densities obtained with the surrogate models are compared to those from the full model in Figure 5.8. As before, we move on to the case of two uncertain parameters. Posterior densities exhibit similar behavior as in the previous model, Figure 5.9. For the Spalart-Allmaras turbulence model with six uncertain parameters, we see similar results to that of the inhomogeneous covariance function, with the posteriors for κ and c_{v1} in Figure 5.10 showing some differences compared to the full model results.

5.4.2.3 Correlated inhomogeneous covariance

Since length scales in turbulent flows are set differently based on the region of the flow, it makes sense to incorporate that structure in the uncertainty model. While we keep the assumption of a multiplicative error model (5.48), we choose a covariance function with a variable length scale [104, 111],

$$\langle \boldsymbol{\varepsilon}(z)\boldsymbol{\varepsilon}(z')\rangle = \sigma^2 \left(\frac{2l(z)l(z')}{l^2(z)+l^2(z')}\right)^{1/2} \exp\left(-\frac{(z-z')^2}{l^2(z)+l^2(z')}\right), \qquad (5.52)$$

again, σ is a calibration parameter, and the length scale function $l(z)$ is given by,

$$l(z) = \begin{cases} l_{\text{in}} & \text{for } z < z_{\text{in}} \\ l_{\text{in}} + \frac{l_{\text{out}} - l_{\text{in}}}{z_{\text{out}} - z_{\text{in}}}(z - z_{\text{in}}) & \text{for } z_{\text{in}} \leq z \leq z_{\text{out}} \\ l_{\text{out}} & \text{for } z > z_{\text{out}}, \end{cases} \tag{5.53}$$

where $l_{\text{in}} = l_{\text{in}}^{+}/Re_{\tau}$, $z_{\text{in}} = z_{\text{in}}^{+}/Re_{\tau}$, and l_{in}^{+}, z_{in}^{+}, l_{out}, and z_{out} are additional calibration parameters.

Posterior probability densities using this variable length covariance structure indicate similar agreement as in the previous two multiplicative error models for all turbulence model parameters. Very little difference is seen between the posteriors with one or two uncertain parameter, see Figures 5.11 and 5.12. Note that Figure 5.13 actually shows better agreement between the posterior distributions for κ and c_{v1} than the results obtained using the homogeneous covariance structure.

We expect the final model based on the multiplicative error assumption (5.48) to be superior to the two simpler models. Nonetheless, it represents an uncertainty model based on the mean flow velocity only. If we truly hope to capture uncertainty in the RANS model we should focus on the uncertainty associated with the Reynolds stress tensor.

5.4.3 Reynolds stress uncertainty model

Finally, we introduce an uncertainty model based on the Reynolds stress. While more complex, and thus more difficult to implement in practice, a Reynolds stress uncertainty model is appealing since it directly targets

the source of error.

The uncertainty model for Reynolds stress proposed by Oliver and Moser [104], takes the form,

$$\left\langle \boldsymbol{u}_i' \boldsymbol{u}_j' \right\rangle^+ (z;\xi) = T^+(z;\xi) - \boldsymbol{\varepsilon}(z;\xi) \tag{5.54}$$

where T^+ is the Reynolds shear stress computed by the approximate turbulence model, $\boldsymbol{\varepsilon}$ represents the error field as before, and $\left\langle \boldsymbol{u}_i' \boldsymbol{u}_j' \right\rangle^+$ is the predicted Reynolds stress.

Note that (5.54) does not lead to a prediction of the mean velocity explicitly; in order to predict the mean flow one must first compute the Reynolds stress T^+ governed by the turbulence model. Then the predicted Reynolds stress $\left\langle \boldsymbol{u}_i' \boldsymbol{u}_j' \right\rangle^+$ obtained from (5.54) is used to complete the momentum equations,

$$-\frac{d}{dz}\left(\frac{1}{Re_\tau}\frac{d\left\langle u \right\rangle^+}{dz} - \left\langle \boldsymbol{u}_i' \boldsymbol{u}_j' \right\rangle\right) = 1, \tag{5.55}$$

which must then be solved for the mean velocity $\langle u \rangle^+$. As a result, realizations of the solution do not necessarily satisfy the turbulence momentum equations (5.11) [104].

We must still choose a description for the error field $\boldsymbol{\varepsilon}$. Sticking with [104], we assume a zero-mean Gaussian with covariance,

$$\langle \boldsymbol{\varepsilon}(z)\boldsymbol{\varepsilon}(z') \rangle = k_{\text{in}}(z,z') + k_{\text{out}}(z,z'), \tag{5.56}$$

where k_{in} models the error near the wall and k_{out} represents the error far from

the wall. The choices made in [104] are,

$$k_{\text{in}}(z,z') = \sigma_{\text{in}}^2 \left(1 - \frac{(z-z')^2}{l_{\text{in}}^2} - \frac{(z-z')^2}{\Delta^2} - \frac{l_{\text{in}}^2 z z'}{\Delta^2 \Delta^2}\right) \times \exp\left(-\frac{1}{2}\frac{(z-z')^2}{l_{\text{in}}^2} - \frac{1}{2}\frac{(z^2+z'^2)^2}{\Delta^2}\right), \tag{5.57}$$

$$k_{\text{out}}(z,z') = \sigma_{\text{out}}^2 \left(1 - \frac{(z-z')^2}{l_{\text{out}}^2}\right) \exp\left(-\frac{1}{2}\frac{(z-z')^2}{l_{\text{out}}^2}\right), \tag{5.58}$$

where $l_{\text{in}} = l_{\text{in}}^+/Re_\tau$, $\Delta = C_d l_{\text{in}}$ and $\sigma_{\text{out}} = C_s/Re_\tau$. The additional calibration parameters for this uncertainty model are σ_{in}, l_{in}^+, C_d, C_s, l_{out}.

Even though the Reynolds stress uncertainty model differs significantly from the three multiplicative error models discussed above, Bayesian calibration with all of the models leads to qualitatively similar results. The one-parameter model shows relatively good agreement for all of the parameters, see Figure 5.14, while some discrepancies for models with two and six uncertain parameters are observed, Figures 5.15 and 5.16, respectively.

The Reynolds stress uncertainty model, while appealing from a theoretical standpoint, may be overly complex for the problem considered here. Oliver and Moser concluded that this stochastic model was superior to the multiplicative error models, however the multiplicative model with correlated inhomogeneous covariance was almost as good and is easier to implement in practice; moreover the additional PDE solve for the Reynolds stress uncertainty model makes it more computationally intensive than the multiplicative approach. In the next section we will carry out a similar Bayesian model comparison leading to similar conclusions.

5.4.4 Model selection

Some of the above models are obviously deficient while others may be overly complex for the present analysis; all models are now evaluated based on their agreement with the calibration data. With the model set $\mathcal{M}$ comprised of the four models proposed in this section, we are prepared to move forward with the application of the Bayesian model comparison procedure to our adaptive surrogate model for the turbulent channel flow problem.

In [104], the authors examine four turbulence models in addition to the four uncertainty models described in the previous section; since we have only discussed the turbulence model of Spalart and Allmaras, our model selection procedure is performed on a subset of the model class used in [104]. Here the model class is comprised of uncertainty models given in the previous section. While one may argue that a model, for example the Reynolds stress uncertainty model, is more probable than the others, we assume that all models are given an equal prior plausibility $P(M_i|\mathcal{M}) = 1/4$; in other words, we ignore any intuition or knowledge we may have in regards to how the error is distributed in the channel. Thus, in equation (5.30), the model evidence $E(M_i|\boldsymbol{q}, \mathcal{M})$ is the only component unique to each model, making it the determining factor in model selection.

Table 5.3 reports the evidence computed for each of the four models and reproduces the relevant portion of Table 2 from [104]. While the numerical val-

	surrogate	full model
independent homogeneous	-1.457	8.862
correlated homogeneous	1.963	8.045
correlated inhomogeneous	164.9	164.0
Reynolds stress	164.8	169.0

Table 5.3: Evidences computed for the four uncertainty models. ($\log(E)$ is reported in the table.)

ues themselves differ[1], the results are qualitatively similar. As expected, the two multiplicative error models with homogeneous covariance structures have very small evidences; clearly the error in the turbulence model is not homogeneous across the channel. Interestingly, the multiplicative model with inhomogeneous covariance appears to outperform the much more complex Reynolds stress model. However, if we actually compute the plausibility using the prior, we see that both are nearly equally plausible with $P(M_3|\mathcal{M}) = 0.53$ for the inhomogeneous covariance model and $P(M_4|\mathcal{M}) = 0.46$ for the Reynolds stress model; at this stage either model is equally probable.

Our conclusions are in line with those found in [104] regarding the inability of homogeneous uncertainty models to capture the turbulence modeling error. Their results favor the Reynolds stress model over the correlated inhomogeneous model, but again the two are relatively close in plausibility. In contrast to the use of the full turbulence model, our surrogate based approach took significantly less computational time to complete. Table 5.4 displays the

[1]Differences in the computed evidence can be due to a number of factors including the length and number of Markov chains used as well as other tuning parameters of the sampling strategy.

	surrogate	full model
independent homogeneous	130	1720
correlated homogeneous	162	1906
correlated inhomogeneous	151	1735
Reynolds stress	147	1743
Cumulative	590	7104

Table 5.4: Relative runtime in seconds for the Bayesian calibration of each uncertainty model.

runtime for each of the models using the full turbulence model compared to the surrogate model as well as the cumulative time to run the entire model selection study. Simulations were all run on the same machine to obtain relative compute times. The surrogate leads to at least an order of magnitude fewer seconds of total computation time, even for this one-dimensional problem with moderate resolution. One would expect the savings to be even greater for more complex models. Of course these reported times do not take into account the amount of time needed to actually construct the adaptive surrogate models. It took $9,165$ seconds to complete all 18 iterations of the adaptive procedure to construct the anisotropic surrogate model. Factoring in this time, we see that in reality the computational effort is comparable whether one uses the full model or the adaptive surrogate model. The advantage of performing the analysis with a surrogate model is that the same surrogate can be used for all uncertainty models; thus, the cost can be amortized over the exploration of many different uncertainty models. That is, once a surrogate model has been constructed a new model selection study can be performed rather efficiently, each time we wish to access a newly proposed uncertainty model; making the

surrogate approach a valuable resource for modelers.

5.5 Concluding remarks

In this chapter, we have explored the application of goal-oriented error estimation and adaptivity for problems with uncertainty. Accurate surrogate models were constructed for the Spalart-Allmaras turbulence model and the solution of the RANS equations in a fully-developed channel. The results demonstrate that the newly developed methodology can be a valuable resource to computational scientists in modeling complex physical systems.

Future work in this area should focus on expanding the results of Marzouk and Xiu to a broader class of uncertainty representations. With the established error estimates of Chapter 4, the ability to relate the surrogate approximation error and the posterior error would be a valuable addition to the field. Given a desired level of accuracy in the posterior, one could then determine the level of accuracy that is required from the surrogate model and adaptively construct a surrogate model that achieves the goal, and provide an error estimate to assess the reliability of the whole process.

Further investigation with respect to the calculation of the evidence is also of concern. Accurate estimates of the model evidence require a large number of samples; using a surrogate model in place of the full model would allow for the reduction of sampling error in the evidence calculation to within the error in the surrogate model. More analysis would be needed to establish a direct connection between the two errors.

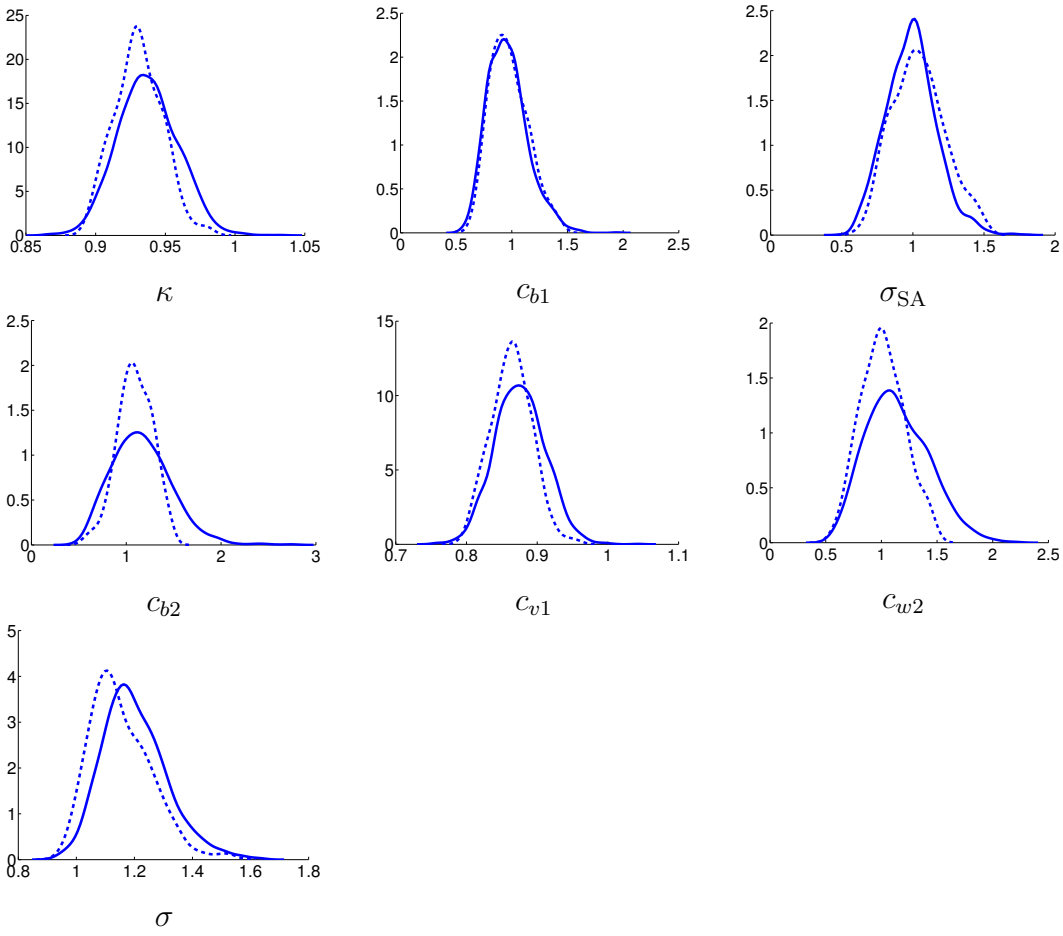

Figure 5.7: Posterior probability densities for the multiplicative error model with independent homogeneous covariance for the SA turbulence model with six uncertain parameters. Full model (solid line) and surrogate model (dashed), where 1 indicates nominal value.

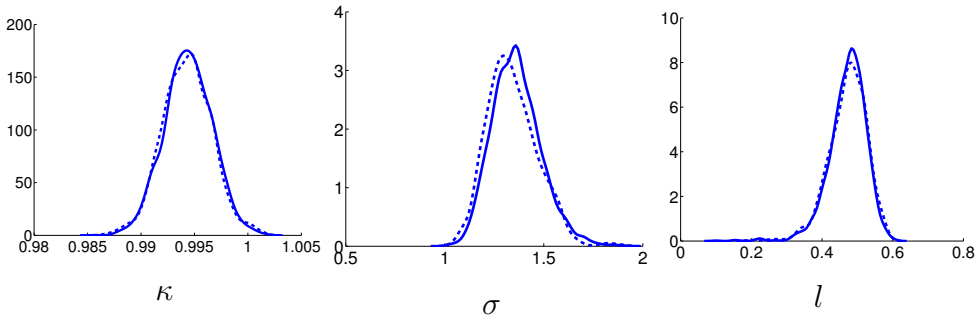

Figure 5.8: Posterior probability densities for the multiplicative error model with correlated homogeneous covariance for the SA turbulence model with uncertain κ. Full model (solid line) and surrogate model (dashed), where 1 indicates nominal value.

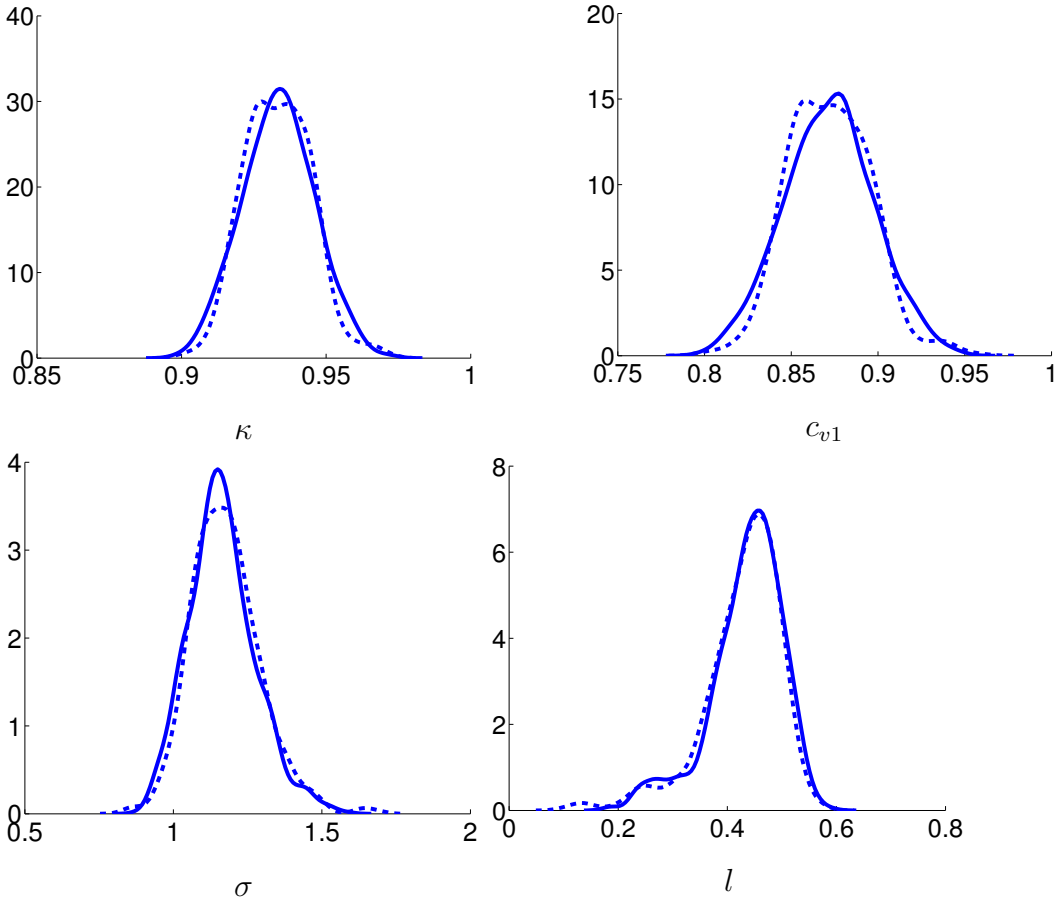

Figure 5.9: Posterior probability densities for the multiplicative error model with correlated homogeneous covariance for the SA turbulence model with uncertain κ and c_{v1}. Full model (solid line) and surrogate model (dashed), where 1 indicates nominal value.

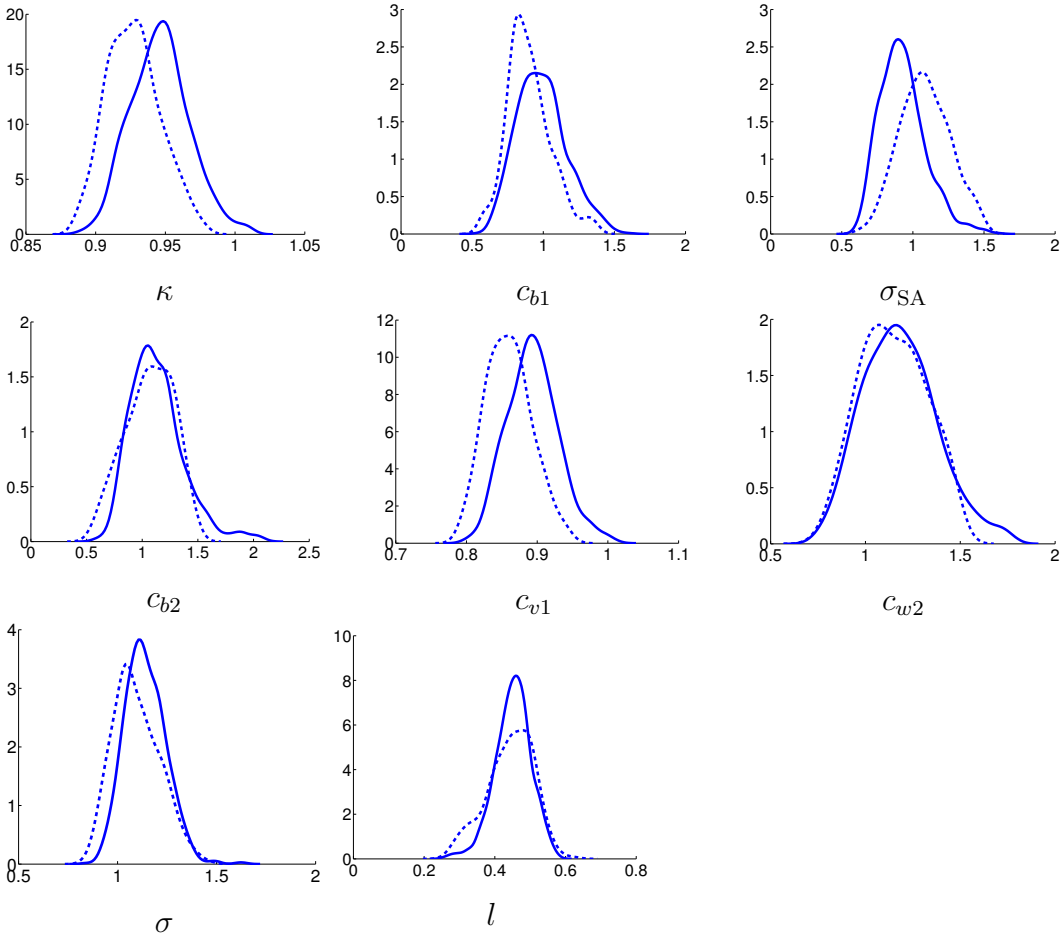

Figure 5.10: Posterior probability densities for the multiplicative error model with correlated homogeneous covariance for the SA turbulence model with six uncertain parameters. Full model (solid line) and surrogate model (dashed), where 1 indicates nominal value.

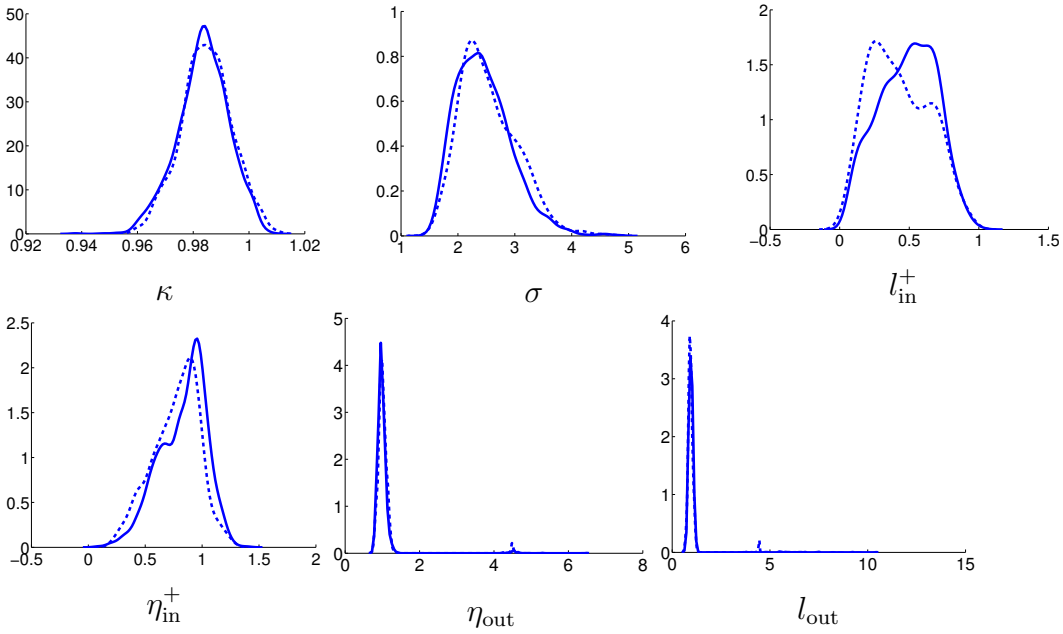

Figure 5.11: Posterior probability densities for the multiplicative error model with correlated inhomogeneous covariance for the SA turbulence model with uncertain κ. Full model (solid line) and surrogate model (dashed), where 1 indicates nominal value.

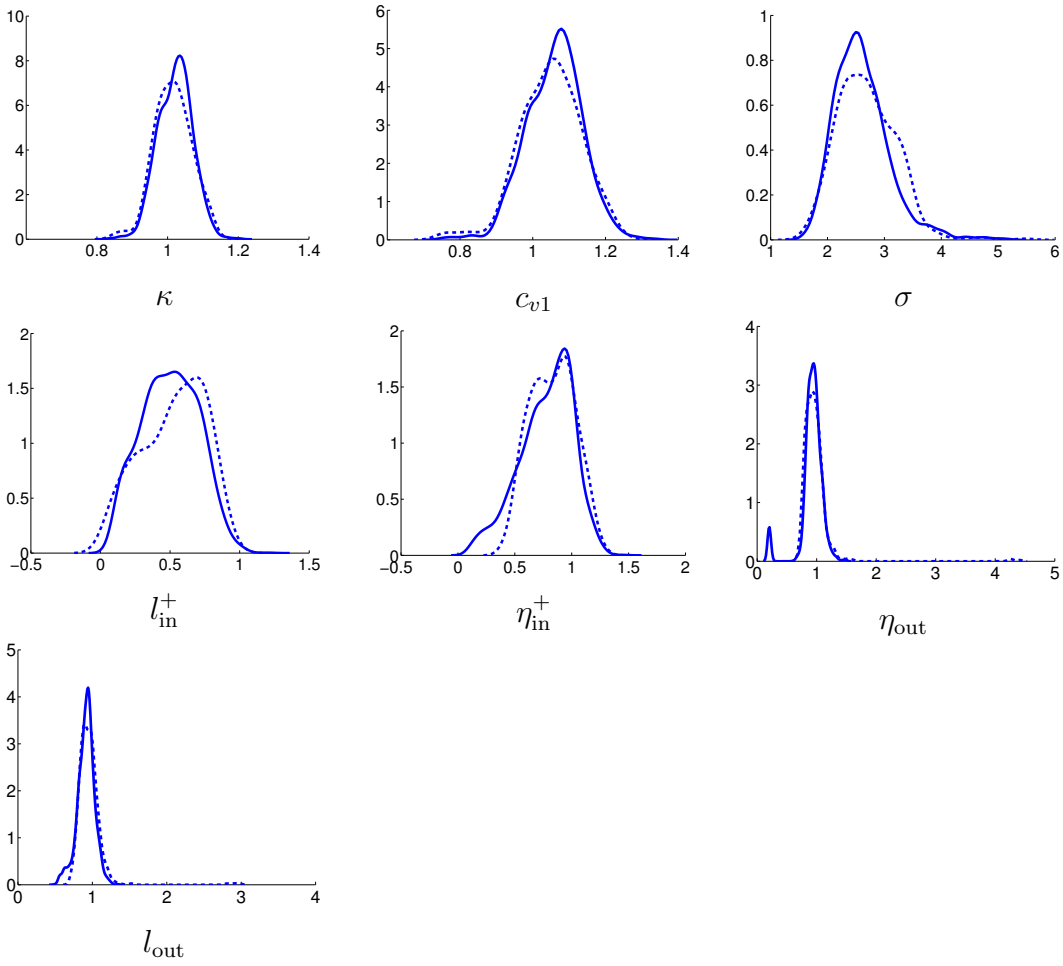

Figure 5.12: Posterior probability densities for the multiplicative error model with correlated inhomogeneous covariance for the SA turbulence model with uncertain κ and c_{v1}. Full model (solid line) and surrogate model (dashed), where 1 indicates nominal value.

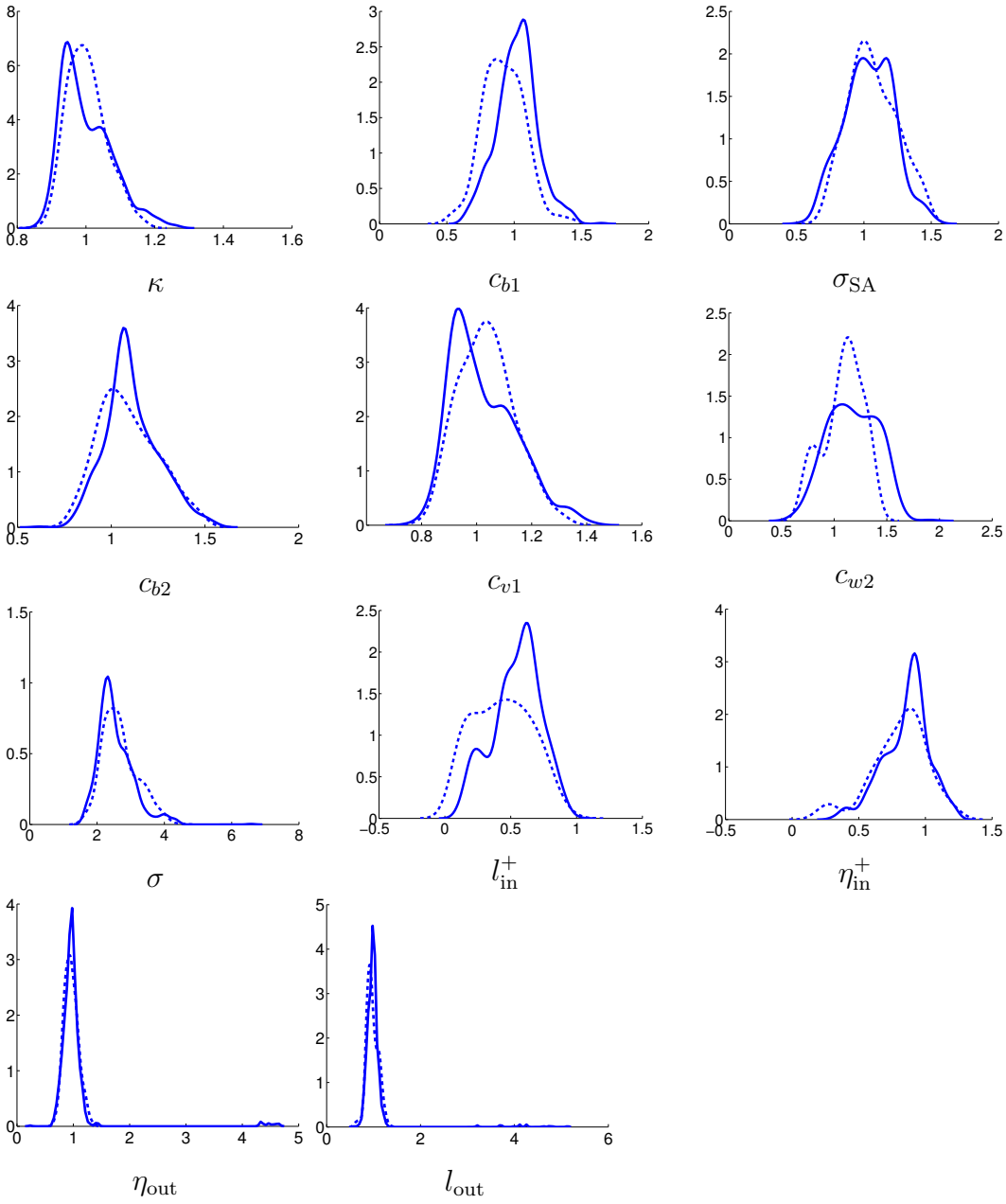

Figure 5.13: Posterior probability densities for the multiplicative error model with correlated inhomogeneous covariance for the SA turbulence model with six uncertain parameters. Full model (solid line) and surrogate model (dashed), where 1 indicates nominal value.

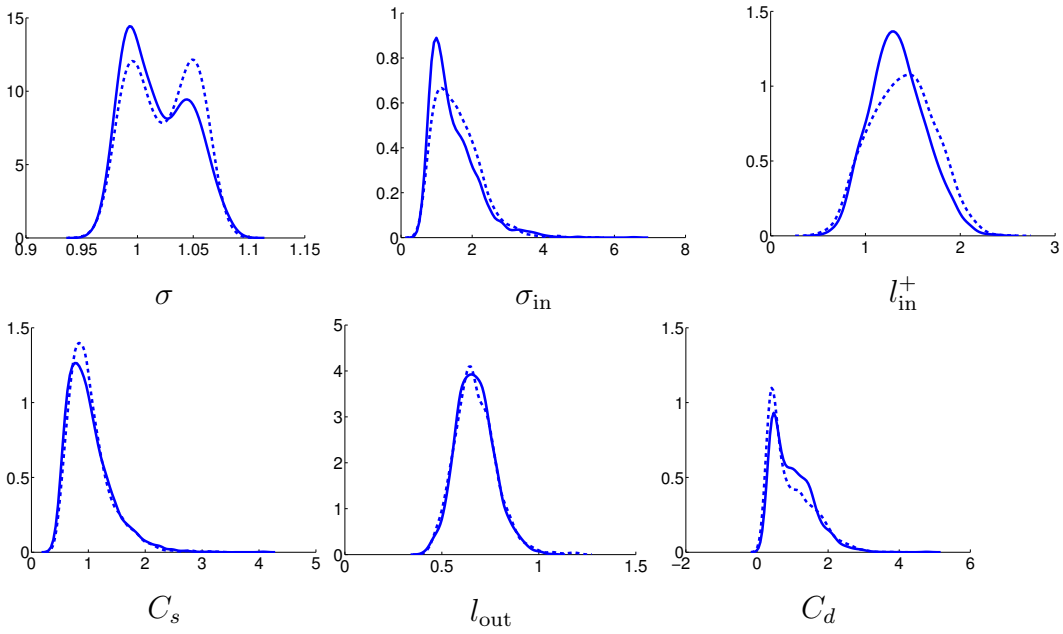

Figure 5.14: Posterior probability densities for the Reynolds stress error model for the SA turbulence model with uncertain κ. Full model (solid line) and surrogate model (dashed), where 1 indicates nominal value.

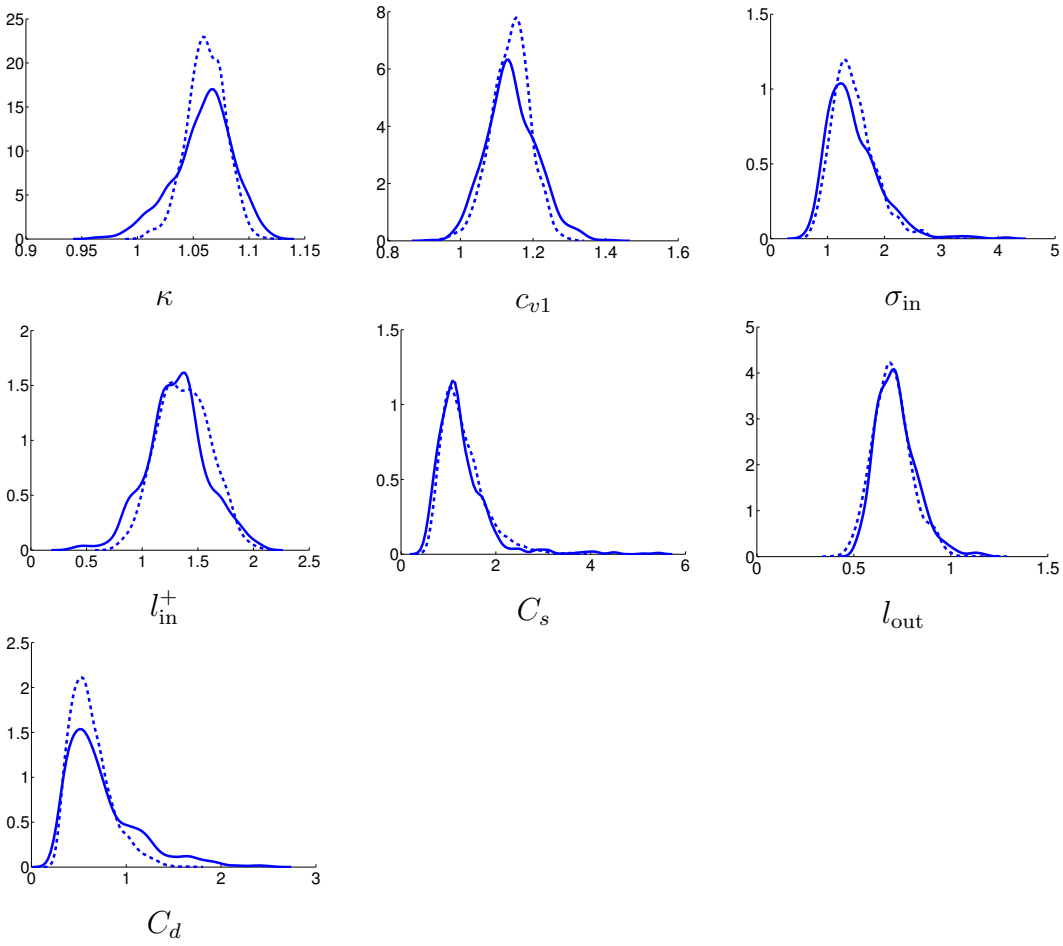

Figure 5.15: Posterior probability densities for the Reynolds stress error model for the SA turbulence model with uncertain κ and c_{v1}. Full model (solid line) and surrogate model (dashed), where 1 indicates nominal value.

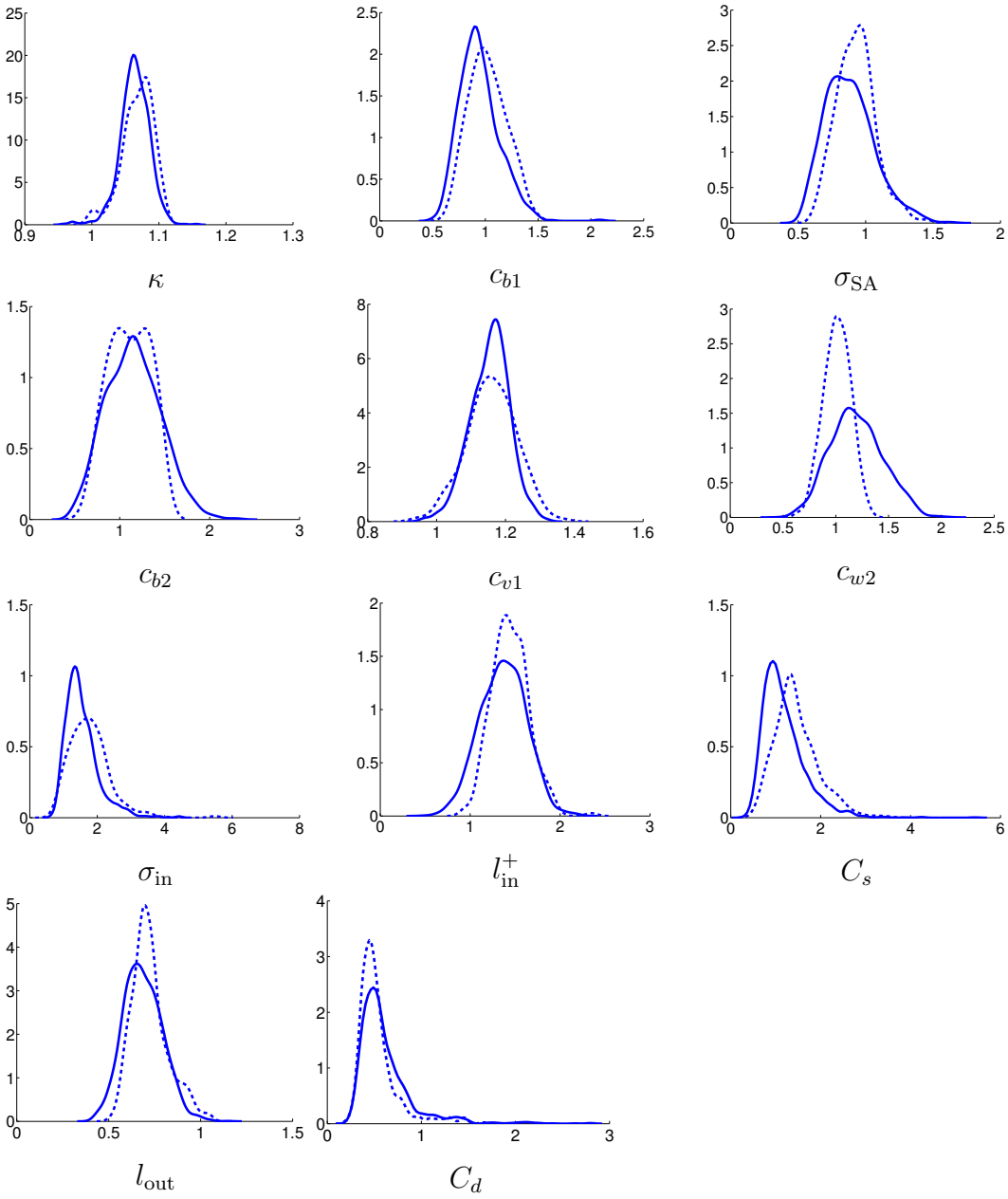

Figure 5.16: Posterior probability densities for the Reynolds stress error model for the SA turbulence model with six uncertain parameters. Full model (solid line) and surrogate model (dashed), where 1 indicates nominal value.

Chapter 6

Conclusions and future work

6.1 Conclusions

In this dissertation, we have proposed a methodology based on the construction of surrogate models and the extension of goal-oriented error estimation techniques for efficient and reliable parameter estimation within a Bayesian study for turbulence modeling.

Following a review of the goal-oriented error estimation theory for linear problems, classical theorems were extended to the case of nonlinear problems. We have also analyzed the effect of neglecting the nonlinear terms in the error estimates, as is often done in the literature. The main conclusion of the investigation is that the nonlinear contributions appeared to have little effect on error estimation or adaptive refinement for Burgers' equation in 1D and Navier-Stokes equations in the case of flow past an obstacle. In these cases, the standard residual error estimator is generally sufficient for both purposes. We have also presented a rather simple diffusion problem to demonstrate that the nonlinear terms may actually dominate the residual term. Further research work would thus be needed to better understand possible influence of these nonlinear terms. Nevertheless, the classical estimator and adaptive ap-

proach proved adequate for the simulation of a flow past an obstacle at low to moderate Reynolds numbers and we proceeded with the analysis of linear and nonlinear problems involving uncertain data.

A posteriori error estimates were developed for second-order differential equations with uncertain parameters. A novel decomposition of the error estimate into contributions from physical and stochastic approximation spaces was shown to properly identify which approximation space should be refined. Adaptive refinement strategies were also developed that took advantage of the indicator for the error in the stochastic approximation. Adaptive mesh refinement in stochastic space and anisotropic p-refinement were demonstrated. The methodology was tested on a number of model problems including that of flow past a cylinder in a channel at low to moderate Reynolds numbers.

Finally, the techniques for goal-oriented error estimation and adaptivity for problems with uncertainty were applied to the study of RANS turbulence models. The objective was to use surrogate models to make the calibration process of these models more efficient. In addition to the theoretical results presented on that topic, we have shown that the approach developed in this thesis could be a valuable resource in applications of engineering interest.

6.2 Future work

We believe we have presented numerical and theoretical evidence that ongoing efforts should be pursued in the investigation of goal-oriented error estimation for nonlinear problems. While the nonlinear diffusion example pre-

sented in Chapter 3 suggests that there may exist initial or boundary-value problems for which one should be careful when neglecting the 'higher-order' terms in the error analysis, preliminary work on mesh adaptation for this problem showed very similar results when including or neglecting the nonlinear contributions in the error estimate. One objective of future work is to find or design a model problem in which the element indicators that include the nonlinear contributions lead to a very different refinement pattern from the one that the standard residual based indicators would provide.

Application of the goal-oriented *a posteriori* error estimation procedure to statistical quantities of interest is another avenue for future investigation. Surrogate models adapted to better predict specific statistical features of the solution would be valuable in predicting rare or extreme events for engineering applications.

Future work on efficient Bayesian inference using surrogate models should include the extension of the theoretical results discussed in Chapter 5 to a broader class of uncertainty representations. Advances on that topic will help relate the surrogate approximation error and the posterior error, hopefully providing a connection between the error estimates for surrogate models derived herein to the error in the posterior distributions of parameters.

Bibliography

[1] M. Ainsworth and J. T. Oden. *A Posteriori Error Estimation in Finite Element Analysis*. John Wiley & Sons, 2000.

[2] S. R. Allmaras, F. T. Johnson, and P. R. Spalart. Modifications and clarifications for the implementation of the spalart-allmaras turbulence model. In *Seventh International Conference on Computational Fluid Dynamics (ICCDF7), Big Island, Hawaii, USA, 9-13 July 2012*, July 9-13 2012.

[3] R. C. Almeida and J. T. Oden. Solution verification, goal-oriented adaptive methods for stochastic advection-diffusion problems. *Comput. Methods Appl. Mech. Eng.*, 199(37-40):2472–2486, 2010.

[4] T. Arbogast and J. Bona. Functional Analysis for the Applied Mathematician. Lecture notes, 2012.

[5] I. Babuška, F. Nobile, and R. Tempone. A stochastic collocation method for elliptic partial differential equations with random input data. *SIAM J. Numer. Anal.*, 45(3):1005–1034, 2007.

[6] I. Babuška and T. Strouboulis. *The Finite Element Method and Its Reliability*. Oxford University Press, 2001.

[7] I. Babuška. The finite element method with Lagrangian multipliers. *Numer. Math.*, 20:179–192, 1973.

[8] I. Babuška and A. Miller. The post-processing approach in the finite element method, Part 1: Calculation of displacements, stresses and other higher derivatives of the displacements. *Internat. J. Numer. Methods Engrg.*, 20(6):1085–1109, 1984.

[9] I. Babuška and A. Miller. The post-processing approach in the finite element method, Part 2: The calculation of stress intensity factors. *Internat. J. Numer. Methods Engrg.*, 20(6):1111–1129, 1984.

[10] I. Babuška and A. Miller. The post-processing approach in the finite element method, Part 3: A posteriori error estimates and adaptive mesh selection. *Internat. J. Numer. Methods Engrg.*, 20(12):2311–2324, 1984.

[11] I. Babuška and W. C. Rheinboldt. A posteriori error estimates for the finite element method. *Internat. J. Numer. Methods Engrg.*, 12:1597–1615, 1978.

[12] I. Babuška and W. C. Rheinboldt. A posteriori error analysis of finite element solutions for one dimensional problems. *SIAM J. Numer. Anal.*, 18:565–589, 1981.

[13] B. Baldwin and H. Lomax. Thin-layer approximation and algebraic model for separated turbulent flows. *AIAA Paper*, 257, 1978.

[14] W. Bangerth and R. Rannacher. *Adaptive Finite Element Methods for Differential Equations*. Birkhauser Verlag, 2003.

[15] R. Becker and R. Rannacher. A feed-back approach to error control in finite element methods: Basic analysis and examples. *East West Journal of numerical mathematics*, 4:237–264, 1996.

[16] R. Becker and R. Rannacher. An optimal control approach to a posteriori error estimation in finite element methods. *Acta Numer.*, 10:1–102, 2001.

[17] P. Billingsley. *Probability and Measure*. John Wiley & Sons, 1995.

[18] P. Binev, W. Dahmen, and R. DeVore. Adaptive finite element methods with convergence rates. *Numerische Mathematik*, 97:219–268, 2004.

[19] D. Braess. *Finite Elements: Theory, Fast Solvers, and Applications in Solid Mechanics*. Cambridge Univ. Press, New York, 2001.

[20] S. Brenner and L. R. Scott. *The Mathematical Theory of Finite Elements Methods*, volume 15 of *Texts in Applied Mathematics*. Springer-Verlag, New York, 2002.

[21] F. Brezzi. On the existence, uniqueness and approximation of saddle-point problems arising from Lagrangian multipliers. *RAIRO Anal. Numér.*, pages 129–151, 1974.

[22] F. Brezzi and R. Falk. Stability of higher-order Hood-Taylor methods. *Siam J. Numer. Anal*, 28(3):581–590, 1991.

[23] F. Brezzi, J. Rappaz, and P. A. Raviart. Finite dimensional approximation of nonlinear problems, Part I: Branches of nonsingular solutions. *Numer. Math.*, 36:1–25, 1980.

[24] S. Brooks, A. Gelman, G. Jones, and X.L. Meng. *Handbook of Markov Chain Monte Carlo*. Chapman & Hall/CRC Handbooks of Modern Statistical Methods. Taylor & Francis, 2011.

[25] C. Bryant and S. Prudhomme. Application of goal-oriented adaptive methods to stochastic partial differential equations. 11th US National Congress on Computational Mechanics, Minneapolis, 25-28 July 2011.

[26] C. Bryant and S. Prudhomme. Application of goal-oriented error estimation methods to statistical quantities of interest. SIAM Conference on Uncertainty Quantification, Raleigh, 2-5 April 2012.

[27] C. Bryant and G. Terejanu. An information-theoretic approach to optimally calibrate approximate models. In *The 50th AIAA Aerospace Sciences Meeting, Nashville, Tennessee, 9-12 January*, 2012.

[28] C. Bryant and G. Terejanu. Optimal data collection under model error. SIAM Conference on Uncertainty Quantification, Raleigh, 2-5 April 2012.

[29] C. Bryant, T. Wildey, and S. Prudhomme. Error control for output quantities of interest in parameterized partial differential equations. SIAM Conference on Computational Science and Engineering, 25 February - March 1 2013.

[30] C. M. Bryant, S. Prudhomme, and T. Wildey. A posteriori error control for partial differential equations with random data. ICES Report 13-08, 2013.

[31] C. M. Bryant, S. Prudhomme, and T. Wildey. Error decomposition and adaptivity for response surface approximations from pdes with parametric uncertainty. *Submitted to SIAM/ASA J. Uncert. Quant.*, 2014.

[32] T. Butler, P. Constantine, and T. Wildey. A posteriori error analysis of parameterized linear systems using spectral methods. *SIAM. J. Matrix Anal. Appl.*, 33:195–209, 2012.

[33] T. Butler, C. Dawson, and T. Wildey. A posteriori error analysis of stochastic spectral methods. *SIAM J. Sci. Comput.*, 33:1267–1291, 2011.

[34] T. Butler and T. Wildey. Adaptive enhancement of surrogate models to accurately predict the probabilities of events. *Submitted to SIAM/ASA J. Uncert. Quant.*, 2014.

[35] D. Calvetti and E. Somersalo. *Introduction to Bayesian Scientific Computing*. Springer, 2007.

[36] R. Cameron and W. Martin. The orthogonal development of non-linear functionals in series of Fourier-Hermite functionals. *Annals of Mathematics*, 48:385–392, 1947.

[37] C. Carstensen, D. Peterseim, and H. Rabus. Optimal adaptive nonconforming FEM for the Stokes problem. *Numerische Mathematik*, 123:291–308, 2013.

[38] C. Carstensen and H. Rabus. An optimal adaptive mixed finite element method. *Mathematics of Computation*, 80(274):649–667, 2011.

[39] S. H. Cheung and J. L. Beck. New Bayesian updating methodology for model validation and robust predictions of a target system based on hierarchical subsystem tests. Technical report, California Institute of Technology, 2008.

[40] S. H. Cheung, T. A. Oliver, E. E. Prudencio, S. Prudhomme, and R. D. Moser. Bayesian uncertainty analysis with applications to turbulence modeling. *Reliability Engineering & System Safety*, 96(9):1137–1149, 2011.

[41] K. Y. Chien. Predictions of channel and boundary-layer flows with a low-Reynolds-number two-equation model of turbulence. *AIAA Journal*, 20(1):33–38, 1982.

[42] P. G. Constantine, M. S. Eldred, and E. T. Phipps. Sparse pseudospectral approximation method. *Computer Methods in Applied Mechanics*

and Engineering, 229-232:1 – 12, 2012.

[43] P. G. Constantine, D. F. Gleich, and G. Iaccarino. Spectral methods for parameterized matrix equations. *SIAM. J. Matrix Anal. Appl.*, 31:2681–2699, 2010.

[44] M. K. Deb, I. Babuška, and J. T. Oden. Solution of stochastic partial differential equations using Galerkin finite element techniques. *Comput. Methods Appl. Mech. Eng.*, 190:6359–6372, 2001.

[45] J. C. Del Alamo, J. Jiménez, P. Zandonade, and R. D Moser. Scaling of the energy spectra of turbulent channels. *Journal of Fluid Mechanics*, 500:135–144, 2004.

[46] P. Drábek and J. Milota. *Methods of nonlinear analysis: applications to differential equations*. Birkhäuser, 2007.

[47] C. F. Dunkl and Y. Xu. *Orthogonal Polynomials in Several Variables*. Cambridge University Press, 2001.

[48] P. A. Durbin. Separated flow computations with the $k - \varepsilon - v^2$ model. *AIAA Journal*, 33:659–664, 1995.

[49] P. A. Durbin and B. A. Petterson Reif. *Statistical Theory and Modeling for Turbulent Flows*. Wiley, 2001.

[50] R. Durrett. *Probability: Theory and Examples*. Duxbury Press, 2004.

[51] K. Eriksson, D. Estep, P. Hansbo, and C. Johnson. Introduction to adaptive methods for differential equations. *Acta Numer.*, pages 105–158, 1995.

[52] K. Eriksson, D. Estep, P. Hansbo, and C. Johnson. *Computational differential equations*. Cambridge University Press, 1996.

[53] A. Ern and J. L. Guermond. *Theory and Practice of Finite Elements*, volume 159 of *Applied Mathematical Sciences*. Springer-Verlag, New York, 2004.

[54] A. Ern and M. Vohralík. Adaptive inexact newton methods with a posteriori stopping criteria for nonlinear diffusion pdes. *SIAM J. Sci. Comput.*, 35(4):A1761–A1791, 2013.

[55] O. G. Ernst, A. Mugler, H.-J. Starkloff, and E. Ullmann. On the convergence of generalized polynomial chaos expansions. *ESAIM: Mathematical Modelling and Numerical Analysis*, 46(2):317–339, October 2011.

[56] D. Estep. A posteriori error bounds and global error control for approximation of ordinary differential equations. *SIAM J. Numer. Anal.*, 32(1):1–48, 1995.

[57] D. Estep, M. G. Larson, and R. D. Williams. *Estimating the error of numerical solutions of systems of reaction-diffusion equations*. American Mathematical Soc., 2000.

[58] B. Ganapathysubramanian and N. Zabaras. Sparse grid collocation schemes for stochastic natural convection problems. *J. Comput. Phys.*, 225(1):652–685, July 2007.

[59] B. Ganis, H. Klie, M. F. Wheeler, T. Wildey, I. Yotov, and D. Zhang. Stochastic collocation and mixed finite elements for flow in porous media. *Comput. Methods Appl. Mech. Engrg*, 197(43-44):3547 – 3559, 2008.

[60] E. C. Gartland Jr. Computable pointwise error bounds and the Ritz method in one dimension. *SIAM J. Numer. Anal.*, 21(1):84–100, 1984.

[61] W. Gautschi. Orthogonal polynomials: applications and computation. *Acta Numerica*, 5:45–119, 1996.

[62] W. Gautschi. *Orthogonal Polynomials: Computation and Approximation*. Clarendon Press, Oxford, 2004.

[63] A. Gelman and D. B. Rubin. Inference from iterative simulation using multiple sequences. *Statistical Science*, 7(4):457–472, 1992.

[64] S. Geman and D. Geman. Stochastic relaxation, Gibbs distributions, and the Bayesian restoration of images. *IEEE Transactions on Pattern Analysis and Machine Intelligence*, PAMI-6(6):721–741, 1984.

[65] T. Gerstner and M. Griebel. Dimension-adaptive tensor-product quadrature. *Computing*, 71(1):65–87, 2003.

[66] C. J. Geyer. Practical Markov Chain Monte Carlo. *Statistical Science*, 7(4):473–483, 1992.

[67] R. Ghanem and J. Red-Horse. Propagation of probabilistic uncertainty in complex physical systems using a stochastic finite element approach. *Physica D: Nonlinear Phenomena*, 133:137–144, 1999.

[68] R. Ghanem and P. Spanos. *Stochastic Finite Elements: A Spectral Approach*. Springer-Verlag, New York, 2002.

[69] M. B. Giles and E. Süli. Adjoint methods for PDEs: a posteriori error analysis and postprocessing by duality. *Acta Numerica*, 11:145–236, 2002.

[70] W. R. Gilks, S. Richardson, and D. J. Spiegelhalter. *Markov Chain Monte Carlo in Practice*. Chapman & Hall, 1996.

[71] D. S. Guignard, F. Nobile, and M. Picasso. A posteriori error estimations for elliptic partial differential equations with small uncertainties. MATHICSE Report 40.2014, 2014.

[72] H. Haario, M. Laine, A. Mira, and E. Saksman. DRAM: Efficient adaptive MCMC. *Statistics and Computing*, 16(4):339–354, 2006.

[73] W. K. Hastings. Monte Carlo sampling methods using Markov chains and their applications. *Biometrika*, 57(1):97–109, 1970.

[74] S. Hoyas and J. Jiménez. Scaling of the velocity fluctuations in turbulent channels up to $Re_\tau = 2003$. *Physics of Fluids*, 18(1):011702, 2006.

[75] S. Hoyas and J. Jiménez. Reynolds number effects on the Reynolds-stress budgets in turbulent channels. *Physics of Fluids*, 20(10):101511, 2008.

[76] J. D. Jakeman and S. G. Roberts. Local and dimension adaptive stochastic collocation for uncertainty quantification. In *Sparse Grids and Applications*, volume 88 of *Lecture Notes in Computational Science and Engineering*, pages 181–203. Springer, Heidelberg, 2013.

[77] E. T. Jaynes. *Probability Theory: The Logic of Science*. Cambridge University Press, 2003.

[78] J. Kaipio and E. Somersalo. *Statistical and Computational Inverse Problems*. Springer, 2005.

[79] D. W. Kelly. The self-equilibration of residuals and complementary a posteriori error estimates in the finite element method. *Internat. J. Numer. Methods Engrg.*, 20:1491–1506, 1984.

[80] M. C. Kennedy and A. O'Hagan. Bayesian calibration of computer models. *J. Royal Statist. Soc. Series B*, 63(3):425–464, 2001.

[81] P. Ladevèze and D. Leguillon. Error estimate procedure in the finite element method and applications. *SIAM J. Numer. Anal.*, 20:485–509, 1983.

[82] O. Le Maître, R. Ghanem, O. Knio, and H. Najm. Multi-resolution analysis of Wiener-type propagation schemes. *J. Comput. Phys.*, 197:502–531, 2004.

[83] O. Le Maître, R. Ghanem, O. Knio, and H. Najm. Uncertainty propagation using Wiener-Haar expansions. *J. Comput. Phys.*, 197(1):28–57, 2004.

[84] O. Le Maître and O. Knio. *Spectral Methods for Uncertainty Quantification: With Applications to Computational Fluid Dynamics*. Springer, 2010.

[85] J. Li and Y. Marzouk. Adaptive construction of surrogates for the Bayesian solution of inverse problems. *SIAM J. Sci. Comput.*, 36:A1164–A1186, 2014.

[86] X. Ma and N. Zabaras. An adaptive hierarchical sparse grid collocation algorithm for the solution of stochastic differential equations. *J. Comput. Phys.*, 228(8):3084–3113, May 2009.

[87] X. Ma and N. Zabaras. An efficient Bayesian inference approach to inverse problems based on an adaptive sparse grid collocation method. *Inverse Problems*, 25(3):035013, March 2009.

[88] Y. Marzouk, H. Najm, and L. Rahn. Stochastic spectral methods for efficient Bayesian solution of inverse problems. *J. Comput. Physics*, 224:560–586, 2007.

[89] Y. Marzouk and D. Xiu. A stochastic collocation approach to bayesian inference in inverse problems. *Communications in computational physics*, 6(4):826–847, 2009.

[90] Y. M. Marzouk and H. N. Najm. Dimensionality reduction and polynomial chaos acceleration of Bayesian inference in inverse problems. *Journal of Computational Physics*, 228(6):1862–1902, April 2009.

[91] L. Mathelin and O. Le Maître. Dual-based a posteriori error estimate for stochastic finite element methods. *Communications in Applied Mathematics and Computational Science*, 2(1):83–115, 2007.

[92] L. Mathelin and O. P. Le Maître. Dual-based error analysis for uncertainty quantification in a chemical system. *PAMM*, 7(1):2010007–2010008, 2007.

[93] N. Metropolis, A. W. Rosenbluth, M. N. Rosenbluth, A. H. Teller, and E. Teller. Equation of state calculations by fast computing machines. *Journal of Chemical Physics*, 29:1087–1092, 1953.

[94] M. S. Mommer and R. Stevenson. A goal-oriented adaptive finite element method with convergence rates. *Siam J. Numer. Anal*, 47(2):861–886, 2009.

[95] R. Morrison, C. Bryant, G. Terejanu, K. Miki, and S. Prudhomme. Optimal data split methodology for model validation. In *Proceedings of*

the World Congress on Engineering and Computer Science 2011 Vol II, WCECS 2011, pages 1038–1043, October 19-21 2011.

[96] R. E. Morrison, C. M. Bryant, G. Terejanu, S. Prudhomme, and K. Miki. Data partition methodology for validation of predictive models. *Computers & Mathematics with Applications*, 66(10):2114–2125, 2013.

[97] R. D. Moser. Turbulence. Lecture Notes, 2013.

[98] F. Nobile, R. Tempone, and C. G. Webster. An anisotropic sparse grid stochastic collocation method for partial differential equations with random input data. *Siam J. Numer. Anal*, 46(5):2411–2442, 2008.

[99] F. Nobile, R. Tempone, and C. G. Webster. A sparse grid stochastic collocation method for partial differential equations with random input data. *Siam J. Numer. Anal*, 46(5):2309–2345, 2008.

[100] J. T. Oden and S. Prudhomme. Goal-oriented error estimation and adaptivity for the finite element method. *Computers & Mathematics with Applications*, 41(5):735–756, 2001.

[101] J. T. Oden and S. Prudhomme. Estimation of Modeling Error in Computational Mechanics. *J. Comput. Physics*, 182:496–515, 2002.

[102] J. T. Oden, S. Prudhomme, A. Romkes, and P. T. Bauman. Multiscale Modeling of Physical Phenomena: Adaptive Control of Models. *SIAM J. Sci. Comput.*, 28(6):2359, 2006.

[103] T. A. Oliver and D. L. Darmofal. Impact of turbulence model irregularity on high-order discretizations. *AIAA Paper*, 953, 2009.

[104] T. A. Oliver and R. D. Moser. Bayesian uncertainty quantification applied to rans turbulence models. *Journal of Physics: Conference Series*, 318(4):042032, 2011.

[105] S. B. Pope. *Turbulent Flows*. Cambridge University Press, October 2000.

[106] J. Pousin and J. Rappaz. Consistency, stability, a priori and a posteriori errors for Petrov-Galerkin methods applied to nonlinear problems. *Numer. Math.*, 69:213–131, 1994.

[107] E. E. Prudencio and K. W. Schulz. The parallel C++ statistical library QUESO: Quantification of uncertainty for estimation, simulation and optimization. In *Euro-Par 2011: Parallel Processing Workshops*, volume 7155 of *Lecture Notes in Computer Science*, pages 398–407. Springer, Heidelberg, 2012.

[108] S. Prudhomme and J. T. Oden. On goal-oriented error estimation for elliptic problems: application to the control of pointwise errors. *Comput. Methods Appl. Mech. Eng.*, 176(14):313 – 331, 1999.

[109] S. Prudhomme and J. T. Oden. Computable Error Estimators and Adaptive Techniques for Fluid Flow Problems. In *Estimation and Adaptive Discretization Methods in Computational Fluid Dynamics, Lecture*

Notes in Computational Science and Engineering, volume 25. Springer-Verlag, 2003.

[110] M. M. Rao and R. J. Swift. *Probability Theory with Applications*, volume 582 of *Mathematics and Its Applications*. Springer-Verlag, New York, 2006.

[111] C. E. Rasmussen and K. I. Williams. *Gaussian Processes for Machine Learning*. MIT Press, 2006.

[112] A. Romkes, C. M. Bryant, and K. S. Surana. A posteriori error estimation of hpk fe solutions of linear boundary value problems in terms of quantities of interest. *Acta Mechanica Solida Sinica*, 23, Special Issue:122–127, 2010.

[113] P. R. Spalart and S. R. Allmaras. A one-equation turbulence model for aerodynamic flows. *Recherche Aérospatiale*, (1):5–21, 1994.

[114] R. Stevenson. Optimality of a Standard Adaptive Finite Element Method. *Foundations of Computational Mathematics*, 7(2):245–269, 2007.

[115] A. Tarantola. *Inverse Problem Theory and Methods for Model Parameter Estimation*. SIAM, 2005.

[116] G. Terejanu, C. M. Bryant, and K. Miki. Bayesian optimal experimental design for the shock-tube experiment. In *Journal of Physics: Conference Series*, volume 410, page 012040, 2013.

[117] R. A. Todor and C. Schwab. Convergence rates for sparse chaos approximations of elliptic problems with stochastic coefficients. *IMA Journal of Numerical Analysis*, 27(2):232–261, 2006.

[118] K. G. van der Zee. *Goal-Adaptive Discretization of Fluid-Structure Interaction*. PhD thesis, Delft University of Technology, The Netherlands, 2009.

[119] R. Verfürth. *A Posteriori Error Estimation Techniques for Finite Element Methods*. Numerical Mathematics and Scientific Computation. Oxford University Press, 2013.

[120] X. Wan and G. Karniadakis. Beyond Wiener-Askey expansions: Handling arbitrary pdfs. *Journal of Scientific Computing*, 27:455–464, 2006.

[121] X. Wan and G. Karniadakis. Error control in multi-element generalized polynomial chaos method for elliptic problems with random coefficients. *Communications in Computational Physics*, 5(2-4):793–820, 2009.

[122] X. Wan and G. Karniadakis. Solving elliptic problems with non-Gaussian spatially-dependent random coefficients. *Computer Methods in Applied Mechanics and Engineering*, 198(21-26):1985–1995, 2009.

[123] X. Wan and G. E. Karniadakis. An adaptive multi-element generalized polynomial chaos method for stochastic differential equations. *J. Comput. Phys.*, 209(2):617–642, 2005.

[124] M. F. Wheeler. A priori l_2 error estimates for galerkin approximations to parabolic partial differential equations. *SIAM J. Numer. Anal.*, 10(4):723–759, 1973.

[125] N. Wiener. The homogeneous chaos. *American Journal of Mathematics*, 60:897–936, 1938.

[126] D. Wilcox. *Turbulence modeling for CFD*. DCW Industries, 2006.

[127] D. C. Wilcox. Reassessment of the scale-determining equation for advanced turbulence models. *AIAA Journal*, 26:1299–1310, 1988.

[128] D. Xiu and G. Karniadakis. The Wiener-Askey polynomial chaos for stochastic differential equations. *SIAM J. Sci. Comput.*, 24:619–644, 2002.

[129] E. Zeidler. *Nonlinear Functional Analysis and its Applications*. Springer-Verlag, New York, 1985.

[130] O. C. Zienkiewicz and J. Z. Zhu. A simple error estimator and adaptive procedure for practical engineering analysis. *Internat. J. Numer. Methods Engrg.*, 24:337–357, 1987.

[131] O. C. Zienkiewicz and J. Z. Zhu. The superconvergent patch recovery and a posteriori error estimates. Part 1: The recovery technique. *Internat. J. Numer. Methods Engrg.*, 33(7):1331–1364, 1992.

[132] O. C. Zienkiewicz and J. Z. Zhu. The superconvergent patch recovery and a posteriori error estimates. Part 2: Error estimates and adaptivity. *Internat. J. Numer. Methods Engrg.*, 33(7):1365–1382, 1992.

[133] G. Žitković. Theory of Probability. Lecture Notes, 2013.

Vita

Corey Michael Bryant was born in Shawnee, KS. He received a Bachelor of Science degree in Mechanical Engineering from the University of Kansas in May 2009, where his research efforts contributed to the publication of [112]. In August of the same year he entered the Computational and Applied Mathematics program at The University of Texas at Austin, under the supervision of Dr. Serge Prudhomme. In the summer of 2012 he was an intern with the Optimization and Uncertainty Quantification Department at Sandia National Labs. Throughout his time in graduate school he presented his work at professional conferences [25, 26, 28, 29], coauthored two journal publications [31, 96] and a number of conference proceedings and technical reports [27, 30, 95, 116].

Address: corey.m.bryant@gmail.com

This dissertation was typeset with LaTeX[†] by the author.

[†]LaTeX is a document preparation system developed by Leslie Lamport as a special version of Donald Knuth's TeX Program.